



NOVA

NOVA SCHOOL OF
SCIENCE & TECHNOLOGY

DEPARTMENT OF CHEMISTRY

RUTE RITA MENDES CANCELA OLIVEIRA FRANCISCO

Bachelor's Degree in Science of Chemical and Biochemical Engineering

POLY(ETHYLENE GLYCOL) DIACRYLATE
IONGEL MEMBRANES REINFORCED WITH
NANOCCLAYS FOR CO₂ SEPARATION

MASTER IN CHEMICAL AND BIOCHEMICAL ENGINEERING

NOVA University of Lisbon

October 2021

POLY(ETHYLENE GLYCOL) DIACRYLATE IONGEL MEMBRANES REINFORCED WITH NANOCLAYS FOR CO₂ SEPARATION

RUTE RITA MENDES CANCELA OLIVEIRA FRANCISCO

Bachelor's Degree in Science of Chemical and Biochemical Engineering

Supervisor: Dr. Luísa Alexandra Graça Neves, Assistant Researcher,
LAQV-REQUIMTE, FCT-NOVA, NOVA University of Lisbon

Cosupervisor: Dr. Liliana Sofia Carvalho Tomé, Assistant Researcher,
LAQV-REQUIMTE, FCT-NOVA, NOVA University of Lisbon

Jury:

President: Dr. Mário Fernando José Eusébio, Assistant Professor,
FCT-NOVA, NOVA University of Lisbon

Examiner: Dr. Mónica Cristina Faria Besteiro, Assistant Researcher
and Invited Professor, *Instituto Superior Técnico*, University
of Lisbon

Supervisors: Dr. Luísa Alexandra Graça Neves, Assistant Researcher,
LAQV-REQUIMTE, FCT-NOVA, NOVA University of Lisbon
Dr. Liliana Sofia Carvalho Tomé, Assistant Researcher,
LAQV-REQUIMTE, FCT-NOVA, Nova University of Lisbon

MASTER IN CHEMICAL AND BIOCHEMICAL ENGINEERING

NOVA University of Lisbon
October 2021

Poly(ethylene glycol) diacrylate longel membranes reinforced with nanoclays for CO₂ separation

Copyright © RUTE RITA MENDES CANCELA OLIVEIRA FRANCISCO, Faculdade de Ciências e Tecnologia, Universidade NOVA de Lisboa.

A Faculdade de Ciências e Tecnologia e a Universidade NOVA de Lisboa têm o direito, perpétuo e sem limites geográficos, de arquivar e publicar esta dissertação através de exemplares impressos reproduzidos em papel ou de forma digital, ou por qualquer outro meio conhecido ou que venha a ser inventado, e de a divulgar através de repositórios científicos e de admitir a sua cópia e distribuição com objetivos educacionais ou de investigação, não comerciais, desde que seja dado crédito ao autor e editor.

AGRADECIMENTOS

Em primeiro lugar, quero agradecer especialmente à minha orientadora, Dra. Luísa Neves, por me ter dado a oportunidade de realizar esta tese sob a sua supervisão, por todo o conhecimento que me transmitiu, pela simpatia e amizade nos bons momentos e também pela compreensão e paciência nos momentos menos bons, motivando-me ao longo da tese e mostrando-se sempre disponível para esclarecer as minhas dúvidas. Agradeço também à minha coorientadora, Dra. Liliana Tomé, que apesar de não ter estado presente durante toda a tese, foi fundamental para a sua realização, contribuindo com novas ideias e sugestões e mostrando um sentido crítico e criativo inspiradores que me encorajaram a continuar a melhorar. Obrigada à minha "coorientadora não oficial", *PhD* Rita Nabais, que me acompanhou e ajudou nos primeiros tempos no laboratório, partilhando comigo a sua experiência e conhecimento, e pelo tempo que disponibilizou para responder às minhas questões e fazer discursos motivacionais.

À Dra. Isabel Nogueira do Instituto Superior Técnico, ao Dr. Nuno Costa e à Dra. Carla Rodrigues do Laboratório de Análises da FCT-NOVA quero agradecer por terem analisado as minhas amostras e terem providenciado alguns dos resultados apresentados nesta tese. Ao Dr. Vítor Alves do Instituto Superior de Agronomia agradeço a disponibilidade e auxílio prestados nos ensaios de perfuração e no tratamento dos respetivos resultados.

Às *Membrane Ladys*, *PhD* Rosa Nascimento, *PhD* Paloma Ortiz, *PhD* Inês Ferreira, Dra. Noémi Jordão e as que já mencionei agradeço pela companhia, apoio e ajuda e por se mostrarem sempre empenhadas em melhorar a nossa qualidade de trabalho no laboratório.

Às minhas colegas Joana Galamba, Anastasiia Keba e Mónica Rocha agradeço pela sua amizade e boa disposição e pelos momentos de convívio e partilha das suas próprias experiências. Um agradecimento a todos os colegas, professores e investigadores com os quais contactei ao longo do curso e que de alguma forma contribuíram para o meu desenvolvimento académico.

Por último, mas não menos importante, obrigada: À minha avó Antónia, ao meu tio Rui e ao meu pai Jorge pela paciência e apoio sempre que precisei; À Sofia Ribeiro pela sua generosidade ao emprestar-me o portátil que me permitiu escrever esta tese; À Joana Moreira,

sempre amiga e com as palavras que eu precisei de ouvir; À Lina, pela ajuda e por uma nova amizade; Ao Dr. Marco Torrado e à Dra. Elsa Lara de que tanto precisei porque infelizmente a vida não traz manual de instruções.

A todos os que contribuíram para a conclusão de uma das etapas mais importantes da minha vida, muito obrigada!

"I was taught that the way of progress was neither swift nor easy."

(Marie Curie)

ABSTRACT

The continuous consumption of fossil fuels has elevated the concentration of carbon dioxide (CO₂) in the atmosphere with severe consequences for the environment. Membrane technology emerged as a potential solution to separate CO₂ from light gases, contributing to Carbon Capture and Storage (CCS). Within the several materials studied for the preparation of membranes, ionic liquids (ILs) are some of the most interesting, mainly due to their tunable properties and good affinity towards CO₂. In this line, iongel membranes combining high IL loadings (≥ 60 wt%) incorporated into a poly(ethylene glycol) (PEG) based polymer network cross-linked by ultraviolet (UV) radiation have been developed. One of the main challenges faced when fabricating these iongel membranes is their limited mechanical resistance due to a gel-like nature, which becomes more accentuated when the concentration of IL increases. To overcome this problem, the addition of low amounts of nanoclay particles (≤ 1 wt%) into the iongel membranes is suggested in this work as a way to reinforce their structure.

Self-standing iongel mixed matrix membranes (MMMs) that were solid yet malleable were prepared in a simple single-pot with different loadings (from 0.2 to 1.0 wt%) of montmorillonite (MMT) nanoclay particles. The iongel MMMs were characterized by several techniques, including attenuated total reflectance Fourier-transform infrared (ATR-FTIR) spectroscopy, thermogravimetric analysis (TGA), scanning electron microscopy (SEM), differential scanning calorimetry (DSC), contact angle and puncture tests in order to assess how their properties affect the CO₂ separation performance from nitrogen (N₂) and methane (CH₄) in pure gas permeation experiments and evaluate their potential to be applied in post-combustion streams and biogas upgrading.

The characterization results revealed that the iongel MMMs can withstand temperatures typical of post-combustion streams (around 120 °C) and that the incorporation of MMT did not have a significant impact on the permeability/selectivity, crystallinity, and hydrophilicity of the iongel MMMs. On the other hand, a concentration of 0.2 wt% MMT evenly dispersed into an iongel MMM was able to increase the mechanical resistance up to 30%, which suggests that future studies focused on the optimization of the preparation of these membranes may allow the addition of higher IL loadings for better CO₂ separation performance while the mechanical stability is maintained.

Keywords: longel membranes; Ionic Liquids; UV cross-linked polymer network; Montmorillonite nanoclay; CO₂ separation.

RESUMO

O consumo contínuo de combustíveis fósseis tem tido consequências graves para o ambiente devido ao aumento da concentração de dióxido de carbono (CO_2) na atmosfera. Uma possível solução para separar o CO_2 de outros gases leves consiste na Captura e Armazenamento de Carbono (CCS) através da tecnologia de membranas. Dentro dos materiais estudados para a preparação de membranas, os Líquidos Iônicos (LIs) são dos mais promissores, principalmente devido às suas propriedades ajustáveis e boa afinidade para o CO_2 . Posto isto, têm sido desenvolvidas membranas de géis iônicos com elevadas concentrações de LIs ($\geq 60 \text{ \% (m/m)}$) incorporados numa rede polimérica entrecruzada por radiação ultravioleta (UV) à base de polietileno glicol (PEG). Porém, a resistência mecânica das membranas de géis iônicos está limitada devido à sua natureza gelatinosa, que é mais acentuada quanto maior for a concentração de LI, tratando-se de um dos maiores desafios inerentes ao seu fabrico. De modo a abordar este problema, este trabalho propõe a adição de pequenas quantidades de partículas de *nanoclay* ($\leq 1 \text{ \% (m/m)}$) às membranas de géis iônicos com o intuito de reforçar a sua estrutura.

Foram preparadas membranas de matriz mista (MMMs) de géis iônicos sólidas e maleáveis, com diferentes concentrações (entre 0.2 e 1.0 \% (m/m)) de partículas do *nanoclay* montmorillonite (MMT). As MMMs de géis iônicos foram caracterizadas por diversas técnicas, entre as quais espectroscopia de infravermelho com transformada de Fourier em modo de refletância total atenuada (ATR-FTIR), análise termogravimétrica (TGA), microscopia eletrónica de varrimento (SEM), calorimetria diferencial de varrimento (DSC), ângulo de contacto e testes mecânicos através de ensaios de perfuração. A caracterização permitiu estudar de que forma as propriedades das MMMs de géis iônicos influenciam o seu desempenho na separação de CO_2 de azoto (N_2) e de metano (CH_4), e assim avaliar o seu potencial para serem aplicadas em correntes de pós-combustão e em purificação de biogás.

Os resultados da caracterização revelaram que as MMMs de géis iônicos têm a capacidade de suportar temperaturas típicas de correntes gasosas de pós-combustão (à volta de $120 \text{ }^\circ\text{C}$) e que a incorporação de MMT não teve um impacto significativo na permeabilidade/seletividade, cristalinidade e hidrofiliabilidade das mesmas. Contudo, a adição de uma concentração de 0.2 \% (m/m) de MMT bem disperso nas membranas de géis iônicos permitiu

aumentar a sua resistência mecânica até 30%. Este resultado sugere que a otimização da preparação das MMMs de géis iónicos em trabalhos futuros, poderá permitir a incorporação de concentrações superiores de LI, de modo a atingir um melhor desempenho na separação de CO₂, e de forma a não comprometer a sua estabilidade mecânica.

Palavras-chave: Membranas de géis iónicos; Líquidos iónicos; Rede polimérica entrecruzada por UV; *Nanoclay* montmorillonite; Separação de CO₂.

INDEX

AGRADECIMENTOS.....	VII
ABSTRACT	XI
RESUMO	XIII
INDEX.....	XV
FIGURE INDEX.....	XVII
TABLE INDEX.....	XIX
LIST OF ABBREVIATIONS.....	XXI
LIST OF VARIABLES	XXV
GREEK LETTERS.....	XXVII
1. INTRODUCTION.....	1
1.1. CONTEXT.....	1
1.2. CO ₂ CAPTURE/SEPARATION TECHNOLOGIES.....	4
1.3. MEMBRANE MATERIALS	9
1.4. MEMBRANE TECHNOLOGY WITH IONIC LIQUIDS.....	16
2. GOAL AND MOTIVATION	31
3. MATERIALS AND METHODS	33
3.1. MATERIALS.....	33
3.2. MEMBRANE PREPARATION.....	36
3.3. MATERIALS CHARACTERIZATION	36
4. RESULTS AND DISCUSSION	43
4.1. FOURIER-TRANSFORM INFRARED (FTIR) SPECTROSCOPY	44
4.2. THERMOGRAVIMETRIC ANALYSIS	47
4.3. CO ₂ SOLUBILITY MEASUREMENTS	51
4.4. SCANNING ELECTRON MICROSCOPY.....	52

4.5.	DIFFERENTIAL SCANNING CALORIMETRY	54
4.6.	CONTACT ANGLE.....	55
4.7.	MECHANICAL PROPERTIES	57
4.8.	PURE GAS PERMEATION EXPERIMENTS	58
5.	CONCLUSION	63
6.	FUTURE WORK.....	65
	REFERENCES.....	67
A.	APPENDIX: RESULTS REPORTED IN THE LITERATURE.....	85
B.	APPENDIX: FOURIER-TRANSFORM INFRARED (FTIR) SPECTROSCOPY.....	93
C.	APPENDIX: THERMOGRAVIMETRIC ANALYSIS	95
D.	APPENDIX: SCANNING ELECTRON MICROSCOPY	97
E.	APPENDIX: MECHANICAL PROPERTIES.....	99
F.	APPENDIX: PURE GAS PERMEATION EXPERIMENTS.....	101

FIGURE INDEX

FIGURE 1.1 - THE CARBON CAPTURE AND STORAGE PROCESS. IMAGE PROVIDED BY THE GLOBAL CCS INSTITUTE. ¹⁰	2
FIGURE 1.2 - SCHEMATIC REPRESENTATION OF CO ₂ CAPTURE SYSTEMS. IMAGES PROVIDED BY THE GLOBAL CCS INSTITUTE. ¹⁰	3
FIGURE 1.3 - SCHEMATIC REPRESENTATION OF CO ₂ SOLVENT ABSORPTION. COURTESY OF CO2CRC LTD. ¹⁹	4
FIGURE 1.4 - SCHEMATIC REPRESENTATION OF CO ₂ ADSORPTION. COURTESY OF CO2CRC LTD. ¹⁹	5
FIGURE 1.5 - SCHEMATIC REPRESENTATION OF CO ₂ CRYOGENIC DISTILLATION. COURTESY OF CO2CRC LTD. ¹⁹	6
FIGURE 1.6 - SCHEMATIC REPRESENTATION OF CO ₂ SEPARATION MEMBRANE. COURTESY OF CO2CRC LTD. ¹⁹	7
FIGURE 1.7 - SCHEMATIC REPRESENTATION OF GAS TRANSPORT MECHANISM THROUGH A DENSE MEMBRANE. ADAPTED FROM ¹⁴⁶	9
FIGURE 1.8 - UPPER BOUND CORRELATION FOR THE SEPARATION OF THE GAS PAIRS CO ₂ /N ₂ AND CO ₂ /CH ₄ . ADAPTED FROM ⁴¹	11
FIGURE 1.9 - STRUCTURE OF NON-MODIFIED MONTMORILLONITE. ²⁰⁵	13
FIGURE 1.10 - MAIN MORPHOLOGIES OF CLAY/POLYMER NANOCOMPOSITES (PHASE SEPARATED, INTERCALATED, AND EXFOLIATED). ADAPTED FROM ⁶⁵	15
FIGURE 1.11 - STRUCTURES OF THE MOST USED IL CATIONS AND ANIONS FOR CO ₂ SEPARATION. ADAPTED FROM ⁸⁶ ..	17
FIGURE 1.12 - SCHEMATIC REPRESENTATION OF A SUPPORTED IONIC LIQUID MEMBRANE (SILM).	18
FIGURE 1.13 - SCHEMATIC REPRESENTATION OF A NEAT PIL MEMBRANE. ADAPTED FROM ¹⁴⁶	21
FIGURE 1.14 - SCHEMATIC REPRESENTATION OF A PIL/IL MEMBRANE. ADAPTED FROM ¹⁴⁶	24
FIGURE 1.15 - SCHEMATIC REPRESENTATION OF A PIL/IL-BASED MMM. ADAPTED FROM ¹⁴⁶	27
FIGURE 3.1 - CHEMICAL STRUCTURE OF THE IDEAL ARRANGEMENT OF PEGDA MOLECULES UPON CROSS-LINKING. ADAPTED FROM ²⁰⁶	34
FIGURE 3.2 - SCHEMATIC REPRESENTATION OF A GAS ABSORPTION SETUP (PI – PRESSURE INDICATOR; TC – TEMPERATURE CONTROLLER; GC – GAS COMPARTMENT; AC – ABSORPTION COMPARTMENT). ADAPTED FROM ¹⁶⁶	38
FIGURE 3.3 - SCHEMATIC REPRESENTATION OF THE THREE INTERFACIAL TENSIONS (γ_{sv} , γ_{sl} , γ_{lv}) AND THE CONTACT ANGLE (θ^y) AS DESCRIBED BY YOUNG’S EQUATION. ADAPTED FROM ¹⁷⁰	39

FIGURE 3.4 - SCHEMATIC REPRESENTATION OF A PURE GAS PERMEATION SETUP (TC – TEMPERATURE CONTROLLER; PI – PRESSURE INDICATOR; V1, V4 – EXHAUST VALVES; V2, V3 – INLET VALVES). ADAPTED FROM ¹⁶⁶	41
FIGURE 4.1 - PICTURES OF THE PREPARED MEMBRANES: NEAT IONGEL (LEFT) AND IONGEL MMM WITH 1.0 WT% MMT LOADING (RIGHT).....	43
FIGURE 4.2 - FTIR SPECTRUM OF MMT.....	44
FIGURE 4.3 - FTIR SPECTRA OF [C ₂ MIM][TF ₂ N] IL, PEGDA AND THE RESPECTIVE NEAT IONGEL MEMBRANE WITH 60 WT% OF [C ₂ MIM][TF ₂ N]. THE DASHED VERTICAL LINES INDICATE THE CHARACTERISTIC PEAKS OF TERMINAL ACRYLATE GROUPS OF PEGDA.....	45
FIGURE 4.4 - FTIR SPECTRA OF MMT, THE NEAT IONGEL AND THE IONGEL MMMS WITH 0.2, 0.5 AND 1.0 WT% MMT LOADING. THE DASHED VERTICAL LINES INDICATE THE CHARACTERISTIC PEAKS OF MMT.	46
FIGURE 4.5 - TGA AND DTGA PROFILES OF MMT.	47
FIGURE 4.6 - TGA PROFILES OF [C ₂ MIM][TF ₂ N], PEGDA AND THE NEAT IONGEL.....	49
FIGURE 4.7 – TGA PROFILES OF MMT, THE NEAT IONGEL AND THE IONGEL MMMS WITH 0.2, 0.5 AND 1.0 WT% MMT LOADING.	50
FIGURE 4.8 - PRESSURE DECAY METHOD APPLIED TO DETERMINE THE CO ₂ SOLUBILITY IN MMT.	51
FIGURE 4.9 - SEM IMAGE OF THE IONGEL MMM WITH 1.0 WT% LOADING OF MMT WITH AN AMPLIATION OF 1000X. THE RED CIRCLES IDENTIFY HOLES ON THE SURFACE.....	54
FIGURE 4.10 - CONTACT ANGLES OBTAINED FOR THE IONGELS WITH 0.0, 0.2, 0.5 AND 1.0 WT% MMT LOADING.....	56
FIGURE 4.11 - CO ₂ , N ₂ AND CH ₄ PERMEABILITIES OF THE IONGELS WITH 0.0, 0.2 AND 0.5 WT% MMT LOADING.....	59
FIGURE 4.12 – CO ₂ SEPARATION PERFORMANCE OF THE PREPARED IONGEL MEMBRANES AND OF OTHER MEMBRANES REPORTED IN THE LITERATURE ^{65,69–71,90,92,93,96,97,100–102,104–106,116,121,124,126–131,134,136,140,144,147–152,156–158,202} (SEE APPENDIX A) PLOTTED ON A CO ₂ /N ₂ ROBESON PLOT. DATA ARE PLOTTED ON A LOG-LOG SCALE AND THE UPPER BOUND IS ADAPTED FROM ROBESON. ⁴¹	61
FIGURE 4.13 – CO ₂ SEPARATION PERFORMANCE OF THE PREPARED IONGEL MEMBRANES AND OF OTHER MEMBRANES REPORTED IN THE LITERATURE ^{29,48,65,69–72,92,93,97,99,104,105,116,121,124,126,128,134,147–149,154,156–158,201} (SEE APPENDIX A) PLOTTED ON A CO ₂ /CH ₄ ROBESON PLOT. DATA ARE PLOTTED ON A LOG-LOG SCALE AND THE UPPER BOUND IS ADAPTED FROM ROBESON. ⁴¹	62
FIGURE C.1 – DTGA PROFILES OF [C ₂ MIM][TF ₂ N], PEGDA AND THE NEAT IONGEL	96
FIGURE C.2 – DTGA PROFILES OF MMT, THE NEAT IONGEL AND THE IONGEL MMMS WITH 0.2, 0.5 AND 1.0 WT% MMT LOADING.....	96
FIGURE E.1 – GRAPHIC REPRESENTATION OF THE PUNCTURE TEST FOR THE IONGEL WITH 0.2 WT% MMT LOADING (TWO REPLICATES).	99
FIGURE F.1 – N ₂ PRESSURE VARIATION IN THE FEED AND PERMEATE COMPARTMENTS AS A FUNCTION OF TIME FOR THE IONGEL WITH 0.5 WT% MMT LOADING.	101
FIGURE F.2 – LINEAR FITTING OF THE IONGEL WITH 0.5 WT% MMT LOADING FOR N ₂ PERMEABILITY CALCULATIONS. .	102

TABLE INDEX

TABLE 1.1 - TYPICAL COMPOSITIONS AND CONDITIONS OF FLUE GAS AND RAW BIOGAS STREAMS.	8
TABLE 1.2 - MOST USED ORGANIC MODIFIERS OF LAYERED SILICATES. ADAPTED FROM ⁶⁴	14
TABLE 3.1 - PROPERTIES OF THE [C ₂ MIM][TF ₂ N] IL USED IN THE PREPARATION OF THE IONGELS. ^{134,161}	34
TABLE 3.2 - PROPERTIES OF THE PEGDA MONOMER USED IN THE PREPARATION OF THE IONGELS. ^{134,207}	35
TABLE 3.3 - PROPERTIES OF THE NANOCLAY MMT USED IN THE PREPARATION OF THE IONGELS. ^{68,163}	35
TABLE 4.1 – ONSET AND DECOMPOSITION TEMPERATURES, TOTAL WEIGHT LOSS, AND RESPECTIVE TEMPERATURE RANGE OF THE IONGEL MEMBRANES WITH 0.0, 0.2, 0.5, AND 1.0 WT% MMT LOADING.....	50
TABLE 4.2 - SEM IMAGES OF THE SURFACE OF THE IONGELS WITH 0.0, 0.2, 0.5, AND 1.0 WT% LOADING OF MMT WITH AN AMPLIATION OF 1000X. THE RED CIRCLES IDENTIFY AGGLOMERATIONS.	53
TABLE 4.3 - GLASS TRANSITION TEMPERATURES (T_g) OF THE IONGEL MEMBRANES WITH 0.0, 0.2, 0.5, AND 1.0 WT% OF MMT LOADING.	54
TABLE 4.4 - PUNCTURE TEST RESULTS (THICKNESS, PUNCTURE STRESS, NORMALIZED PUNCTURE STRESS, AND ELONGATION UPON PUNCTURE) OF THE IONGELS WITH 0.0, 0.2, 0.5, AND 1.0 WT% MMT LOADING.	57
TABLE 4.5 - MEMBRANE THICKNESSES, CO ₂ , N ₂ , AND CH ₄ PERMEABILITIES, AND IDEAL SELECTIVITIES OF THE IONGELS WITH 0.0, 0.2, AND 0.5 WT% MMT LOADING.	59
TABLE 6.1 - COMMERCIALY AVAILABLE SURFACE MODIFIED MMT NANOCCLAYS SUGGESTED AS FILLERS.....	66
TABLE A.1 - CO ₂ /N ₂ AND CO ₂ /CH ₄ SEPARATION PERFORMANCE OF MMMS WITH NANOCCLAY FILLERS REPORTED IN THE LITERATURE.....	85
TABLE A.2 - CO ₂ /N ₂ , CO ₂ /CH ₄ , AND CO ₂ /H ₂ SEPARATION PERFORMANCE OF SILMS WITH DIFFERENT CATIONS REPORTED IN THE LITERATURE... ..	86
TABLE A.3 - CO ₂ /N ₂ AND CO ₂ /CH ₄ SEPARATION PERFORMANCE OF SILMS WITH DIFFERENT ANIONS REPORTED IN THE LITERATURE... ..	87
TABLE A.4 - CO ₂ /N ₂ AND CO ₂ /CH ₄ SEPARATION PERFORMANCE OF PIL MEMBRANES REPORTED IN THE LITERATURE... ..	88
TABLE A.5 - CO ₂ /N ₂ AND CO ₂ /H ₂ SEPARATION PERFORMANCE OF POLYMER/IL COMPOSITE MEMBRANES REPORTED IN THE LITERATURE.....	88

TABLE A.6 - CO ₂ /N ₂ , CO ₂ /CH ₄ , AND CO ₂ /H ₂ SEPARATION PERFORMANCE OF PIL/IL MEMBRANES REPORTED IN THE LITERATURE.....	89
TABLE A.7 - CO ₂ /CH ₄ AND CO ₂ /H ₂ SEPARATION PERFORMANCE OF PIL/IL-BASED MMMS REPORTED IN THE LITERATURE.....	91
TABLE A.8 - CO ₂ /N ₂ SEPARATION PERFORMANCE OF PEG-BASED CROSS-LINKED IONGEL MEMBRANES REPORTED IN THE LITERATURE.....	92
TABLE B.1 - ASSIGNMENTS OF FTIR PEAKS OF MMT.....	93
TABLE B.2 - ASSIGNMENTS OF FTIR PEAKS OF PEGDA.....	93
TABLE B.3 - ASSIGNMENTS OF FTIR PEAKS OF [C ₂ MIM][TF ₂ N].....	94
TABLE D.1 - SEM IMAGES OF THE CROSS-SECTION OF THE IONGELS WITH 0.0, 0.2, 0.5, AND 1.0 WT% LOADING OF MMT WITH AN AMPLIATION OF 500X.....	98

LIST OF ABBREVIATIONS

Abbreviation	Meaning
AA	Amino Acid
AAIL	Amino Acid-based Ionic Liquid
ATR	Attenuated Total Reflectance
CA	Cellulose Acetate
CCS	Carbon Capture and Storage
CH ₄	Methane
CO ₂	Carbon dioxide
DSC	Differential Scanning Calorimetry
FTIR	Fourier- Transform Infrared Spectroscopy
GHG	Greenhouse Gases
IL	Ionic Liquid
IR	Infrared
MEA	Monoethanolamine
MIL	Magnetic Ionic Liquid
MMM	Mixed Matrix Membrane
MMT	Montmorillonite
MOF	Metal Organic Framework
M _w	Molecular weight

N ₂	Nitrogen
N ₂ O	Nitrous oxide
PA	Polyamide
PBI	Polybenzimidazole
PDMS	Polydimethylsiloxane
PEG	Poly(ethylene glycol)
PEGDA	Poly(ethylene glycol) diacrylate
PES	Polyethersulfone
PI	Polyimide
PIM	Polymer of Intrinsic Microporosity
PSA	Pressure Swing Adsorption
PSf	Polysulfone
PTFE	Polytetrafluoroethylene
PVDF	Poly(vinylidene difluoride)
PVDF-HFP	Poly(vinylidene fluoride-co-hexafluoropropylene)
PVP	Poly(vinylpyrrolidone)
SEM	Scanning Electron Microscopy
T_{dec}	Decomposition temperature (°C)
T_g	Glass transition temperature (°C)
TGA	Thermogravimetric Analysis
T_{onset}	Onset temperature (°C)
TSA	Temperature Swing Adsorption
UV	Ultraviolet
ZIF	Zeolitic Imidazolate Framework

Cations	Meaning
[C ₁₆ mim] ⁺	1-Hexadecyl-3-methylimidazolium
[C ₂ mim] ⁺	1-Ethyl-3-methylimidazolium
[C ₄ mim] ⁺	1-Butyl-3-methylimidazolium
[C ₄ mpyr] ⁺	1-Butyl-3-methylpyrrolidinium
[C ₆ mim] ⁺	1-Hexyl-3-methylimidazolium
[P ₄₄₄₄] ⁺	Tetrabutylphosphonium
[P _{6,6,6,14}] ⁺	Phosphonium

Polycations	Meaning
[Pyr ₁₁] ⁺	Poly(diallyldimethylammonium)
[smim] ⁺	Poly(1-styrenemethyl-3-methylimidazolium)

Anions	Meaning
[Ac] ⁻	Acetate
[B(CN) ₄] ⁻	Tetracyanoborate
[BETI] ⁻	Bis(pentafluoroethylsulfonyl)imide
[BF ₄] ⁻	Tetrafluoroborate
[C(CN) ₃] ⁻	Tricyanomethanide
[C ₁ SO ₄] ⁻	Methylsulphate
[CF ₃ SO ₃] ⁻	Trifluoromethanesulfonate
[ClO ₄] ⁻	Perchlorate
[FAP] ⁻	Tris(pentafluoroethyl)trifluorophosphate
[FeCl ₄] ⁻	Tetrachloroferrate

[HFB] ⁻	Hexafluorobenzene
[MnCl ₄] ²⁻	Manganese tetrachloride
[N(CN) ₂] ⁻	Dicyanamide
[NO ₃] ⁻	Nitrate
[PF ₆] ⁻	Hexafluorophosphate
[Pro] ⁻	Prolinate
[Tf ₂ N] ⁻	Bis(trifluoromethylsulfonyl)imide

LIST OF VARIABLES

Variable	Meaning	Units
A	Area	m ²
d	Distance of the probe from the point of contact to the point of puncture	m
F	Applied force	N
l	Membrane thickness	m
P	Permeability	Barrer
p _{feed}	Feed pressure	bar
p _{perm}	Permeate pressure	bar
r	Radius of the probe	m
t	Time	s
V _{feed}	Feed volume	m ³
V _{perm}	Permeate volume	m ³

GREEK LETTERS

Letter	Meaning	Units
α	Ideal selectivity	-
β	Geometric parameter of the permeation cell	m^{-1}
γ_{LV}	Liquid-vapor tension	N/m
γ_{SL}	Solid-liquid tension	N/m
γ_{SV}	Solid-vapor tension	N/m
ε	Elongation upon puncture	%
θ^Y	Young's contact angle	$^\circ$
σ	Puncture stress	Pa
σ_n	Normalized puncture stress	MPa/mm

INTRODUCTION

1.1. Context

Since the Industrial Revolution, fossil fuels have played an important role in our lives as energy resources. They have contributed to a faster technological, social, and economical development of the society. The global consumption of fossil fuels roughly doubled in the last 40 years, relying on oil, natural gas, and coal. In 2020, these resources represented 83% of the global primary energy consumed for electricity, transport, and heating.¹

However, burning fossil fuels lead to a major impact on air quality and public health due to greenhouse gas (GHG) emissions.² Gases such as carbon dioxide (CO₂), methane (CH₄), and nitrous oxide (N₂O) accounted for 98% of these emissions in 2019.³ These gases trap the infrared radiation from the sun and create a greenhouse effect, resulting in global warming and climate changes. In particular, CO₂ is the most abundant and remains in the atmosphere for a longer period of time.⁴ The natural absorbing processes that balance the concentration of CO₂ in the atmosphere, like photosynthesis, are no longer sufficient to maintain a stable climate.⁵ Consequently, the period from 2016-2020 was the warmest on record, with 1.1°C above the pre-industrial era,⁶ which triggered several problems like changes in the precipitation patterns, severe storms, and sea-level rise.⁵

Many efforts have been made to limit and stabilize GHG emissions. In 2015, the Paris Agreement gathered world leaders to discuss policies favorable to a more sustainable development. It was settled the goal of limiting temperature rise to 2 °C, or preferably to 1.5 °C.⁷ To make this possible, global CO₂ emissions would need to fall 45% from 2010 levels by 2030, in order to reach “net zero” around 2050.⁸ However, global emissions of CO₂ from fossil fuels have reached a new record in 2019, being 62% higher than 1990 emissions.⁶ This means that inevitably some of the CO₂ still have to be removed from the air.⁸

A possible solution for reducing greenhouse gas emissions consists on the implementation of clean energy sources and the development of Carbon Capture and Storage (CCS) technology. CCS can be used in stationary sources of CO₂, like power plants and industries, which account for half of the total emissions.⁹

CCS consists of three steps (**Figure 1.1**).¹⁰ First, CO₂ is captured from the generating source and separated, a process that accounts for 75% of the total cost of this technology and increases electricity production cost by 50%. Even though these numbers vary according to the process, it is mandatory to find ways to reduce the cost of capture.¹¹ Then, the gas is compressed into a liquid, in order to be easily transported via pipeline to a storage area, where it is typically stored at 150 bar.⁹ The need for storage is based on the fact that the industrial global demand for CO₂ as feedstock is much smaller than the global production (250 Mt market vs. 52 Gt emitted per year).¹² Thus, CO₂ is injected into underground geological formations, such as oil and gas reservoirs, deep saline formations, and unminable coal beds. Deep ocean storage is also currently being investigated.^{13,14}

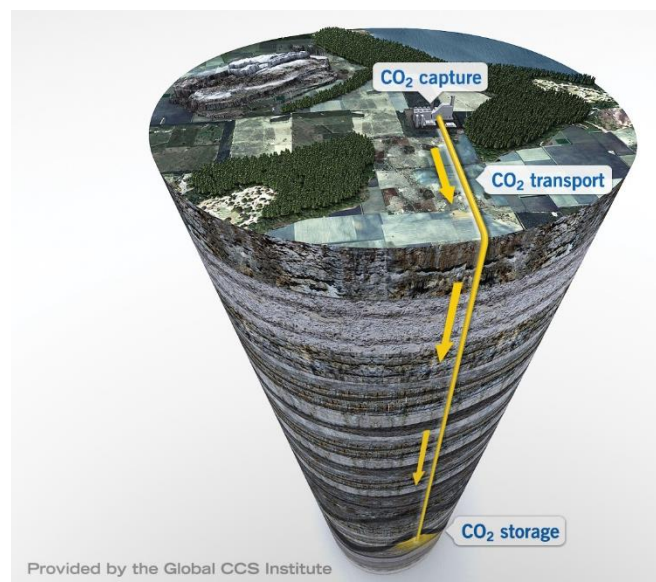


Figure 1.1 - The Carbon Capture and Storage process. Image provided by the Global CCS Institute.¹⁰

Since replacing all the energy-generating systems for clean alternatives in the short term is almost impossible, efforts are being made in the development of CCS technology to reduce the amount of CO₂ in the atmosphere and help to mitigate global warming and climate changes. However, this technology still presents many challenges that prevent it from being implemented on large scale, mainly due to its high energy costs. A power plant equipped with a CCS system and access to a storage site would need roughly 10-40% more energy for capture and compression than an equivalent plant without CCS.¹⁴

There are three approaches to capture CO₂ from fossil fuels (schematically represented in **Figure 1.2**):¹⁰ post-combustion, pre-combustion, and oxyfuel combustion. The choice of the capture technology depends on process conditions such as the concentration of CO₂, pressure of the gas stream, and fuel type (gas or solid).¹⁴

In a post-combustion system, the fuel is combusted with air, generating a stream of flue gas composed mainly of nitrogen (N₂) and CO₂ (stream conditions available in **Table 1.1**). Usually, this system uses a liquid solvent, like monoethanolamine (MEA) to absorb CO₂ with a concentration of 3-15% by volume.¹⁴ In the pre-combustion system, the fuel reacts with steam and air or oxygen (O₂). This produces hydrogen (H₂) and carbon monoxide (CO) that reacts with steam in a second reactor, generating more H₂ and 35-40% by volume of CO₂, usually at 20 bar. The separation of these gases allows for H₂ to be used as an energy source in the power plant.^{15,16} Post-combustion and pre-combustion systems for power plants can capture 85-95% of the produced CO₂. It is possible to obtain higher efficiency, although it increases the process expenses significantly, as well as the equipment dimension.¹⁵ Oxyfuel combustion is a less developed approach that contemplates the complete combustion of fuel by reacting it with high purity oxygen (95-99% by volume). This process produces a flue stream highly concentrated in CO₂ (80% by volume). Before storage, the stream is dehydrated and purified. The main disadvantage comes from the high costs associated with oxygen purification (separation from air, mainly N₂) by cryogenic distillation.^{14,16}

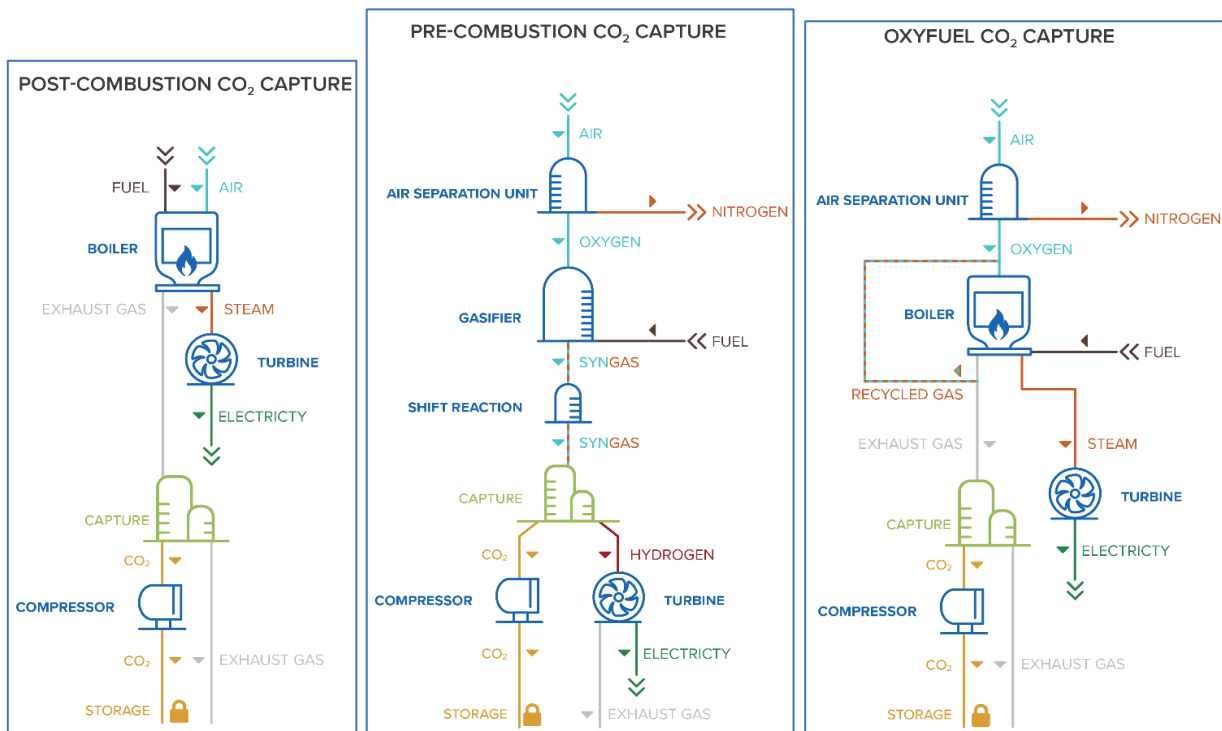


Figure 1.2 - Schematic representation of CO₂ capture systems. Images provided by the Global CCS Institute.¹⁰

In order to separate the CO₂ produced in the previously mentioned systems, four methods can be applied: Absorption, adsorption, cryogenic distillation, and membranes. Other hybrid processes will not be mentioned in this thesis.^{16,17}

1.2. CO₂ capture/separation technologies

Absorption

Absorption occurs when the molecules in the bulk phase, that present affinity towards a specific solvent, are chemically or physically absorbed. Absorption is commonly used for the treatment of gas streams with acid gases, like CO₂.^{16,18} This process is schematically represented in **Figure 1.3**.¹⁹

In chemical absorption, CO₂ reacts with chemical solvents forming a weakly bonded intermediate compound, which can be separated by applying heat. This process is being used in the chemical industry for 70 years. The most used solvent is an aqueous solution of alkanolamines, such as MEA.¹¹ Despite its maturity, this technology has some drawbacks. The capacity of the absorbent is limited, and this process requires high energy consumption. In order to capture 90% of CO₂ from flue gas, an amine absorption system can increase the cost of electricity by 50-90%, which is above the value established by the US Department of Energy of less than 35% increase for 90% capture.²⁰ Significant losses of solvent may take place by evaporation or oxidization if the stream is highly concentrated in O₂ and also, the equipment can suffer corrosion when in contact with the solvent.¹⁶

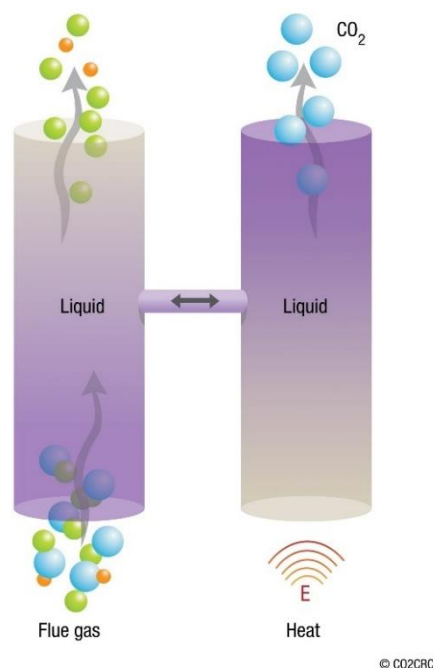


Figure 1.3 - Schematic representation of CO₂ solvent absorption. Courtesy of CO2CRC Ltd.¹⁹

Physical absorption is dependent on the solubility of CO₂ in the solvent, which is related to the partial pressure and temperature of the gas. In this case, the regeneration of the solvent is achieved by heating or decreasing the pressure. The application of this process is frequently done with Selexol™, a liquid glycol-based solvent, in a pressurization/depressurization cycle. The advantage of physical solvents is that they usually have a higher absorption rate than chemical solvents, but they also tend to be less selective.^{11,15}

Adsorption

Adsorption is another method used for CO₂ separation and it consists on the adhesion of molecules present within a liquid or a gas to a solid surface, which is called adsorbent (Figure 1.4).¹⁹ The most common processes to separate CO₂ from gas mixtures are pressure swing adsorption (PSA) and temperature swing adsorption (TSA), which differ in the way the adsorbent is regenerated. The gas stream flows through a packed bed of adsorbent at high pressure or low temperature until the concentration of the gas reaches an equilibrium. The bed is regenerated by reducing the pressure or increasing the temperature, respectively. PSA is considered technically and economically more viable than TSA given that its regeneration time is significantly lower. For PSA, the regeneration of the adsorbent may be performed in a few seconds, while for TSA it may take hours.^{16,18}

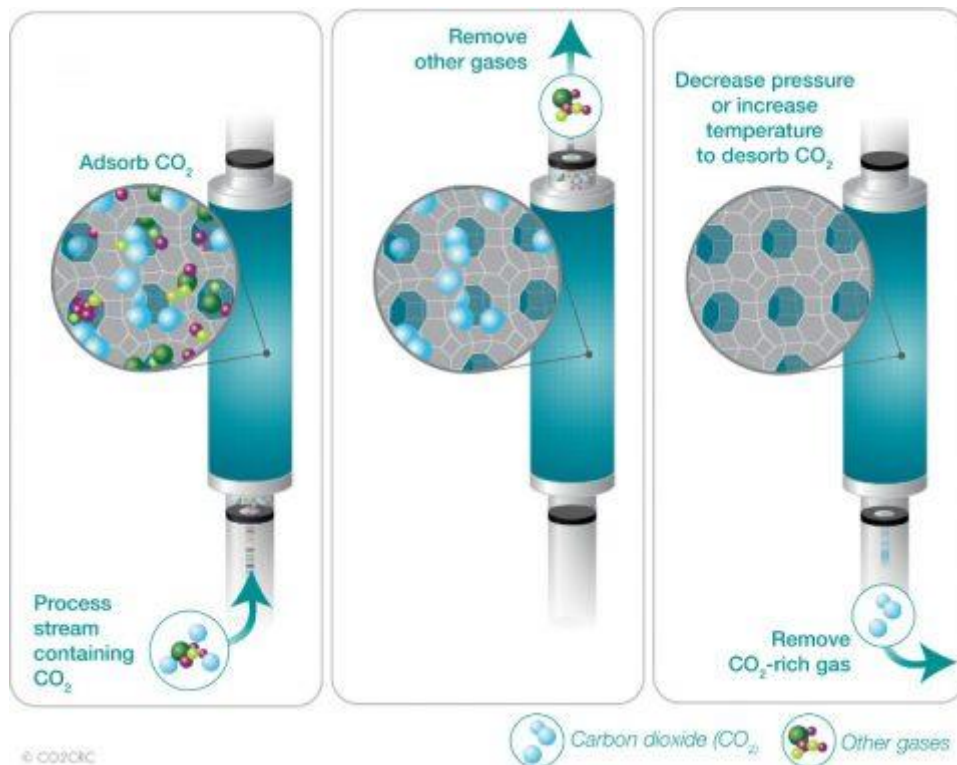


Figure 1.4 - Schematic representation of CO₂ adsorption. Courtesy of CO2CRC Ltd.¹⁹

The adsorbent must have high CO₂ capacity and selectivity, which will influence the purity of the produced CO₂ stream. The adsorption/desorption kinetics should be fast, while the stability of the adsorbent must be maintained during several cycles. Adsorbents used in post-combustion capture should be thermally stable up to 120-150 °C in oxidative environments, and adsorbents for pre-combustion or oxyfuel combustion need to be stable up to 350-400 °C. Materials like activated carbon, zeolites, and metal-organic frameworks (MOFs) have been considered for this purpose. One of the challenges reported is the ability to achieve high CO₂ capacity and selectivity in the presence of water (H₂O), since these molecules compete with CO₂ for binding sites.^{12,21}

Despite being suited for industrial applications, adsorption is often a cyclic process, which represents a major drawback since a continuous process would be more practical. However, this process has several advantages compared to chemical or physical absorption, such as higher capacity and selectivity, ease of handling, and requires less regeneration energy.^{16,21}

Cryogenic Distillation

Cryogenic distillation allows the separation of CO₂ from highly concentrated streams (typically > 80% by volume), such as oxyfuel combustion. This process (represented in **Figure 1.5**)¹⁹ is performed by cooling and condensing the gas mixture.¹⁸ The main advantage is the ability to produce high purity CO₂, usually up to 98%, directly in a liquid state, which is ready for final use or sequestration, without the need for compression. The process also eliminates the need for water supply and treatment, operates at atmospheric pressure, and does not require chemicals that cause corrosion of the equipment. However, the amount of energy needed to provide refrigeration significantly raises

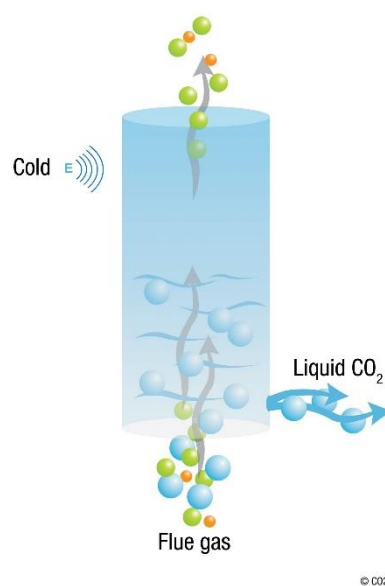


Figure 1.5 - Schematic representation of CO₂ cryogenic distillation. Courtesy of CO2CRC Ltd.¹⁹

the expenses, meaning that cryogenic distillation is only economically attractive when process integration is employed and the cold duty necessary can be obtained at a relatively low cost. Another obstacle to be considered is the formation of dry ice, which may cause blockages in the equipment. The same happens with water and some components that need to be previously removed from the stream.^{16,22,23}

Membranes

This technology consists on the passage of a feed stream of gas through a selective barrier, the membrane (**Figure 1.6**).¹⁹ Even though it is a less mature technology, the use of membranes has several advantages like compactness, high energy efficiency and the ability to retrofit to an upstream process. Moreover, it is environmentally friendly, flexible to scale up or down and works in a continuous mode.^{24,25} A study from the manufacturer Membrane Technology and Research (MTR) concluded that with process optimization and a two-stage membrane system with slight feed compression and partial permeate vacuum, membranes could be competitive with other technologies to separate CO₂ from gaseous streams.²⁰

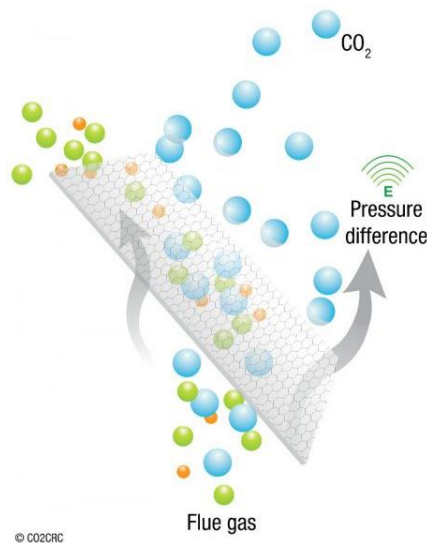


Figure 1.6 - Schematic representation of CO₂ separation membrane. Courtesy of CO2CRC Ltd.¹⁹

Membranes for gas separation can be applied in several processes like hydrogen recovery, air separation, separation and recovery of organics from gas streams, air and natural gas dehydration, and the main focus of this thesis, CO₂ separation.²⁴ The streams approached in this thesis, as well as their typical compositions and conditions, are available in **Table 1.1**.

The flue gas from post-combustion processes is the main source of CO₂, with concentrations of 3-15% by volume. These low concentrations, high temperature (up to 120°C),²⁶ and the pressure of the stream (around 1.5 bar) make it challenging to achieve a level of purity higher than 95% and recovery higher than 90% proposed by the US

Department of Energy.²⁷ These targets may lead to an increase in energy consumption and membrane area, which will raise the overall operation costs.

Table 1.1 - Typical compositions and conditions of flue gas and raw biogas streams.

Stream	Composition (by volume)	Water content (by volume)	Temperature (°C)	Pressure (bar)	Ref.
Flue gas (CO ₂ /N ₂)	3 - 15% CO ₂ 65 - 75% N ₂	5 - 10%	35 - 120	1.5	26,27
Biogas (CO ₂ /CH ₄)	35 - 45% CO ₂ 55 - 65% CH ₄	1 - 7%	25 - 35	1	26-28

Biogas is a mixture of gases, mainly CO₂ and CH₄, produced from the anaerobic digestion of biological waste from several sources such as municipal sewage treatment, human or animal waste, and farm agricultural waste.^{27,29} The composition of raw biogas streams depends on the process conditions and the type of biodegradable material.³⁰ The use of biogas as an energy source not only reduces the volume of accumulated waste, but also creates a renewable alternative to fossil fuels that can be used as vehicle fuel or to produce heat and electricity replacing natural gas.^{29,30} As an energy source, biogas needs to be composed of at least 95% by volume of CH₄. Therefore, CO₂ in a concentration of 35-45% by volume, at low pressure and temperature (1 bar and 25-35°C), should be removed to increase the calorific value of biogas and meet imposed regulations.^{27,29} Biogas upgrading or landfill gas recovery consists on the separation of CO₂ from CH₄ and according to Baena-Moreno *et al.*, membranes are the current technology that presents the lower overall costs and an acceptable efficiency for this process.²⁸

To meet the required specifications in terms of CO₂ purity and separation efficiency mentioned above, it is mandatory to overcome two major challenges of membrane technology. On one hand, the membrane separation performance should be optimized. That is, CO₂/N₂ and CO₂/CH₄ selectivities higher than 40 and 30, respectively, are pointed out as requirements to an energy-efficient process.³¹ On the other hand, membrane stability (chemical, thermal and mechanical) should be addressed to assure long-term operation.³¹ Therefore, different types of membranes have been designed and investigated, such as polymeric, inorganic, Mixed Matrix Membranes (MMMs), and Ionic Liquid (IL) based membranes.

1.3. Membrane Materials

Polymeric Membranes

Polymers are the most commercialized materials to fabricate gas separation membranes.³² The ability to form films, good processability, and mechanical properties are some of the reasons for the popularity of these materials.²⁰ The polymeric membranes used are dense or asymmetric (composed of a thin dense layer and a porous layer just for support),³³ and generally transport CO₂ by a solution-diffusion mechanism.^{32,34} In this case, the CO₂ transport depends on gas solubility and diffusivity. A pressure gradient across the membrane acts as a driving force, leading CO₂ to absorb onto the upstream side of the membrane, then diffuse through the membrane, and finally to desorb at the downstream side (**Figure 1.7**).³² On the other hand, some polymeric membranes use a facilitated transport mechanism, in which specific reactive carriers incorporated in the membrane, like amines and alkaline carbonate solutions, react reversibly with CO₂ and facilitate its transport through the polymer.²⁰

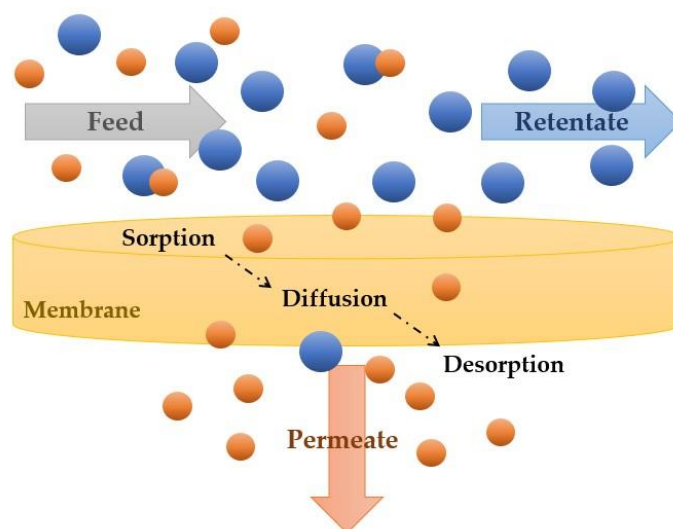


Figure 1.7 - Schematic representation of gas transport mechanism through a dense membrane. Adapted from ¹⁴⁶.

In the solution-diffusion mechanism, the solubility of a gas species depends on its condensability and the affinity between the gas molecules and membrane material. The diffusivity can be related to the membrane's free volume that exists between the polymer chains and the size of the gas molecules.²⁰ The permeability is a product of the solubility coefficient and the diffusivity coefficient, and measures the ability of the membrane to permeate gas molecules (**Equation 9** from **Section 3.3**).²⁶ The ability of the membrane to accomplish a gas separation is given by the real selectivity, or just selectivity, determined from permeation experiments using gas mixtures, that mimic real gas streams.³⁵ As a preliminary study, the ideal selectivity can be determined using pure gas permeation

experiments to measure how well the membrane can differentiate one gas from another. The ideal selectivity is given by the ratio of two pure gas permeabilities (**Equation 8** from **Section 3.3**).^{20,26} For polymeric membranes used in CO₂ separation experiments usually, the ideal selectivity tends to be higher than the real selectivity, since the use of gas mixtures often leads to a plasticization effect due to dissolved CO₂ and competitive sorption between gases.³⁶

Most of the polymeric membranes used in gas separation processes are made of cellulose acetate (CA), polysulfone (PSf), polydimethylsiloxane (PDMS), polyethersulfone (PES) and polyimides (PIs). Rubbery polymers, like PDMS (used above their glass transition temperature (T_g)), which have highly mobile polymer chains and plenty of free volume, are associated with high permeabilities but also with low selectivities.²⁰ These characteristics hinder gas purity, making rubbery polymers less appropriate to separate CO₂ in industrial applications, such as treating flue gas from post-combustion processes, natural gas purification, or hydrogen production (the three major sources of CO₂).²⁰ Therefore, the most commonly used polymers are glassy ones (used below their T_g) that are more rigid and selective due to their densely packed polymer chains but also present lower permeabilities.^{20,24,25,37}

Nevertheless, polymeric membranes have some drawbacks that limit their commercialization, such as plasticization and ageing effects, which damage their structure and decrease their long-term performance. Plasticization occurs when highly condensable gases, like CO₂, are absorbed in the membrane and cause swelling, increasing polymer chain mobility and free volume. In this line, the gas permeability will increase, and the membrane will become less selective.^{20,25} In order to overcome membrane plasticization, several strategies have been proposed,²⁵ such as the incorporation of crosslinking agents,³⁸ thermal treatments,³⁹ and polymer blending.⁴⁰ Moreover, physical ageing occurs when the membrane loses some free volume, leading to a decrease in gas permeability.^{20,25}

Polymeric membranes also suffer from another limitation, an intrinsic trade-off, which means that membranes with high permeabilities consequently have poor selectivity and vice-versa. This relationship between permeability and selectivity is given by an empirical upper bound first described by Robeson in 1991 and updated in 2008 with newly available data.^{20,41} One of the main goals of researchers is to prepare membranes with gas separation performances that surpass the Robeson upper bound.³⁷ In 2019, a group of researchers prepared benzotriptycene-based membranes composed of Polymers of Intrinsic Microporosity (PIMs), achieving exceptionally high gas separation results, in particular for CO₂/N₂ and CO₂/CH₄ gas pairs.⁴² Some of the obtained data were placed considerably above the previously reported Robeson upper bounds and parallel to them, which allowed for their redefinition and settled a new goal for gas separation

membranes. The results obtained in the scope of this thesis were compared with the 2008 Robeson upper bounds, represented in **Figure 1.8**,⁴¹ since these are more frequently used.

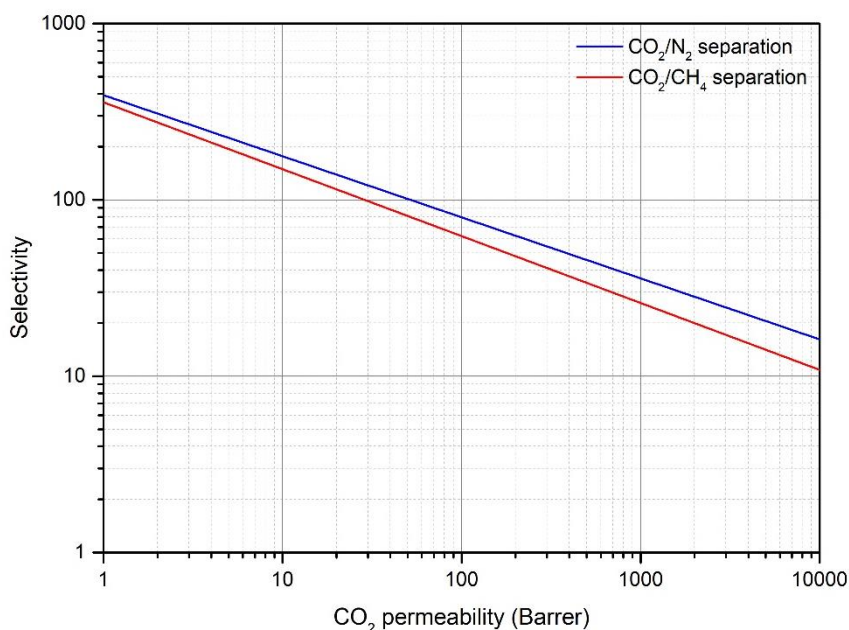


Figure 1.8 - Upper bound correlation for the separation of the gas pairs CO₂/N₂ and CO₂/CH₄. Adapted from ⁴¹.

Inorganic Membranes

As an alternative, inorganic membranes are also used for gas separation and are characterized by their chemical and thermal stability, as well as high gas selectivity. However, careful handling is required due to their brittleness and the operation costs are much higher than polymeric membranes as they are difficult to manufacture on a large scale without defects.^{24,25} These membranes can be made of several materials like metal,⁴³ carbon-based molecular sieves,⁴⁴ and ceramics which include silica and zeolites.^{45,46}

Mixed Matrix Membranes

In order to combine the best features of organic and inorganic materials and overcome the trade-off limitations, a new class of membranes was created named Mixed Matrix Membranes (MMMs).²⁰ These membranes consist of one or more types of inorganic particles dispersed within an organic continuous phase. The biggest challenge of these membranes comes from the defects that may take place in the polymer-particle interface due to poor adhesion. These defects can be reflected in a significant drop in selectivity and membrane gas separation performance. Therefore, the filler must be chosen carefully, considering its type, size, loading, and dispersion capacity.^{20,24,47,48}

The fillers that are mainly used to prepare MMMs can be porous like zeolites,^{48,49} carbon nanoparticles, which include molecular sieves⁵⁰ and carbon nanotubes,⁵¹ MOFs,^{52,53} and zeolitic imidazolate frameworks (ZIFs).⁵⁴ They can also be non-porous such as nanoclays,⁵⁵ graphene oxide,⁵⁶ and metal oxides which include silica (SiO₂),⁵⁷ titanium dioxide (TiO₂),⁵⁸ and magnesium oxide (MgO).⁵⁹ The incorporation of fillers into an organic matrix can create additional pathways between the polymer chains for the gas molecules to cross, increasing diffusivity and, if the filler has an affinity for CO₂, improving solubility as well.²⁰ The option of introducing ILs into MMMs has also been investigated as a way to improve the components' adhesion and/or enhance CO₂ separation performance. For instance, Shindo *et al.* investigated the effect of incorporating different [C₄mim][Tf₂N] IL loadings (up to 66 wt%) into composite membranes combining polyimide and zeolite particles on gas permeation.⁶⁰ The results showed that increasing IL content can decrease interfacial voids and enhance CO₂/N₂ and CO₂/CH₄ selectivity. Mohshim *et al.* incorporated [C₂mim][Tf₂N] IL into polyethersulfone-SAPO-34 MMMs.⁶¹ At 20 wt% loading, the CO₂/CH₄ selectivity was more than three times higher than for the pure MMM.

Clay minerals are a natural nonporous inorganic filler that can be incorporated into membranes. A literature review from Jamil *et al.* indicates enhanced thermal, mechanical, electrical, and barrier properties when a very low amount of clay (≤ 10 wt%) is incorporated into polymer composite membranes.⁶² These materials have attracted great interest due to their appealing properties since they are widely available at low cost and have interesting physicochemical characteristics such as developed specific surface area, ion exchange properties, thermal stability and are benign to the environment.^{63,64}

The most commonly used clay minerals for the preparation of nanocomposites are layered silicates, also called phyllosilicates, and can be divided into three main categories: Kaolinite, Smectite, and Illite or Mica. One of the most important clays is montmorillonite (MMT), included in the Smectite group, due to its ability to be dispersed into polymeric matrices, high specific area of 750-800 m²/g, and non-toxicity, besides being highly abundant and inexpensive.^{64,65} MMT has a 2:1 phyllosilicate structure, which means that is composed of 1 nm layers made of alumina octahedra sheets between two sheets of silica tetrahedra. These layers are bonded together by weak interactions like Van der Waals forces, which allows them to be separated.⁶³ The MMT layers have a negative charge, since some of the silicon ions (Si⁴⁺) are replaced by aluminum ions (Al³⁺), and some aluminum ions are replaced by magnesium (Mg²⁺) or iron ions (Fe²⁺/Fe³⁺).⁶³ Consequently, the interlayer space (average of 1 - 2 nm¹) is occupied with exchangeable

¹ For example, Qiao *et al.* reported an interlayer space of 0.88 nm for MMT with Na⁺ cations in the interlayers.⁷⁰

cations like sodium (Na^+) or potassium (K^+), that have an affinity for polar groups like water, which may also be in the interlayer space in substantial quantities causing MMT to expand.^{66,67} The interlayer thickness of hydrated MMT is 1.45 nm. When the structure is dehydrated the interlayer space reaches a height of 0.28 nm.⁶⁴ The structure of MMT is schematically represented in **Figure 1.9**².

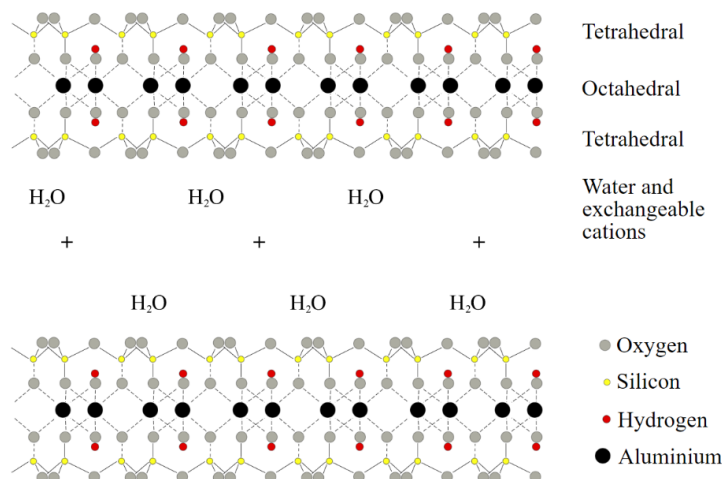


Figure 1.9 - Structure of non-modified montmorillonite.²⁰⁵

In order to successfully incorporate MMT particles within a polymeric matrix, a structure with increased organophilicity should be used. When the interlayer cations are exchanged by organic modifiers like those listed in **Table 1.2**,⁶⁴ MMT becomes more organophilic and the interlayer space increases favoring the compatibility and intercalation of polymer chains.^{67,68} Organophilic MMT is commercially available but can also be prepared by ion-exchange reactions.⁶⁵

Depending on the degree of interaction between the components, polymer/clay nanocomposites can present three different morphologies: phase-separated, intercalated, and exfoliated (**Figure 1.10**). When there are no interactions, the phases are separated. Intercalation occurs when polymer chains are inserted into the interlayer space of clays, causing them to expand and weakening the layer interactions. In the exfoliated morphology, the clay layers are dispersed randomly into the polymeric matrix due to the maximum penetration of polymer chains. The polymer/clay interaction is a consequence of several factors like organic modification of the clay, the amount of organic modifier, the organic modifier polarity, polymer type, and composite synthesis technique.⁶⁵

² This figure is licensed under the Creative Commons Attribution-Share Alike 2.5 Generic license.²⁰³

Table 1.2 - Most used organic modifiers of layered silicates. Adapted from ⁶⁴.

Organic Modifier	Chemical structure
Methyl tallow bis-2-hydroxyethyl quaternary ammonium	$\begin{array}{c} \text{CH}_2\text{CH}_2\text{OH} \\ \\ \text{CH}_3 - \text{N}^+ - \text{T} \\ \\ \text{CH}_2\text{CH}_2\text{OH} \end{array}$
Dimethyl dehydrogenated tallow quaternary ammonium	$\begin{array}{c} \text{CH}_3 \\ \\ \text{H}_3\text{C} - \text{N}^+ - \text{HT} \\ \\ \text{HT} \end{array}$
Dimethyl hydrogenated tallow 2-ethylhexyl quaternary ammonium	$\begin{array}{c} \text{CH}_3 \\ \\ \text{H}_3\text{C} - \text{N}^+ - \text{C}_8\text{H}_{17} \\ \\ \text{HT} \end{array}$
Dimethyl benzyl hydrogenated tallow quaternary ammonium	$\begin{array}{c} \text{CH}_3 \\ \\ \text{CH}_3 - \text{N}^+ - \text{CH}_2\text{-Ph} \\ \\ \text{HT} \end{array}$
Dimethyl dialkyl tallow ammonium	$\begin{array}{c} \text{T} \\ \\ \text{CH}_3 - \text{N}^+ - \text{T} \\ \\ \text{CH}_3 \end{array}$
Trioctyl methyl ammonium	$\begin{array}{c} \text{C}_8\text{H}_{17} \\ \\ \text{CH}_3 - \text{N}^+ - \text{C}_8\text{H}_{17} \\ \\ \text{C}_8\text{H}_{17} \end{array}$
Polyoxy propylene methyl diethyl ammonium	$\begin{array}{c} \text{C}_2\text{H}_5 \\ \\ \text{CH}_3 - \text{N}^+ - (\text{CH}_2\text{CHO})_{25}\text{H} \\ \quad \\ \text{C}_2\text{H}_5 \quad \text{CH}_3 \end{array}$
Octadecyl amine	$\text{CH}_3(\text{CH}_2)_{16}\text{CH}_2\text{NH}_2$
Dimethyl octadecyl amine	$\begin{array}{c} \text{H} \\ \\ \text{CH}_3(\text{CH}_2)_{16}\text{CH}_2 - \text{N}^+ - \text{CH}_3 \\ \\ \text{CH}_3 \end{array}$
Hexadecyl trimethyl ammonium	$\begin{array}{c} \text{CH}_3 \\ \\ \text{CH}_3(\text{CH}_2)_{14}\text{CH}_2 - \text{N}^+ - \text{CH}_3 \\ \\ \text{CH}_3 \end{array}$
Dodecyl triphenyl phosphonium	$\begin{array}{c} \text{Ph} \\ \\ \text{Ph} - \text{P}^+ - \text{CH}_2(\text{CH}_2)_{10}\text{CH}_3 \\ \\ \text{Ph} \end{array}$
Hexadecyl tributyl phosphonium	$\begin{array}{c} \text{C}_4\text{H}_9 \\ \\ \text{CH}_3(\text{CH}_2)_{14}\text{CH}_2 - \text{P}^+ - \text{C}_4\text{H}_9 \\ \\ \text{C}_4\text{H}_9 \end{array}$
Dodecyl trimethyl phosphonium	$\begin{array}{c} \text{CH}_3 \\ \\ \text{CH}_3(\text{CH}_2)_{10}\text{CH}_2 - \text{P}^+ - \text{CH}_3 \\ \\ \text{CH}_3 \end{array}$

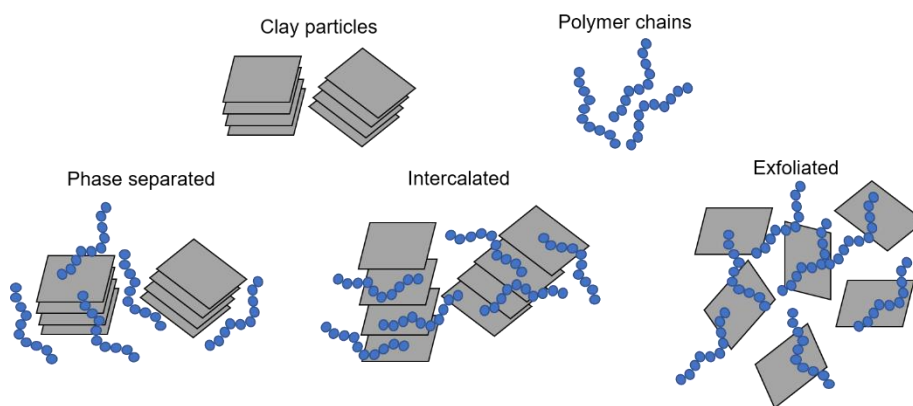


Figure 1.10 - Main morphologies of clay/polymer nanocomposites (phase separated, intercalated, and exfoliated). Adapted from ⁶⁵.

MMT started to be investigated as a reinforcing filler for nanocomposites in the automotive industry in the 1990s by Toyota Research Group.⁶² Several studies have been reported since then considering nanoclays as enhancers of gas separation performance using MMMs (**Table A.1** from **Appendix A**), and enhancers of mechanical properties. Zuhairun *et al.* examined the effect of incorporating Cloisite® 15A (organically modified clay) into a PSf matrix on the gas transport properties of asymmetric MMMs.⁶⁹ At 1 wt% loading, the CO₂ permeability was enhanced by 270% (from 5 to 19 Barrer) with a slight reduction in CO₂/CH₄ selectivity (from 23 to 21) compared to neat PSf. The authors justified this change with the disruption of polymer chain packing in the matrix caused by unexfoliated clay layers.

A different approach was reported by Qiao *et al.* that prepared MMMs for CO₂ separation by bonding and aligning MMT clay layers onto porous PSf support (45 nm of mean pore diameter) using polyvinylamineacid as a polymer linker (it was used a ratio of MMT to polyvinylamineacid of 13:1).⁷⁰ The interlayer space of the aligned clay particles (0.88 nm) served as highly permeable transport channels for CO₂ since the hydroxyl groups on the layered walls have a strong affinity towards this gas. The research group performed the gas separation experiments with gas mixtures at 50 °C, obtaining for the CO₂/CH₄ gas pair a selectivity of 138 and a CO₂ permeability of 85 Barrer. For the CO₂/N₂ gas pair, a selectivity of 123 and a CO₂ permeability of 82 Barrer were obtained. The results are above the respective 2008 Robeson upper bounds.

Behroozi *et al.* prepared defect-free MMMs using Pebax2533 and Cloisite® 15A.⁶⁵ At 2 bar and 10 wt% clay loading, the CO₂ permeability decreased by 28% compared to the neat polymer (from 240 to 187 Barrer), due to an increase in tortuosity and diffusion pathway caused by the well-dispersed clay particles into the polymer. Although, at 6 bar, the CO₂ permeability and CO₂/CH₄ selectivity increased, since the solubility of highly condensable gases, like CO₂, increases with increasing pressure. The best CO₂/CH₄ selectivity accomplished was 9 at 6 bar with 6 wt% clay loading.

A similar conclusion was reported by Jamil *et al.* that prepared MMMs with cellulose acetate (CA) and different bentonite (non-modified clay) loadings for CO₂/CH₄ and CO₂/N₂ separations.⁷¹ The tortuosity caused by well-dispersed clay particles decreased gas permeabilities up to 2 wt% clay loading. However, at 1 wt% (4 bar), CO₂/CH₄ selectivity increased by 79%, and CO₂/N₂ selectivity increased by 123% compared to neat CA. For that same composition, it was reported a 64% and 200% improvement in the elastic modulus and hardness of the MMM, respectively, compared to the neat membrane.

Kalantari *et al.* incorporated talc, a less common clay filler, into a PSf matrix.⁷² Using a concentration of 0.1 wt% talc with pressures in the range 3 - 7 bar or 0.3 wt% talc loading with 3 bar, the prepared MMMs were able to separate CO₂ completely, not allowing CH₄ molecules to pass through the membrane. However, for higher talc loadings up to 0.5 wt%, both gases permeations increased, while the CO₂/CH₄ selectivity decreased due to the formation of unselective voids in the polymer-filler interface.

The incorporation of inorganic particles into polymeric matrices can also be interesting bearing other purposes in mind, especially when considering the versatility of nanoclays. Coelho *et al.* introduced clay particles into biopolymeric membranes to enhance their barrier properties and mechanical stability for packing applications, limiting oxygen contact with food products.⁶⁷ Clays can also be used as fillers for polymer electrolytes in the field of lithium-based batteries. Their large specific area provides good contact with the polymers, combining high cation exchange capacity that enhances ionic conductivity and improving the solubility of lithium salts.⁷³ Bordes *et al.* reviewed the research done in the development of biopolyester with nanoclay systems for packing, agricultural, or biomedical applications and concluded that when the filler incorporation was successful, an improvement in thermal stability, mechanical reinforcement, biodegradability, and barrier properties was obtained.⁷⁴

The abovementioned results describe the successful improvements obtained in MMMs' performance for gas separation applications (**Table A.1** from **Appendix A**), pointing out that nanoclay particles are a good filler option for the development of membranes for flue gas treatment and biogas upgrading.

1.4. Membrane Technology with Ionic Liquids

Ionic Liquids

Ionic Liquids (ILs) are salts composed of an organic cation and an inorganic or organic anion that have melting points below 100°C, making them liquids at room temperature. This feature is caused by the asymmetry of the ions, which leads to weak

interactions and low packing efficiency, and by the delocalization of their charges.²⁶ One of the most interesting characteristics of ILs is that they can be designed to suit the envisioned application. This means that their properties can be manipulated by the selection and combination of different cations and anions or by the addition of specific functional groups.⁷⁵

Diverse applications of ILs have been studied during the last years. In electrochemistry, to take advantage of their high conductivity, ILs are utilized as electrolytes in energy-related applications such as batteries,⁷⁶ chemical sensors,⁷⁷ and fuel cells.⁷⁸ They can be used for biomedical applications, for example in drug delivery systems⁷⁹ and sensors.⁸⁰ They can also be a replacement for volatile organic solvents in organic reactions,⁸¹ catalysis,⁸² extractions,⁸³ and separation,⁸⁴ due to their negligible vapour pressure.⁸⁵ In particular, and since 2001, ILs have also been studied for CO₂ separation,⁸⁶ mainly due to the interactions established between the quadrupole moment of the CO₂ molecules and their electrical charges.²⁶

Usually, both the ions influence CO₂ separation, but the anion has been found to have a higher impact in this application than the cation.²⁶ Some examples of cations include ammonium, phosphonium, pyridinium, pyrrolidinium, and imidazolium with different alkyl chain sizes.⁸⁶ In imidazolium cations, increasing the alkyl chain length leads to a higher CO₂ permeability and solubility, probably because it decreases the interaction between the ions of the IL, which causes a higher free volume to accommodate CO₂ molecules, that become more available to interact with the ILs' anions.²⁶ The anions can be fluorinated, halogens, phosphates, sulfonates, carboxylates, acetates, and cyano-functionalized.²⁶ The structures of the most used IL cations and anions for CO₂ separation are presented in **Figure 1.11**.⁸⁶

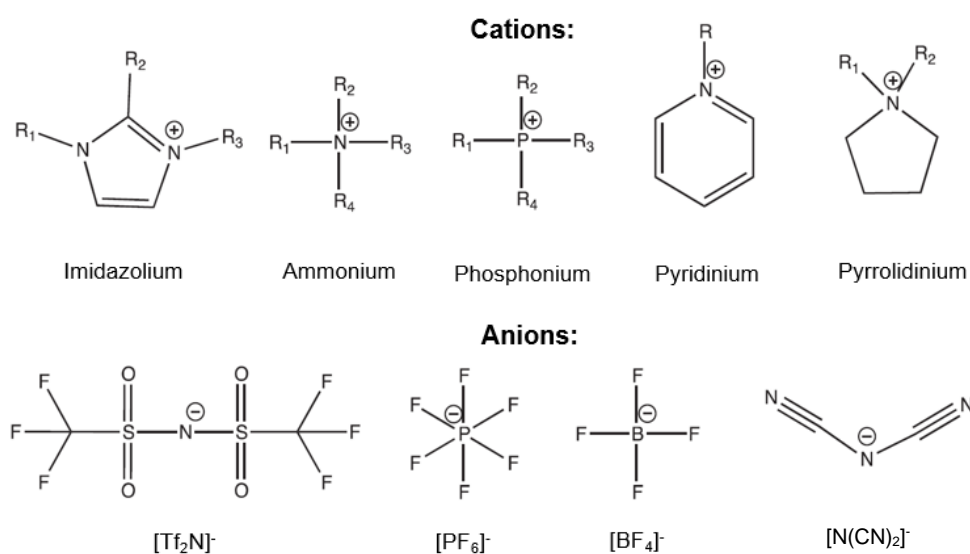


Figure 1.11 - Structures of the most used IL cations and anions for CO₂ separation. Adapted from ⁸⁶.

Supported Ionic Liquid Membranes

Supported liquid membranes consist of inert porous supports completely impregnated with a solvent, which gets immobilized within the pores by capillary forces.²⁶ When the solvent used is an IL, they are named Supported Ionic Liquid Membranes (SILMs) (Figure 1.12).⁸⁶ Compared to organic solvents, the low volatility and high viscosity of ILs are advantages, since the use of ILs help to reduce the solvent losses by evaporation and leakage from the support. Typically, SILMs can be prepared by three methods: immersion, pressure, or vacuum.²⁶ The use of SILMs approach instead of the neat IL for CO₂ separation reduces the necessary amount of IL.

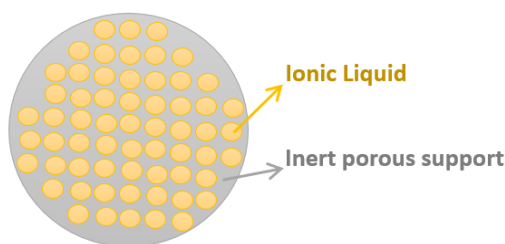


Figure 1.12 - Schematic representation of a supported ionic liquid membrane (SILM).

The supports can be polymeric or ceramic and should be selected considering the chemical compatibility with the IL and the porous support pore size.^{26,75,87} Polymeric supports include nylon,⁸⁸ polypropylene,⁸⁹ polyvinylidene fluoride (PVDF),^{35,90} polytetrafluoroethylene (PTFE),⁹¹⁻⁹³ PES,⁹⁰ and PSf.⁹⁴ Ceramic supports, for example, titanium oxide (TiO₂) and aluminum oxide (Al₂O₃),⁹⁵ are preferred due to their resistance to very high temperatures and mechanical stability.

Several SILM systems have been studied over the years combining different IL cations and anions to suit the aimed applications. In particular, the use of SILMs in gas permeation experiments is an excellent way to determine the effect of the chemical structure of an IL on CO₂ separation performance.²⁶ Considering the IL cation, most studies regarding CO₂ separation have been done using imidazolium cations, possibly due to their early commercial availability and a structure that is easily modified for CO₂ separation, providing better results.²⁶ The influence of the alkyl chain length of imidazolium cations on SILMs' CO₂ separation performance was explored by Neves *et al.*⁹⁶ The [PF₆]⁻ anion was combined with imidazolium cations of different chain lengths (C₄, C₆, and C₈) and the authors found that the gas permeabilities (CO₂, N₂, and H₂) of SILMs increase with the increase in the imidazolium chain length. On the other hand, several authors reported the use of different modifications of imidazolium cations on SILMs in order to improve their CO₂ separation properties. A combination of the [Tf₂N]⁻ anion with fluoroalkyl functionalized imidazolium cations studied by Bara *et al.* showed a decrease in both CO₂ permeability and CO₂/CH₄ and CO₂/N₂ selectivities with the increase in fluoroalkyl length, possibly due to higher IL viscosities.⁹⁷ Although, the CO₂/CH₄ separation was improved

when the fluoroalkyl groups were added to the imidazolium cations. Later, Hojniak *et al.* prepared SILMs with nitrile/glycol difunctionalized imidazolium and pyrrolidinium cations and obtained CO₂/CH₄ and CO₂/N₂ selectivities 2.3 times higher than those obtained for the studied cations with only the glycol group.⁹⁸ Shahkaramipour *et al.* synthesized SILMs with imidazolium-based geminal dicationic ILs with different alkyl spacers between the cations and reported the CO₂ permeability, as well as the CO₂/CH₄ selectivity, were higher when the [C₆mim][Tf₂N] IL was used as opposed to those obtained for C₃[mim]₂[Tf₂N]₂ and C₆[mim]₂[Tf₂N]₂, due to their higher viscosities.⁹⁹

Besides imidazolium-based IL, other cations have been explored for the preparation of SILMs. Mahurin *et al.* synthesized SILMs with different benzyl-functionalized cations combined with the [Tf₂N]⁻ anion for CO₂/N₂ separation.¹⁰⁰ The pyridinium and imidazolium-based ILs exhibited better CO₂ permeabilities than the pyrrolidinium-based IL. On the other hand, the addition of the benzyl group increased the ILs' viscosity which lowered the CO₂ permeability, however, enhanced the CO₂/N₂ selectivity compared to their non-functionalized analogs. Hillesheim *et al.* prepared SILMs with different thiazolium-based ILs combined with the [Tf₂N]⁻ anion, that presented lower CO₂ permeabilities than SILMs with imidazolium-based ILs due to higher viscosities.¹⁰¹ Later on, excellent results were reported by Mahurin *et al.* that used new IL cations that resemble an opened imidazolium structure.¹⁰² SILMs with [(N₁₁)₂CH][Tf₂N] and [(N₁₁)₂N][Tf₂N] ILs reached the 2008 Robeson upper bound with a CO₂ permeability of 1800 Barrer and a CO₂/N₂ selectivity of 29.

The previously mentioned results about the effect of the IL cation on the CO₂ separation performance of SILMs are listed in **Table A.2** from **Appendix A**. Results about CO₂ separation of SILMs with different IL anions are available in **Table A.3** from **Appendix A**.

Regarding the IL anion, different chemical structures have been used to investigate the effect on the CO₂ separation performance of SILMs (**Table A.3** from **Appendix A**). Mahurin *et al.* used ILs with cyano-functionalized anions and compared their performance with ILs having the most popular anion, [Tf₂N]⁻.¹⁰³ The high CO₂ solubility of cyano-functionalized anions was shown to increase SILMs performance on CO₂/N₂ separation, especially when the number of cyano groups of the anion increased. Good results were obtained by Tomé *et al.* with the study of the gas permeation properties of SILMs based on ILs with sulfate anions, achieving the 2008 Robeson upper bound when the [C₂mim][C₁SO₄] IL was used.¹⁰⁴ Santos *et al.* reported the influence of the temperature on SILMs performance with immobilized acetate-based ILs.¹⁰⁵ At 25°C, [C₂mim][Ac] and [C₄mim][Ac] achieved the 2008 Robeson upper bound for CO₂/N₂ separation. In order to obtain an environmentally friendly CO₂ separation process, Tomé *et al.* synthesized SILMs combining the cholinium cation and non-hazardous anions like levulinate [Lev]⁻, lactate [Lac]⁻, glycolate [Gly]⁻, and malonate [Mal]⁻.⁹² Despite the good results obtained for

CO₂/CH₄ and CO₂/N₂ separations, the performance of the membranes was limited by the ILs high viscosity.

In what concerns CO₂ facilitated transport through SILMs, but considering the anion effect, it is important to mention amino acid-based ionic liquids (AAILs). Despite their high viscosity as the main drawback, AAILs have amine groups as CO₂ carriers and are biocompatible and biodegradable. Several studies regarding this class of ILs were done by Kasahara *et al.*^{106,107} For instance, the effect of different amino acid (AA) based anions (glycine, alanine, proline, and serine) combined with the same phosphonium cation on CO₂/N₂ separation was investigated.¹⁰⁶ The performance of the membrane with the IL that had the proline anion, at 100°C and low CO₂ partial pressure (0.1 bar) with dry gases exceeded the 2008 Robeson upper bound.

Another interesting liquid phase for SILMs is the use of magnetic ionic liquids (MILs), which have metal-based anions that confer a magnetic character to their structure. Albo *et al.* prepared SILMs with MILs that combined phosphonium cations and magnetic anions for CO₂/N₂ separation.⁹⁰ The group obtained the best CO₂ separation performance with the membrane containing [P_{6,6,6,14}]₂[MnCl₄] with a CO₂ permeability of 203 Barrer and a CO₂/N₂ selectivity of 41. Furthermore, IL mixtures have also been immobilized into SILMs. Tomé *et al.* reported that a mixture of anions with different chemical features changed the IL's viscosity and molar volume, properties that could be manipulated to improve the CO₂ separation performance of SILMs.⁹³

Regardless of the wide variety of chemical structures of ILs that can be used to prepare SILMs, this type of membranes has a major drawback. When performing gas permeation experiments, if the transmembrane pressure applied is higher than the capillary forces of the support, the IL may be displaced from the pores causing a reduction in selectivity.⁸⁶ Therefore, the use of SILMs is restricted to low-pressure applications. Nevertheless, if the temperature of the application is high enough, the IL becomes less viscous and may leak from the pores.²⁶

Poly(ionic liquid) Membranes

Poly(ionic liquid)s or polymeric ionic liquids (PILs) are a subclass of polyelectrolytes with the monomer repeating units bearing IL species, connected through a polymeric backbone to form a macromolecular architecture (**Figure 1.13**).¹⁰⁸ PILs bring together the good processability and durability of polymers with the unique characteristics of ILs,¹⁰⁹ although their physical properties are not always directly related to those of the components.¹⁰⁸ Most PILs are non-crystalline solid materials with good chemical and thermal stability. However, PILs are less thermally stable than IL monomers since this property is limited by the chemical structure of the polymeric backbone.¹⁰⁸ Therefore,

depolymerization, scission, and thermal degradation of the structure may take place at high temperatures.¹⁰⁸

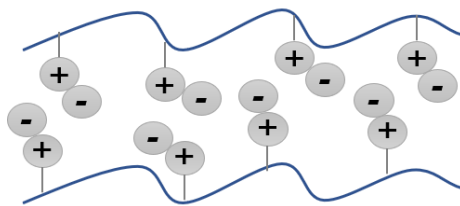


Figure 1.13 - Schematic representation of a neat PIL membrane. Adapted from ¹⁴⁶.

PILs can be divided into polycations, that feature a cation in the backbone part of each monomer, polyanions, that feature an anion and polyzwitterions, that bear a cation and an anion.¹⁰⁹ The variation of their chemical composition, structure type (for example linear, star-shaped, or hyper-branched), and the ability to bond to other types of polymers to form PIL block copolymers allows the development of numerous different polymers.¹⁰⁸ PILs can be prepared by direct polymerization of IL monomers or chemical modification of existing polymers, using different techniques,^{86,109} such as radical polymerization,¹¹⁰ step-growth polymerization,¹¹¹ ring-opening metathesis polymerization,¹¹² and polycondensation polymerization.¹¹³ Cross-linked PIL networks can be also synthesized using thermal or ultraviolet (UV) radical polymerization.¹¹⁴

Most of the synthesized PILs are polycations prepared by step-growth polymerization, usually bearing an imidazolium cation in the polymer backbone obtained from different monomers like vinylic,¹¹⁵ styrenic,¹¹⁶ (meth)acrylic, and (meth)acrylamide,¹¹⁷ ethylene glycol,¹¹⁸ vinyl ether,¹¹⁹ and norbornene.¹¹² Besides, cations like tetraalkyl ammonium,¹¹⁰ pyridinium,¹²⁰ pyrrolidinium,¹²¹ guanidinium,¹²² or piperidinium¹²³ with vinylic, styrenic or methacrylic backbones can also be used. These PILs were combined with counter anions such as $[\text{BF}_4]^-$, $[\text{PF}_6]^-$, $[\text{CF}_3\text{SO}_3]^-$, $[\text{NO}_3]^-$, $[\text{Tf}_2\text{N}]^-$, $[\text{N}(\text{CN})_2]^-$, $[\text{FeCl}_4]^-$, $[\text{ClO}_4]^-$ and alkyl sulphonates.¹⁰⁹ On the other hand, polyanions have also been prepared,¹²⁴ mostly by radical polymerization, although in a much smaller number due to the difficulty associated with their synthesis.¹⁰⁹ Their backbone was obtained from (meth)acrylate, styrenic or vinylic monomers that can feature sulphonate, carboxylate, phosphoric, or amide anions, combined with counter cations like alkyl-imidazolium or tetraalkylammonium.¹⁰⁹

In order to overcome the mechanical instability of SILMs caused by IL leakage at transmembrane pressure differences above 1 - 2 bar, PIL membranes have also been investigated for CO_2 separation.¹⁰⁸ This type of material behaves like a polymer in terms of gas transport and provides good CO_2 /light gas selectivity.¹⁰⁸ However, PILs permeability to CO_2 is much lower than analogous ILs due to their solid nature.

The first neat PIL membranes for CO_2 separation were presented by Noble's group, with a study of the effect of systematic variations of PILs' structure on gas separation

performance.¹¹⁶ By the variation of the *n*-alkyl substituents length of IL monomers, these investigators obtained the best CO₂/N₂ separation with a selectivity of 32, the best CO₂/CH₄ selectivity of 38, both with a CO₂ permeability of 9 Barrer. They have concluded that the CO₂ permeability increased in a non-linear way as the *n*-alkyl substituent increased in length.⁷⁵

After that, this and other groups have studied several structurally different PILs with modifications in their backbones, cations, and anions (**Table A.4** from **Appendix A**), and showed that these membranes provide CO₂/N₂ and CO₂/CH₄ selectivities on par or higher than those observed for SILMs.¹²⁵ For instance, Bara *et al.* synthesized PIL membranes from IL monomers containing polar oligo(ethylene glycol) and nitrile-terminated alkyl substituents linked to imidazolium cations.¹²⁶ The PIL membranes fabricated with polar groups provided CO₂/N₂ and CO₂/CH₄ separations about 50% higher than when alkyl substituents with comparable length were used in PIL structures. Another approach was reported by Shaligram *et al.*, who studied the effect of substitution asymmetry on the CO₂ separation performance of PIL-based membranes.¹²⁷ The imidazole groups of two different polybenzimidazole (PBI) backbones, were substituted by *n*-butyl or 4-*tert*-butylbenzyl, both with a bulky nature, while the other substituent was kept as methyl. This asymmetry was showed to enhanced CO₂ permeability by disturbing PIL's chain packing. The effect of the type of anion and substituent were also studied, with [Tf₂N]⁻ and [HFB]⁻ and 4-*tert*-butylbenzyl providing the best gas permeabilities, respectively.

Even though PILs afford solid stable membranes, their major drawback is the substantial drop in both gas permeability and diffusivity when compared to their analogous liquid phases in SILMs. Therefore, different approaches have been explored to increase gas permeability and diffusivity, including the development of PIL/IL composite membranes (a PIL framework incorporating a certain amount of "free" IL),^{121,128-132} the incorporation of fillers to obtain MMMs,^{29,133} and the use of cross-linked polymer networks to prepare gel membranes containing large amounts of IL (> 50 wt%).^{36,114,124,134}

Polymer/Ionic Liquid Composite Membranes

Polymer/IL composite membranes, also known as polymer/IL gels, ionogels, or ionogels, are a type of dense gel-like membranes.^{26,86} These membranes are comprised of an IL entrapped into the spaces between the chains or clusters of a polymeric matrix.²⁶ Their synthesis is generally done by a solvent casting method with solvent evaporation.²⁶ Regarding the materials used for the membranes' preparation, the polymers should be mechanically, chemically, and thermally stable,²⁶ and the ILs must have a high affinity towards CO₂ and low viscosity.⁷⁵ The compatibility between the polymer and IL should also be addressed to avoid phase separation and leakage of the IL from the membrane.²⁶

The most used copolymer for the preparation of polymer/IL composite membranes is poly(vinylidene fluoride-co-hexafluoropropylene) (PVDF-HFP) due to its high free volume and reported success in gas separation,²⁶ although other polymers like polyether-polyamide block-copolymer (Pebax) due to a high CO₂/N₂ selectivity,¹³⁵ poly(vinylidene difluoride) (PVDF),¹³⁶ and PIs¹³⁷ have also been used.⁸⁶ The ILs commonly used have fluorinated anions, such as [Tf₂N]⁻,^{138,139} [BF₄]⁻,¹⁴⁰ [CF₃SO₃]⁻,¹³⁵ and [FAP]⁻¹⁴¹ or others like [B(CN)₄]⁻¹³⁶, combined with imidazolium cations of variable alkyl chain length, from [C₂mim]⁺ to [C₁₆mim]⁺.

Polymer/IL composites were first considered as solid electrolytes for energy applications due to their high conductivity.¹⁴² Later, this type of membranes started to be used for gas separation as an approach to solving the instability issues of SILMs, while trying to maintain similar CO₂ separation performances.^{26,86,143} In 2009, Hong *et al.* successfully developed the first polymer/IL membranes for CO₂/N₂ separation, reporting extraordinary performance results when 66 wt% of [C₂mim][BF₄] was combined with a PVDF-HFP polymer matrix.¹⁴⁰ A CO₂ permeability of 400 Barrer and a CO₂/N₂ selectivity of 60 surpassed the 2008 Robeson upper bound, while the membrane maintained its thermal stability up to 300 °C.

Later, Uchytel *et al.* studied the separation of CO₂ from CH₄ using PVDF-HFP membranes with different loadings of the IL.¹³⁹ At 70 wt% [C₆mim][Tf₂N] loading, the CO₂ permeability was almost 1000 times higher than for the neat polymer and a 100 times higher than the IL. This is an unexpected outcome since the membrane's CO₂ permeability is usually between the permeabilities of the pure components. These results were justified by the creation of new transport channels in the composite matrix. A heterogeneous membrane of PVDF with 66 wt% [C₄mim][B(CN)₄], stable up to 5 bar of transmembrane pressure, was reported by Chen *et al.* with a CO₂ permeability of 1778 Barrer and a CO₂/N₂ selectivity of 41.¹³⁶ The heterogeneity was believed to be a result of the absence of molecular-level interactions that could restrain gas permeability in miscible IL-based blends.

In 2014, Kasahara *et al.* reported a new type of polymer/IL composite membranes combining a UV cross-linked polymer network with AAILs that act as CO₂ carriers enhancing CO₂ permeability.¹⁴⁴ The authors believed that this soft but elastic network would provide additional support to the membrane, with the IL immobilized in the network's voids. A free-standing membrane with 70 wt% [P₄₄₄₄][Pro] and a poly(vinylpyrrolidone) (PVP) matrix was used in mixed gas permeation experiments at 100 °C and with a CO₂ partial pressure of 0.03 bar. A remarkable CO₂ permeability of 6700 Barrer and CO₂/N₂ selectivity of 170 were achieved with good mechanical stability up to 1 MPa.

After several studies reported with polymer/IL composite membranes (**Table A.5** from **Appendix A**), some conclusions could be taken. Higher loadings of IL swell the polymer matrix, increasing gas diffusion.¹⁴⁵ The IL affinity for CO₂ results in higher solubility,

enhancing the membranes' CO₂ separation performance.⁷⁵ In sum, the results reported in the literature indicate a higher CO₂ permeability compared to the neat polymers, despite a slight decrease in CO₂/N₂ and CO₂/CH₄ selectivities as expected for polymeric membranes and predicted by the 2008 Robeson upper bound.^{20,41,86} Increasing the IL loading can also reduce the polymer's crystallinity since the IL acts as a plasticizer making the membrane more flexible and permeable.^{26,75,140} However, the membrane loses mechanical stability, making the preparation of self-standing membranes with high IL loadings more challenging. Additionally, the type of polymers used to prepare these membranes are not charged, which means that no strong ionic interactions could be established between the polymer and the IL. When high contents of IL (> 50 wt%) are entrapped into the tight spaces between the polymer chains, high-pressure differentials compress the membrane causing IL leakage, therefore limiting the working pressure and the membranes' long-term separation performance.¹⁴⁶

PIL/IL Membranes

Alternatively, the development of a specific type of polymer/IL composite membranes, the PIL/IL membranes has also been explored (Table A.6 from Appendix A). Taking advantage of the strong electrostatic interactions established between the components is possible to prepare robust materials with good CO₂ separation performance.^{143,147} PIL/IL membranes represent an approach to improve the gas permeabilities of PIL membranes while maintaining mechanical stability.²⁶ The synthesis of PIL/IL membranes is based on the polymerization of IL monomers in the presence of "free" IL (Figure 1.14).

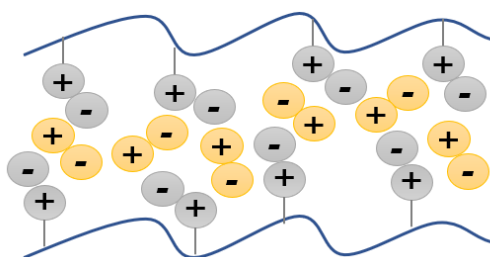


Figure 1.14 - Schematic representation of a PIL/IL membrane. Adapted from ¹⁴⁶.

The proof of concept for PIL/IL composite membranes for CO₂ separation was presented by Bara *et al.* that prepared stable membranes through the photopolymerization of imidazolium-based IL styrene monomers in the presence of 20 mol% non-polymerizable [C₂mim][Tf₂N].¹⁴⁷ This approach provided a 400% improvement of CO₂ permeability (from 9 to 44 Barrer) and an increase of CO₂/N₂ selectivity by 33% (from 32 to 39) compared to the analogous neat PIL membrane. Following the same line, Bara *et al.* studied the effect of changing the free imidazolium-based IL anion on the membranes' separation performance.¹⁴⁸ The membrane that incorporated the IL with the largest molar

volume, [C₂mim][Tf₂N], provided the best gas permeabilities (60 Barrer for CO₂), probably because the IL occupied more space between the polymer chains, allowing for a faster gas diffusion. The CO₂/N₂ and CO₂/CH₄ selectivities were slightly lower than those of the neat PIL membrane, but higher than most SILMs. Later, the same group examined functionalization effect of the free imidazolium-based IL cation.¹⁴⁹ Among alkyl, ether, nitrile, fluoroalkyl and siloxane groups incorporated, the membrane with ether functionalized cations provided the best separation performance with a 231% increase in CO₂ permeability (from 16 to 53 Barrer) despite a decrease in both CO₂/N₂ and CO₂/CH₄ selectivities relative to the neat PIL.

Moreover, Noble's group made considerable efforts regarding different imidazolium-based PILs for CO₂ separation.¹⁴³ The group developed a two-stage casting process that allowed the preparation of a thin PIL/IL membrane (selective layer of 100 nm) with 58 wt% [C₂mim][Tf₂N] and great performance (CO₂ permeability of 610 Barrer and CO₂/N₂ selectivity of 22).¹⁵⁰ Further improvements led to the fabrication of cross-linked PIL/IL membranes with higher IL content (80 wt% [C₂mim][Tf₂N]), good gas separation properties (CO₂ permeability of 500 Barrer and CO₂/N₂ selectivity of 24), and good mechanical stability.¹⁵¹ These PIL/IL membranes were synthesized by Carlisle *et al.* using two alternative methods to the typical use of cross-linkable IL monomers: Cross-linking a curable PIL/IL blend or cross-linking a neat curable PIL and swelling it with free IL. These methods provided advantages such as faster gelation rates and less solution penetration into the porous support. On the other hand, and bearing in mind the low CO₂ partial pressure in flue gas streams (**Table 1.1**), McDanel *et al.* developed an epoxide/amine PIL/IL composite membrane by step-growth polymerization for facilitated transport of CO₂.¹⁵² The results showed that facilitated transport of CO₂ only occurred in the presence of water vapor, improving when the CO₂ partial pressure is lower, which led to a better CO₂/N₂ separation. On the other hand, the use of hydrophilic IL [C₂mim][N(CN)₂] provided better results than hydrophobic IL [C₂mim][Tf₂N], since less humidity is required to achieve the sufficient water content for the reaction of CO₂ with amine functional groups. This membrane provided remarkable results under low CO₂ partial pressure and humidified mixed gas conditions (CO₂ permeability of 900 Barrer and CO₂/N₂ selectivity of 140), surpassing the 2008 Robeson upper bound.

Bearing in mind that the studies regarding PIL/IL membranes for CO₂ separation were mostly focused on the imidazolium cation, Tomé *et al.* have also been studying pyrrolidinium-based PILs with different structural variations.^{121,128-132,153} The advantage of these PILs is that their preparation only includes a metathesis reaction of a halide anion of a commercially available polymer for a more hydrophobic counter-anion, followed by filtration of the precipitated polymer.¹²¹ Comparatively, the preparation of imidazolium-

based PILs is more complex, involving several synthesis and purification steps and controlled polymerization conditions.^{114,116,126}

In their first report, Tomé *et al.* prepared membranes using poly[pyr₁₁][Tf₂N] as PIL combined with variable amounts of [pyr₁₄][Tf₂N] as "free" IL by a solvent casting method.¹²¹ The results showed that the CO₂ separation properties of poly[pyr₁₁][Tf₂N] are of the same order of magnitude as those of imidazolium-based PILs containing the [Tf₂N]⁻ anion. The incorporation of IL into the PIL proved to be an advantageous way to enhance CO₂/N₂ selectivity (from 22 to 32 at 20 wt% IL). Later, Tomé *et al.* synthesized pyrrolidinium random copolymers with counter-anion mixtures and prepared PIL/IL membranes with 20 wt% [pyr₁₄][Tf₂N].¹²⁸ The results showed that it is possible to adjust the gas permeation properties of the membranes by introducing a second PIL counter-anion with a different chemical structure, as it impacts the polymer chains interaction and packing efficiency. Further studies led to the development of novel pyrrolidinium-based PILs with cyano counter-anions, showing that gas permeabilities were dependent on the number of cyano groups in the anion.¹²⁹ In particular, the preparation of a [C(CN)₃]⁻ based membrane with 60 wt% [C₂mim][C(CN)₃] provided excellent performance for flue gas treatment, surpassing the 2008 Robeson upper bound with a CO₂ permeability of 439 Barrer and a CO₂/N₂ selectivity of 64. Tomé *et al.* also prepared membranes of pyrrolidinium-based PILs having three different molecular weights (M_w) and incorporated different contents of IL (20, 40 or 60 wt% [C₂mim][C(CN)₃]).¹³⁰ The results indicated that smaller polymer chains (lower M_w) improved gas permeability, probably due to higher chain mobility in a less packed matrix and high IL contents led to superior CO₂/N₂ separation performance. Considering the great results obtained with pyrrolidinium-based PIL/IL membranes bearing fluorinated or cyano functionalized anions for CO₂/N₂ separation, Tomé *et al.* explored these membranes potential also for biohydrogen production.^{132,153} Promising results were obtained, with a CO₂/H₂ separation performance superior to the respective upper bound.

More recently, Kammakakam *et al.* developed the first anionic PIL/IL membrane via photopolymerization.¹²⁴ Self-standing membranes were prepared, combining a PIL with delocalized sulfonimide anions pendant from the polymer backbone and mobile imidazolium counter-cations, with 0.5 and 1 equiv amount of free IL [C₂mim][Tf₂N] to the two newly designed polymerizable anionic ILs, and 20 wt% of cross-linker poly(ethylene glycol) diacrylate (PEGDA) as the composite matrix. The authors reported a CO₂ permeability of 20 Barrer and a remarkable CO₂/CH₄ selectivity of 119, reaching the 2008 Robeson upper bound.

PIL/IL-based Mixed Matrix Membranes

In order to improve the CO₂ separation efficiency, as well as thermal and mechanical stability of PIL/IL membranes, three-component MMMs with solid fillers (**Figure 1.15**), such as zeolites,^{48,154} and MOFs,^{29,133} have also been investigated (**Table A.7** from **Appendix A**).

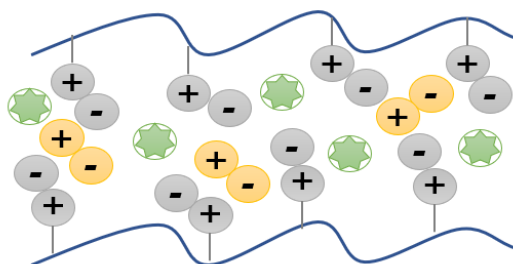


Figure 1.15 - Schematic representation of a PIL/IL-based MMM. Adapted from ¹⁴⁶.

Zeolites are a type of porous, crystalline silicate-based frameworks with pore sizes close to the diameter of light gas molecules.⁴⁸ Regarding this type of filler, Singh *et al.* examined and optimized the factors affecting CO₂/CH₄ separation using cross-linked PIL/IL/zeolite MMMs.⁴⁸ The membrane comprising 50 wt% poly([smim][Tf₂N]), 20 wt% [C₂mim][Tf₂N], and 30 wt% SAPO-34 achieved the best performance (CO₂ permeability of 260 Barrer and CO₂/CH₄ selectivity of 90), outperforming the 2008 Robeson upper bound. Later on, Dunn *et al.* developed cross-linked PIL/IL/zeolite MMMs for CO₂/CH₄ separation, based on curable PIL prepolymers, instead of a mixture of IL monomer and cross-linker.¹⁵⁴ The results demonstrated that by adjusting the prepolymer chain length is possible to control polymer gelation rate and resistance to support penetration, when casting onto ultrafiltration membranes, which improved gas separation performance.

On the other hand, MOFs represent a class of crystalline and porous materials that consist of a three-dimensional hybrid network formed by organic bridging ligands and inorganic metal nodes linked through coordination bonds, which makes for a well-defined structure with specific pore sizes that can accommodate light gases.¹⁵⁵ The presence of organic ligands leads to easier incorporation of MOFs into polymers to produce MMMs, as opposed to zeolites.¹⁵⁵ Nabais *et al.* prepared MMMs combining poly([pyr₁₁][Tf₂N]), [C₄mpyr][Tf₂N] and three different MOFs (Cu-BTC, MIL-53 and ZIF-8).¹³³ An increase in MOF content (up to 30 wt%) led to overall better CO₂/H₂ separation, with membranes performances that surpassed the 2008 Robeson upper bound. Recently, Sampaio *et al.* studied the impact of different loadings of MOF-5 (10 – 30 wt%) on CO₂/CH₄ separation performance of MMMs comprising poly([pyr₁₁][Tf₂N]) and [C₂mim][BETI].²⁹ Despite an 88% selectivity decrease at 30 wt% MOF-5, the results also demonstrated a 133%

increase in CO₂ permeability, both probably due to the MOF's large cavity size relative to the gases' diameter.

The results reported so far indicate PIL/IL-based MMMs as a promising strategy to solve the permeability/selectivity issues of polymeric membranes and to overcome the brittleness of inorganic membranes. However, the optimization of factors that affect gas separation (filler type and loading, PIL structure and cross-linking density) must continue to be addressed, as well as experiments with real operational conditions in order to produce defect-free membranes with high performance.

Cross-linked polymer/IL Membranes

Another relevant and simpler strategy is the preparation of polymer/IL composites in a single-pot using commercially available non-ionic polymer networks. The preparation of these membranes can be done by thermal or UV-initiated polymerization of the desired non-ionic polymer network in the presence of "free" IL.¹³⁴ In particular, excellent results have been reported in terms of CO₂ separation using poly(ethylene glycol) (PEG) (Table A.8 from Appendix A), since this polymer contains several ether groups, known for their high affinity for CO₂.¹⁴⁵ However, its crystallinity represents a limitation for CO₂ permeability. For instance, Lin *et al.* increased the CO₂ permeability by 10 times by cross-linking a PEGDA membrane, in comparison to a semi-crystalline PEG one, without significant sacrifice in CO₂/N₂ selectivity.¹⁵⁶ The decrease in crystalline zones and increase of the amorphous phase made the polymer more flexible, which facilitated CO₂ transport. On the other hand, the presence of "free" IL also helps to reduce crystallinity.¹⁴⁵ In this line, different researchers have recently studied this type of cross-linked polymer/IL membranes for CO₂ separation, frequently named PEG-based cross-linked iongels.

Kusuma *et al.* studied the compatibility between several ILs and two different cross-linked polymer matrices, PEGDA and PEGDA copolymer with a thiol functionalized polysiloxane, by preparing iongels with 40 vol% IL loading.¹⁵⁷ They concluded that ILs with imidazolium and pyridinium cations combined with the anion [Tf₂N]⁻ promote thermal stability and good miscibility with the cross-linked PEG network.¹⁵⁷ In further studies, Kusuma *et al.* incorporated several ILs having the anion [Tf₂N]⁻ and 1,3-substituted imidazolium cations into a cross-linked PEG network.¹⁵⁸ ILs with short alkyl terminal substituents increased gas permeability since they allowed superior polymer chain mobility. When a 60 vol% [C₂mim][Tf₂N] was used, a CO₂ permeability of 530 Barrer and a CO₂/N₂ selectivity of 31 was obtained.

More recently, Martins *et al.* studied the influence of anion structure on the properties of cross-linked PEGDA iongels for CO₂/N₂ separation.¹³⁴ The performance of the iongel with 70 wt% [C₂mim][C(CN)₃] supported in a porous polyamide (PA) filter was able

to surpass the 2008 Robeson upper bound, but future improvements regarding mechanical stability should be addressed to avoid the use of a porous support. The results of this study also showed that iongels with fluorinated IL anions ($[\text{Tf}_2\text{N}]^-$) presented better mechanical properties than those fabricated with cyano-functionalized IL anions.

Taking into account all the literature reviewed and mentioned throughout this introduction, it is understood that the combination of membrane technology with ILs has great potential to emerge as an economic and environmentally friendly approach to separate CO_2 from light gases, replacing some of the more mature technologies used today. For instance, some of the reported IL-based membranes showed better separation performance than the commercially available ones, represented by the 2008 Robeson upper bound. However, there is still room for improvement for IL-based membranes to be applied in industrial conditions. In particular, two major challenges need to be tackled: maintain mechanical stability while achieving high separation performance. It is believed that the development of robust PEG-based cross-linked iongel membranes for CO_2 separation from post-combustion streams and biogas upgrading is an excellent approach to overcome these issues. Considering its simple single-pot preparation with reduced environmental impact combined with high content of CO_2 -philic ILs, it can be affirmed that this is a promising approach and future developments should focus on the iongels' mechanical stability.

GOAL AND MOTIVATION

The main goal of this thesis was to improve the mechanical stability of iongel membranes composed of UV-cross linked PEGDA with 60 wt% content of the IL [C₂mim][Tf₂N] by incorporating different loadings of MMT nanoclay particles. The membrane preparation was done in order to fabricate self-standing iongels desired for CO₂ separation from flue gas of post-combustion streams and biogas upgrading.

The iongels were prepared with MMT concentrations of 0.2 wt%, 0.5 wt%, and 1.0 wt%. The reason behind the selection of such MMT loadings was due to the fact that the incorporation of small amounts of MMT into polymeric membranes has been reported in the literature to improve mechanical properties,^{67,71} thus allowing the membranes to withstand a wider range of process conditions, and in some cases to facilitate CO₂ separation from light gases.^{69,70,72}

The characterization of the materials (MMT and iongel membranes) included attenuated total reflectance Fourier-transform infrared (ATR-FTIR) spectroscopy, thermogravimetric analysis (TGA), CO₂ solubility measurements, scanning electron microscopy (SEM), differential scanning calorimetry (DSC), contact angle, puncture tests to evaluate mechanical properties, and pure gas permeation experiments using CO₂, N₂, and CH₄ at 30°C and a transmembrane pressure differential of 0.7 bar. The characterization was done in order to have a better understanding of the physico-chemical properties of the materials and how they influence the CO₂ separation performance regarding CO₂/N₂ and CO₂/CH₄ gas pairs.

MATERIALS AND METHODS

3.1. Materials

The membranes were prepared using the following materials: the IL 1-ethyl-3-methylimidazolium bis(trifluoromethylsulfonyl)imide ($[C_2mim][Tf_2N]$, 99 wt% pure) provided by IoLiTec GmbH (Germany), the monomer poly(ethylene glycol) diacrylate (PEGDA, $M_w = 575$ g/mol) acquired from Sigma-Aldrich (Spain) and the nanoclay Nanomer[®] I.34TCN, montmorillonite (MMT) clay surface modified with 25-30 wt% methyl dihydroxyethyl hydrogenated tallow ammonium purchased from Sigma-Aldrich (Germany). The photoinitiator used was 2-hydroxy-2-methylpropiophenone (DAROCUR, 97 wt% pure) provided by Sigma-Aldrich (Spain).

For the CO₂ solubility measurements (**Section 4.3**) and the pure gas permeation experiments (**Section 4.8**), the following gases were supplied by Praxair (Portugal): nitrogen, N₂ (industrial grade, 99.99%), methane, CH₄ (> 99.99% purity) and carbon dioxide, CO₂ (high purity grade, 99.998%).

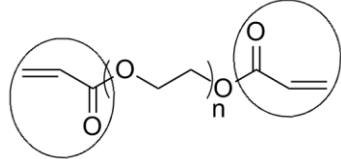
$[C_2mim][Tf_2N]$ IL

The $[C_2mim][Tf_2N]$ IL, bearing an imidazolium cation and a fluorinated anion, was selected for the iongels' preparation, since it has been reported to have high CO₂ permeabilities and selectivities in studies regarding the effect of the IL structure on the permeation properties of SILM configurations.^{91,93,159} The properties of $[C_2mim][Tf_2N]$ are presented in **Table 3.1**.

PEGDA

In order to increase structural density and make the iongel self-standing, a PEGDA crosslinked polymeric network was selected for this work (**Figure 3.1**). The iongels were obtained by UV photopolymerization of the terminal acrylate groups of PEGDA in the

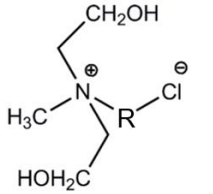
Table 3.2 - Properties of the PEGDA monomer used in the preparation of the iongels.^{134,207}

Name	Poly(ethylene glycol) diacrylate
Abbreviation	PEGDA
Molecular formula	$(C_2H_4O)_n C_6H_6O_3$
Molecular weight	575 g/mol
Density (25°C)	1.12 g/cm ³
Viscosity (25°C)	57 cP
CO₂ loading capacity	126 mmol/g
Water content	< 0.2 %
Water solubility (20°C)	Soluble
Structure ^{162 3} (The acrylate groups are marked in circles)	

MMT

Montmorillonite was used as filler in this work to improve the mechanical properties of PEGDA-based iongel materials. For the preparation of the iongels, the nanoclay MMT modified with 25 – 30 wt% methyl dihydroxyethyl hydrogenated tallow ammonium was used, and its properties are listed in **Table 3.3**.

Table 3.3 - Properties of the nanoclay MMT used in the preparation of the iongels.^{68,163}

Name	Montmorillonite
Abbreviation	MMT
Molecular formula (non-modified)	$M_x(Al_{4-x}Mg_x)Si_8O_{20}(OH)_4$ M – Monovalent cation; x – degree of isomorphous substitution ($0.5 < x < 1.3$)
Surface organo-modifier	25 – 30 wt% Methyl dihydroxyethyl hydrogenated tallow ammonium
Density	1.7 g/cm ³
Particle size	$\leq 20 \mu m$
pH	6.5 – 7.0
Structure of organo-modifier (Adapted from ¹⁶⁴)	 R – Hydrogenated Tallow

³ This figure is licensed under the Creative Commons Attribution-Share Alike 3.0 Unported license.²⁰⁴

3.2. Membrane Preparation

Neat Iongel Membranes

To prepare the neat iongel membranes, the following protocol was followed. First, the [C₂mim][Tf₂N] IL was added to PEGDA in a vial and the solution was stirred for 1 hour at room temperature on a magnetic stirrer plate (Magnetic Emotion Mix 15 eco, Germany). The solution was prepared with 60 wt% IL (0.6 g) and 40 wt% PEGDA (0.4 g). The quantities were measured on an analytical balance (Kern ABJ 220-4NM, Germany). Next, UV photopolymerization was performed to fabricate the neat iongel membranes. The necessary amount of radical photoinitiator (3 wt% of PEGDA) was magnetically stirred into the vial for a few seconds and the solution was poured onto a glass plate and covered with a quartz plate on top. The plates were separated by spacers to assure the desired iongel thickness and diameter and secured in place with clips. Then, the neat iongel solution was exposed to UV light with a wavelength of 365 nm and an intensity of 1.723 mW/cm² for 10 minutes. After that, the neat iongel was peeled from the plates and stored in a Petri dish.

Iongel Mixed Matrix Membranes

The preparation of the iongel MMMs, started with the addition of the necessary amounts of MMT to [C₂mim][Tf₂N]. The iongel MMMs were prepared with different percentages of nanoclay, namely 0.2 wt% (2 mg), 0.5 wt% (5 mg) and 1 wt% (10 mg), and 60 wt% of IL (0.6 g). The solutions were magnetically stirred for 20 minutes at room temperature and sonicated for 1 hour in an ultrasonic bath (Bandelin Sonorex Digitec, Germany), in order to obtain a good dispersion of the nanoclay in the IL. Afterwards, the necessary amount of PEGDA to complete 1 g was added and the solutions were stirred for 1 hour at room temperature. Lastly, the iongel MMMs were fabricated by UV photopolymerization following the same steps previously described for the preparation of the neat iongel membranes.

3.3. Materials Characterization

Fourier-Transform Infrared (FTIR) Spectroscopy

Attenuated total reflectance Fourier-transform infrared (ATR-FTIR) spectroscopy was used in order to identify the characteristic peaks of MMT, [C₂mim][Tf₂N] and PEGDA. The iongel membranes' spectra were collected to confirm the incorporation of the components and to determine possible interactions established between them. The success

of photopolymerization of the iongels was checked as well. Samples with 1 x 1 cm of each iongel membrane were used and enough liquid to cover the crystal was necessary in the case of [C₂mim][Tf₂N] and PEGDA. The equipment used was a Perkin Elmer Spectrum Two spectrometer with the software Spectrum that collected data using 10 scans from 400 to 4000 cm⁻¹.

Thermogravimetric Analysis

Thermogravimetric analysis (TGA) is a technique that monitors the degradation of a sample, while it is being heated at a controlled and constant temperature in a controlled atmosphere. The resulting data is collected as a percentage of weight loss in function of time or temperature and allows the study of the sample's thermal stability.¹⁶⁵ TGA of the iongel membranes and the respective components were carried out to assess their thermal stability when submitted to temperatures up to 120 °C, considering one of the possible applications for the iongel membranes, CO₂ separation from post-combustion streams.²⁶ The onset temperature (T_{onset}), defined as the temperature at which the material starts to decompose that corresponds to the point at which the baseline slope changes during heating, and the decomposition temperature (T_{dec}), defined as the temperature at 50% weight loss, were both determined.^{134,165}

Measurements were performed in Lass Evo TGA-DTA/DSC 1600°C PG from Setaram (France) on a temperature range of 25 - 600°C, at a heating rate of 10 °C min⁻¹ and under argon atmosphere. The sample was weighted to have at least 10 mg. The TGA was performed by the technician Dr. Carla Rodrigues from *Laboratório de Análises*, LAQV-REQUIMTE at NOVA School of Science and Technology (FCT-NOVA).

CO₂ Solubility Measurements

To evaluate if there is any affinity of the MMT nanoclay towards CO₂, gas solubility measurements were performed using the apparatus shown in **Figure 3.2**, following a pressure decay method previously described elsewhere.¹⁶⁶ The setup includes two separated stainless-steel compartments immersed in a water bath, one for the sample and one for the gas. The temperature of the water was kept constant at 30 °C by a thermostat (Julabo Corio C, Germany) and the pressure in the gas compartment was measured at each second by a transducer (Druck PDCR 910, UK). Pressure values were collected over time using the software LabView.

To make sure that the gas compartment (GC) only had CO₂, the experiment began with a purge. A sample with 0.5 g of MMT was placed in a glass cup inside the absorption compartment with valve 3 closed. Then, the gas compartment was pressurized at 0.7 bar with pure CO₂ while valves 1 and 2 were closed. The necessary time passed to guarantee

that there were no significant changes in pressure due to temperature variation. When the pressure stabilized, valve 3 was opened, allowing for CO₂ to be in contact with MMT. The affinity of MMT for CO₂ is detected if there is a pressure decay, resulting from the absorption of gas by the sample.

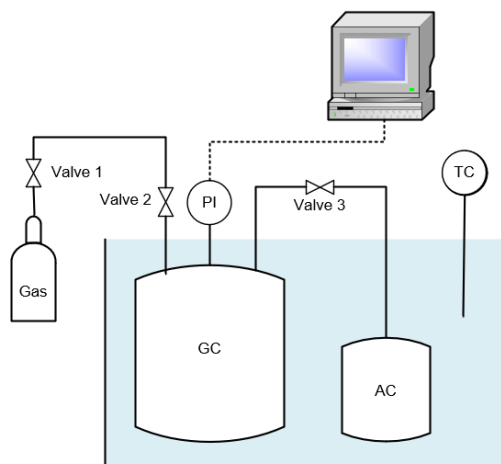


Figure 3.2 - Schematic representation of a gas absorption setup (PI – Pressure indicator; TC – Temperature controller; GC – Gas compartment; AC – Absorption compartment). Adapted from ¹⁶⁶.

Scanning Electron Microscopy

In order to examine their morphology, the iongel membranes were characterized by scanning electron microscopy (SEM). The interactions between a high-energy beam of electrons and the surface of the iongel membranes gave information about their morphology.¹⁶⁷ Since the iongel membranes are meant for gas permeation experiments considering a solution-diffusion mechanism, a dense structure is required thus, the compatibility between both the MMT and iongel matrix was studied.

A SEM device from JOEL, model 7001F with an electron beam intensity of 10 kV was used by the technician Dr. Isabel Nogueira at MicroLab, *Instituto Superior Técnico, Universidade de Lisboa*. Samples with 1 x 1 cm of the iongel membranes were covered with a thin layer of Au-Pd before characterization. The SEM images were collected from surface and cross-section with magnifications of 50x, 500x, 1000x, and 50x, 200x, 500x, respectively.

Differential Scanning Calorimetry

Differential scanning calorimetry (DSC) is an analysis used to determine the material's thermal properties and phase transitions, like glass transition, crystallization, and melting point. DSC is performed by monitoring the changes in a material's heat capacity (C_p) with the temperature. These changes are detected by variations in the heat flow while a sample is submitted to heating or cooling.¹⁶⁸

The samples of the iongel membranes were prepared with at least 10 mg each and analyzed in a Setaram DSC 131 device, under a nitrogen atmosphere, with heating and cooling cycles between -130 °C to room temperature and from room temperature to 300 °C. The analyses were carried out by the technician Dr. Carla Rodrigues from *Laboratório de Análises*, LAQV-REQUIMTE at NOVA School of Science and Technology (FCT-NOVA).

Contact Angle

When a drop of liquid is sitting on top of a solid surface, it is possible to measure a contact angle. The contact angle is defined as the angle between the solid surface plane and a tangent to the drop of liquid that meets the point where three phases are in contact. Young's equation describes this system and is used for ideal situations with a smooth solid surface.¹⁶⁹ The equation defines the contact angle (θ^Y) as an equilibrium between a drop of liquid and three interfacial tensions: solid-vapor (γ_{SV}), solid-liquid (γ_{SL}), and liquid-vapor (γ_{LV}), and is represented in **Equation 1** and **Figure 3.3**.¹⁷⁰

$$\cos \theta^Y = \frac{\gamma_{SV} - \gamma_{SL}}{\gamma_{LV}} \quad (\text{Eq. 1})$$

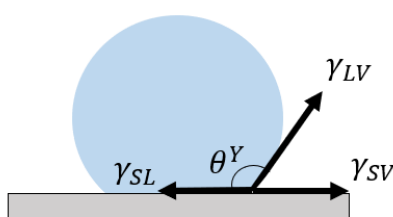


Figure 3.3 - Schematic representation of the three interfacial tensions (γ_{SV} , γ_{SL} , γ_{LV}) and the contact angle (θ^Y) as described by Young's equation. Adapted from ¹⁷⁰.

The drop may be of different liquids. When water is used and the contact angle measured is inferior to 90°, the surface is considered hydrophilic. If the angle is superior to 90°, the surface is hydrophobic.

In this case, the iongel membranes were cut into squares of 1x1 cm and placed flat on top of glass slides. The analysis was performed by the deposition of a drop of distilled water or glycerol with a syringe on the membrane surface. The goniometer CAM100 (KSV Instruments LTD) controlled by the software CAM100 collected 10 frames with intercalation of 1000 ms and calculated the right and left contact angles. Three replicates were made, and the mean value was determined.

Mechanical Properties

The mechanical properties of the iongel membranes were analyzed by puncture tests, which were performed at *Instituto Superior de Agronomia* from *Universidade de Lisboa* with the assistance of Professor Vítor Alves. This technique studies a material's capacity to resist or transmit an external force without breaking or deforming its original structure.

Two identical iongel membranes were prepared for the measurements, performed at room temperature using a TA XT Plus Texture Analyzer (Stable Micro Systems, UK). This equipment has a cylindrical probe with a diameter of 2 mm that punctures a hole on the iongel membrane at a constant velocity of 1 mm s⁻¹. One replicate was performed for each iongel membrane, from which the mean value of the obtained puncture stress and elongation upon puncture was determined.

The texture analyzer is controlled by software (Exponent) that records the applied force as a function of time and distance. The puncture stress was calculated according to **Equation 2**.

$$\sigma = \frac{F}{A} \quad (\text{Eq. 2})$$

Where σ is the puncture stress (Pa), F is the maximum force applied by the probe (N) and A is the cross-sectional area of the probe (m²). The cross-sectional area of the probe is determined using the following equation, where r is the probe radius (m).

$$A = \pi r^2 \quad (\text{Eq. 3})$$

In order to rigorously compare the results obtained for the iongel membranes with slightly different thicknesses, the puncture stress values were normalized as follows:

$$\sigma_n = \frac{\sigma}{l} \quad (\text{Eq. 4})$$

Where σ_n is the normalized puncture stress (MPa/mm), and l is the iongel membrane's thickness (mm). The elongation upon puncture was obtained by **Equation 5**.

$$\varepsilon = \left(\frac{\sqrt{h^2 - d^2} - h}{h} \right) \times 100 \quad (\text{Eq. 5})$$

Where ε is the elongation upon puncture (%), h is the radius of the iongel membrane exposed in the cylindrical hole of the sample holder (mm) and d is the distance of the probe from the point of contact to the point of puncture (mm).

Pure Gas Permeation Experiments

The main purpose of this work is the preparation of iongel membranes that can be used for CO₂ separation from flue gas streams (CO₂/N₂) and biogas upgrading (CO₂/CH₄). The pure gas permeation experiments provide data that allowed the determination of the permeability and the ideal selectivity of the membranes for different gas pairs.

For these experiments, a gas permeation setup was used, like the one described in **Figure 3.4**. This setup is composed of a stainless-steel cell with two compartments of identical volume, that represent the feed and the permeate. The cell is immersed in a water bath and the temperature is maintained at 30 °C by a thermostat (Julabo Corio C, Germany). Connected to each compartment is a transducer (Jumo type 404327, Germany) that measures the respective pressure variation at every second. These measurements are recorded over time in the computer using the software PicoLog.

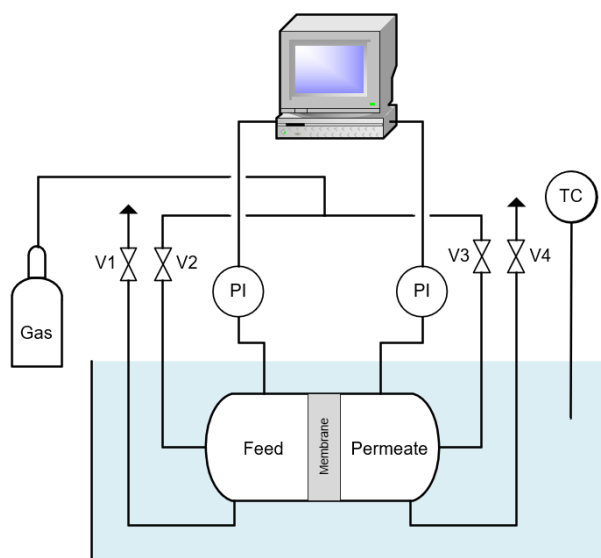


Figure 3.4 - Schematic representation of a pure gas permeation setup (TC – Temperature controller; PI – Pressure indicator; V1, V4 – Exhaust valves; V2, V3 – Inlet valves). Adapted from ¹⁶⁶.

The experiments began with the purge of the cell compartments to guarantee that only the desired gas was in the cell. Then the cell was pressurized at 0.7 bar and left the necessary time for the pressure to stabilize due to temperature variations. Finally, the driving force was applied by quickly opening and closing the outlet valve of the permeate compartment which creates a pressure difference between the compartments. The pressure variation at each second was recorded since the instant t_0 when the driving force was applied. The pressure decreased in the feed compartment and increased in the permeate compartment until the equilibrium was reached.

The iongel membrane's permeability is determined by **Equation 6**:

$$\frac{1}{\beta} \times \ln\left(\frac{\Delta P_0}{\Delta P}\right) = P \times \frac{t}{l} \quad (\text{Eq. 6})$$

Where β is the experimental geometric parameter of the cell (m^{-1}), ΔP_0 is the pressure difference between the feed and the permeate compartments at the instant t_0 (bar), ΔP is the pressure difference between the feed and the permeate compartments over time (bar), P is the iongel membrane's permeability (m^2/s), t is time (s) and l is the iongel membrane's thickness (m). Permeability is often given in Barrer ($1 \text{ Barrer} = 1 \times 10^{-10} \text{ cm}^3(\text{STP})\cdot\text{cm}\cdot\text{cm}^{-2}\cdot\text{s}^{-1}\cdot\text{cmHg}^{-1} = 8.3 \times 10^{-13} \text{ m}^2/\text{s}$).¹⁷¹

The permeability was obtained from the slope when $1/\beta \ln(\Delta P_0/\Delta P)$ was plotted as a function of t/l . The constant β is given by **Equation 7**.

$$\beta = A \times \left(\frac{1}{V_{\text{feed}}} + \frac{1}{V_{\text{perm}}} \right) \quad (\text{Eq. 7})$$

Where A is the iongel membrane area (m^2), V_{feed} is the volume of the feed compartment (m^3) and V_{perm} is the volume of the permeate compartment (m^3).

The value β was determined with an N_2 permeation experiment to calibrate the cell. It was used a PDMS membrane with a known permeability for N_2 of $2.08 \times 10^{-10} \text{ m}^2/\text{s}$ ¹⁷² and an average thickness of $117 \mu\text{m}$. The method followed was the one described above, and β was obtained from the slope when $1/P \ln(\Delta P_0/\Delta P)$ was plotted as a function of t/l .

The iongel membranes' ideal selectivity is defined by the ratio of the permeabilities between gas A and gas B, as indicated by **Equation 8**.

$$\alpha = \frac{P_A}{P_B} \quad (\text{Eq. 8})$$

Where α is the ideal selectivity, P_A is the permeability to gas A (Barrer) and P_B is the permeability to gas B (Barrer).

To understand the gas transport in the prepared iongel membranes, it is important to have in mind that these are dense membranes and thus, the gas transport is determined by a solution-diffusion mechanism, in which the permeability (P) of a certain gas is dependent on its diffusivity (D) and solubility (S), as stated by **Equation 9**.

$$P = D \times S \quad (\text{Eq. 9})$$

RESULTS AND DISCUSSION

The preparation of the iongel membranes with 60 wt% IL and different amounts of MMT incorporated (0.0, 0.2, 0.5, 1.0 wt%), resulted in solid, yet malleable free-standing membranes, that could be handled carefully without damage. Before UV polymerization, the prepared mixtures looked homogeneous, indicating that the components were miscible at room temperature. The optical transparency of the neat iongel suggested good compatibility between [C₂mim][Tf₂N] and the cross-linked PEGDA network. The iongel MMMs, despite being more opaque, also appeared homogeneous and defect-free, becoming slightly less malleable as the MMT concentration increased. Pictures of the neat iongel and the iongel MMM with the highest loading of MMT can be seen in **Figure 4.1**.

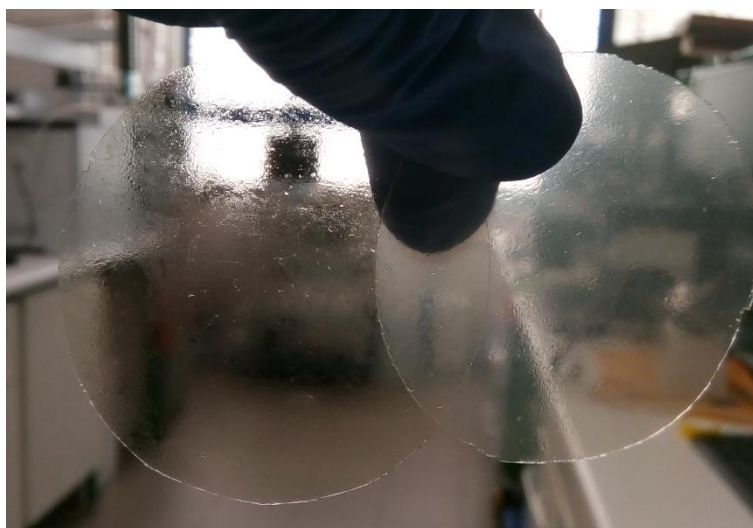


Figure 4.1 - Pictures of the prepared membranes: neat iongel (left) and iongel MMM with 1.0 wt% MMT loading (right).

The different starting materials and iongel membranes, were characterized by ATR-FTIR, TGA, and the CO₂ solubility in MMT was assessed. The techniques to characterize the prepared iongel membranes also included SEM, DSC, contact angle, and mechanical properties. Lastly,

pure gas permeation experiments were also carried out. The obtained results are presented and discussed below.

4.1. Fourier-Transform Infrared (FTIR) Spectroscopy

The MMT used was characterized by ATR-FTIR. The obtained spectrum is presented in **Figure 4.2**, while the respective peak assignments are listed in **Table B.1** from **Appendix B**.

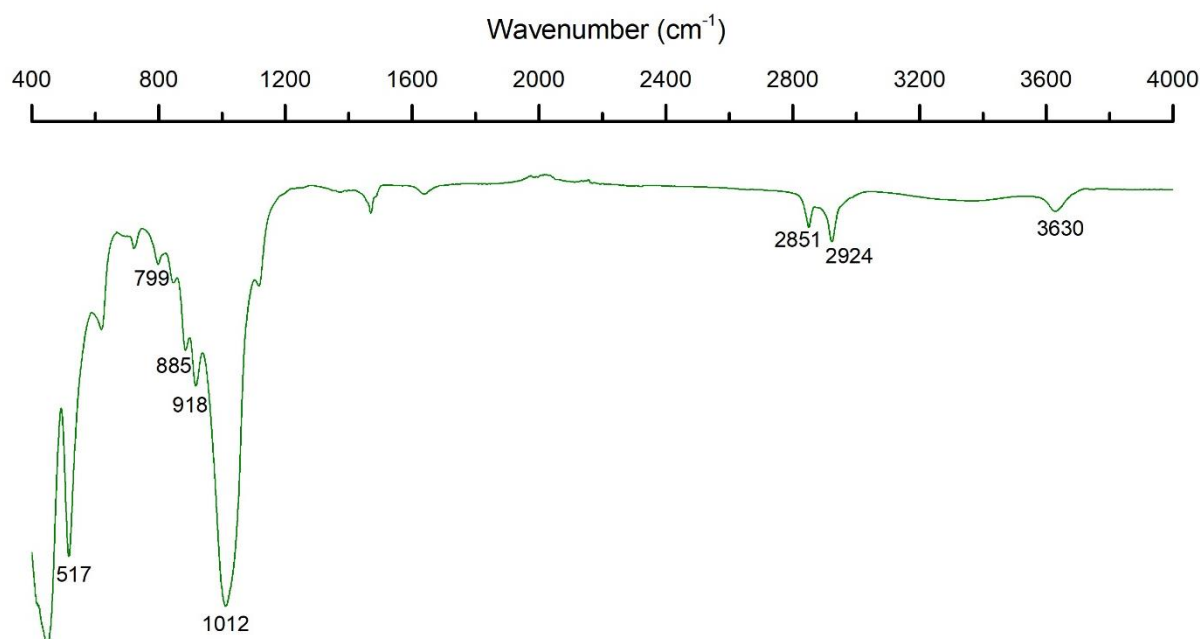


Figure 4.2 - FTIR spectrum of MMT.

The identified peaks of MMT are similar to those reported in the literature.^{173–175} In particular, the peaks observed at 517 cm^{-1} and 1012 cm^{-1} correspond to Si-O bending and stretching of the sheets of silica tetrahedra, respectively. The peaks detected at 799 cm^{-1} , 885 cm^{-1} , and 918 cm^{-1} are associated with the bending of AlMgOH, AlFeOH, and AlAlOH functional groups, respectively. This agrees with what was previously mentioned when describing the MMT structure. The aluminum ions in the sheets of alumina octahedra could have been replaced by magnesium or iron ions, which originated this infrared (IR) pattern. The peaks at 2851 cm^{-1} and 2924 cm^{-1} are related to the C-H bending of CH_2 and CH_3 groups present in the MMT organic modifier. The broad peak at 3630 cm^{-1} is attributed to the stretching of several structural OH groups associated with Al-OH and Si-OH from alumina and silica sheets. This peak may also be associated with the hydroxyl groups of the MMT organic modifier.

Although Jarrar *et al.* reported peaks at 3405 cm^{-1} and 1640 cm^{-1} for an identical MMT provided by the same supplier, that were associated with the water present in clay interlayers,¹⁷³ these peaks were not identified in the obtained spectrum. This could be explained by different water contents present in different batches.¹⁷⁶

The prepared iongel membranes, as well as their major components, [C₂mim][Tf₂N] and PEGDA, were characterized by ATR-FTIR spectroscopy as well. The results are displayed in **Figure 4.3** and **Figure 4.4**, where the spectrum called “Neat iongel” (black line) is the same for both figures. The peak assignments are available in **Table B.2** and **Table B.3** from **Appendix B**. This technique allowed the identification of the components' functional groups, verify their successful incorporation into the iongel membranes, and detect possible interactions that might be established between them.

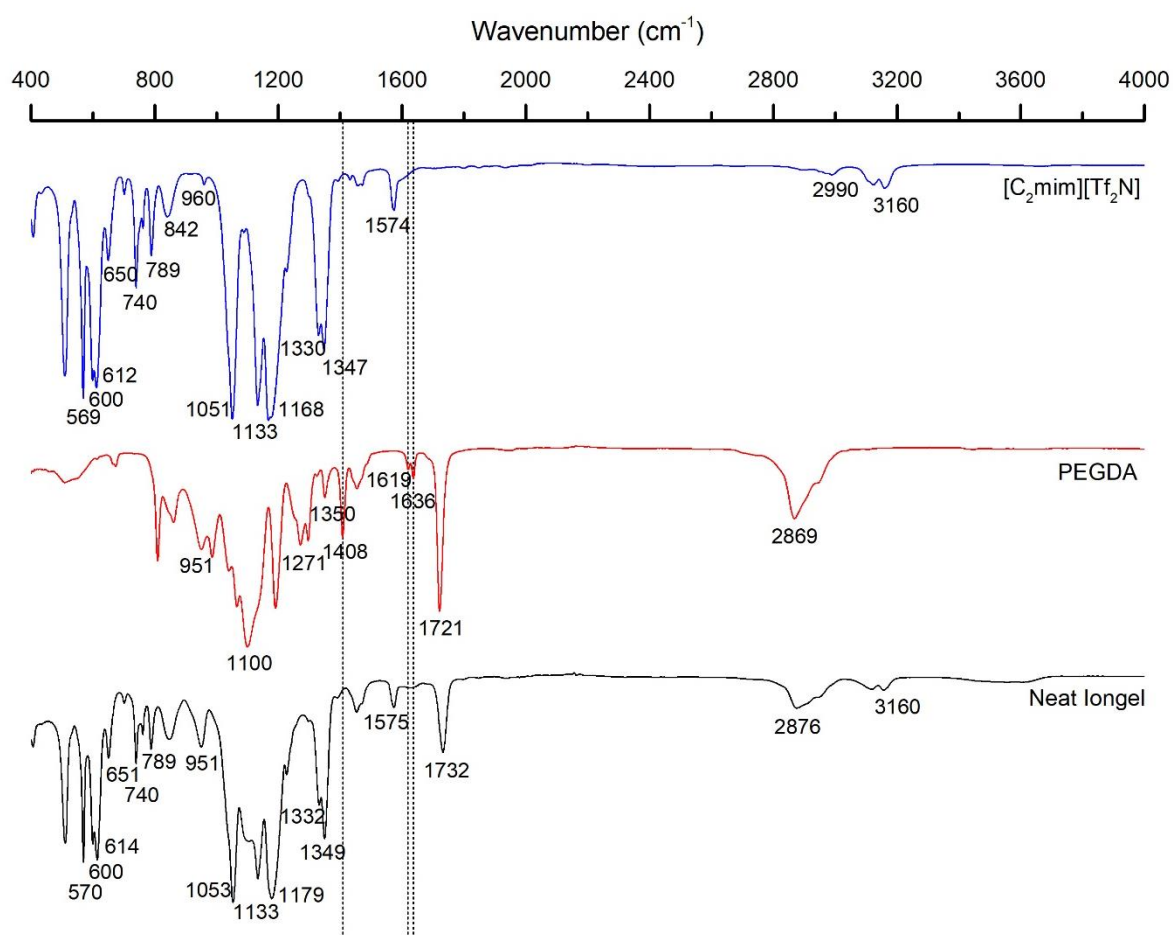


Figure 4.3 - FTIR spectra of [C₂mim][Tf₂N] IL, PEGDA and the respective neat iongel membrane with 60 wt% of [C₂mim][Tf₂N]. The dashed vertical lines indicate the characteristic peaks of terminal acrylate groups of PEGDA.

The FTIR spectrum of [C₂mim][Tf₂N] IL is mostly dominated by characteristic peaks of the anion, which is in agreement to what has been published in the literature.^{133,134,177,178} For example, some of the most intense peaks are assigned to 1051 cm⁻¹ (S-N-S asymmetric stretching), 1133 cm⁻¹ (S=O symmetric stretching), 1168 cm⁻¹ (CF₃ asymmetric stretching), and 1347 cm⁻¹ (S=O asymmetric stretching). The peaks associated with the IL cation can also be identified, for example, at 740 cm⁻¹ for the CH₃N, CH₂N, and imidazolium ring bending, and at 3160 cm⁻¹ for the stretching modes of C-H and imidazolium ring.

The FTIR spectrum obtained for PEGDA is also in agreement with the literature,^{134,145,179} with peaks detected at 1100 cm⁻¹ from the C-O-C symmetric stretching of ether groups, at

1721 cm^{-1} from C=O symmetric stretching, and 2869 cm^{-1} from C-H stretching. The dashed vertical lines in **Figure 4.3** point out the characteristic peaks of the terminal acrylate groups of the PEGDA monomer. At 1408 cm^{-1} the peak is assigned to C-H bending, while the peaks at 1619 cm^{-1} and 1636 cm^{-1} are attributed to the stretching modes of the acrylate groups. When the neat iongel spectrum is analyzed, it can be seen that these three peaks disappeared, confirming the formation of a cross-linked PEGDA network. Moreover, the assigned peak to 1100 cm^{-1} from the spectrum of the PEGDA monomer becomes less intense and undetectable when incorporated into the iongels. This indicates that the high amount of IL present may act as a plasticizer by swelling the polymeric network, which alters the polymer chain interactions and limits the stretching vibration of ether groups.¹⁶⁰

In the spectrum of the neat iongel, the peaks of its components can be identified without considerable shifts in wavenumber. This implies that $[\text{C}_2\text{mim}][\text{Tf}_2\text{N}]$ and PEGDA were well incorporated into the neat iongel and that no evident chemical interactions were detected between them, which is in agreement to what was previously observed.¹³⁴

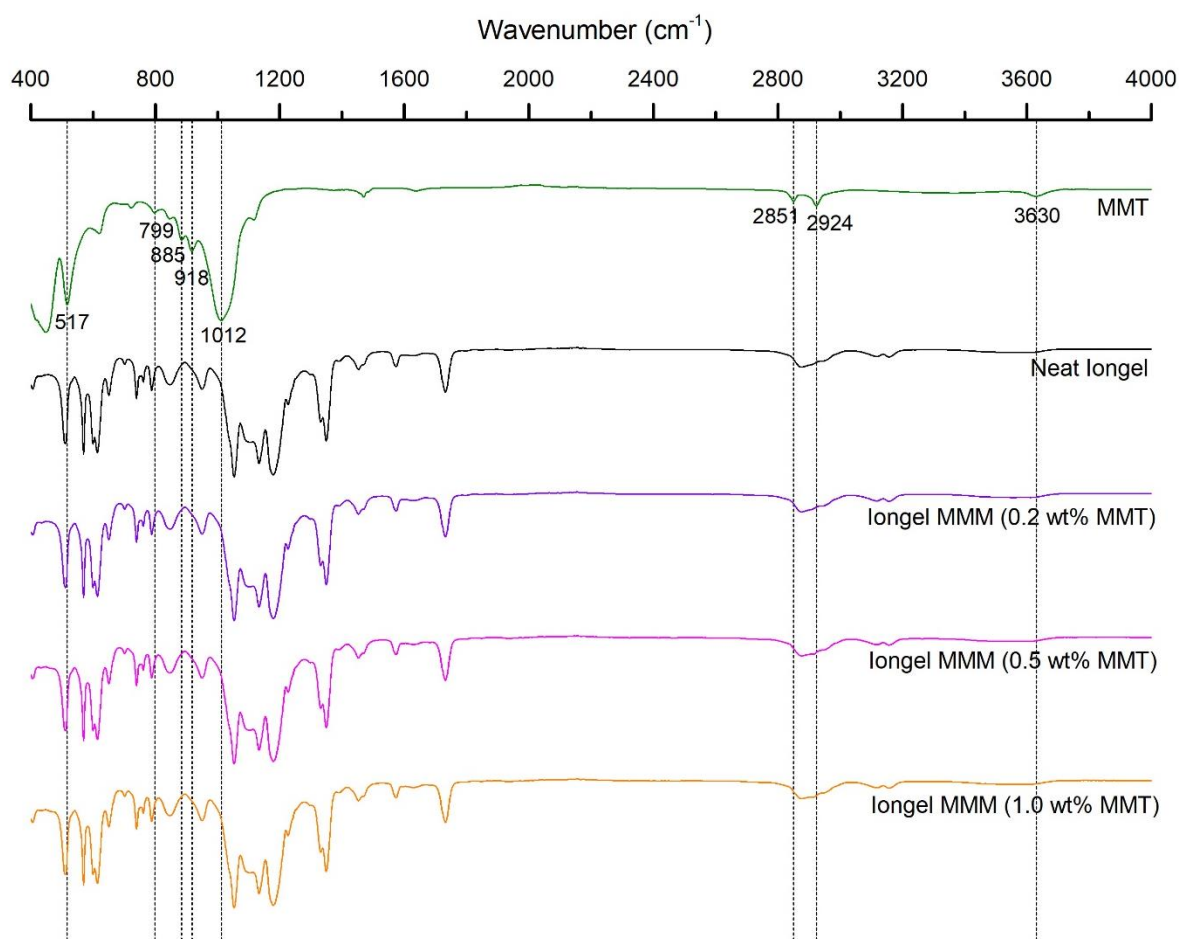


Figure 4.4 - FTIR spectra of MMT, the neat iongel and the iongel MMMs with 0.2, 0.5 and 1.0 wt% MMT loading. The dashed vertical lines indicate the characteristic peaks of MMT.

Figure 4.4 shows the FTIR spectrum of the MMT nanoclay, which was already discussed, as well as the spectra of the prepared iongel membranes with different compositions of MMT incorporated. The dashed vertical lines across the spectra indicate the wavenumbers corresponding to MMT peaks. Considering the iongel membranes' spectra, it can be seen that they are coincident with each other, since no new peaks appeared from the presence of MMT. Moreover, there was no location shift in characteristic peaks of the IL or PEGDA. Consequently, it is not possible to confirm the incorporation of nanoclay into the iongel MMMs only based on ATR-FTIR characterization. A likely explanation is that the very small quantities of MMT used (≤ 1 wt%) were not enough to be detected by this technique. However, the simple visual observation of the prepared iongel MMMs suggests that the incorporation of the MMT was successful, since the neat iongel, which is transparent, becomes slightly more opaque with the addition of increasing amounts of nanoclay. On the other hand, the similarity between the iongel membranes' spectra indicates that the IL and PEGDA were properly incorporated in all the prepared iongel membranes and that the photopolymerization was successful.

4.2. Thermogravimetric Analysis

TGA of MMT was performed in order to study its thermal stability. The obtained thermograms represented in **Figure 4.5** show the nanoclay weight loss and the weight loss velocity, both as a function of temperature. The latter allowed the identification of the temperatures corresponding to peaks of weight loss.

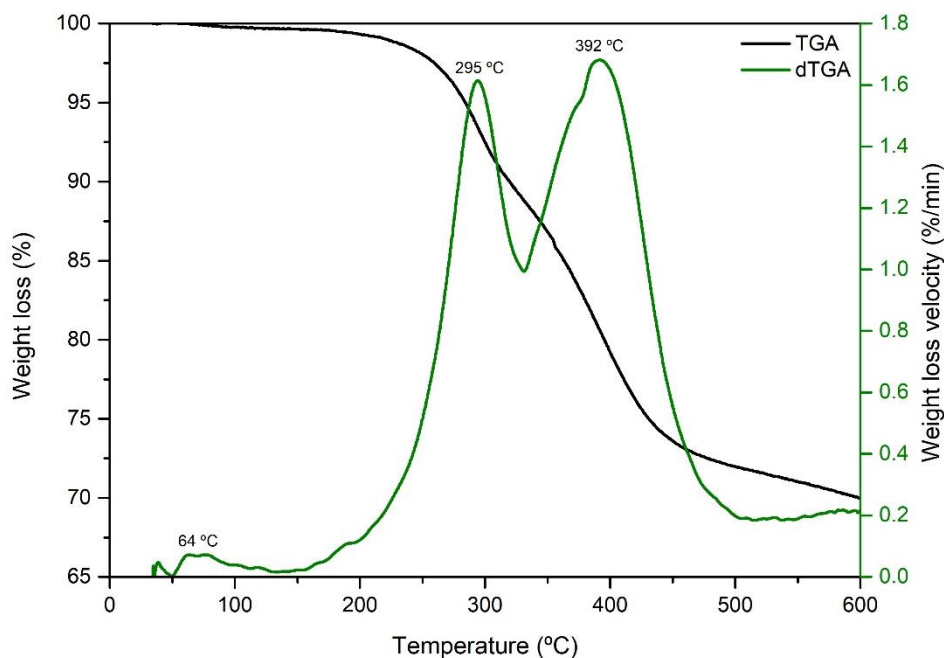


Figure 4.5 - TGA and dTGA profiles of MMT.

The TGA profile of MMT is similar to those reported in the literature,¹⁸⁰⁻¹⁸² starting with a slight weight loss in the range of 50-150 °C that corresponded to the evaporation of water physically adsorbed to the clay's surface, followed by interlayer water.¹⁸⁰⁻¹⁸² This agrees with the FTIR characterization (**Section 4.1**) that did not detect peaks related to water in the MMT structure, since the water corresponded only to 0.3% of its weight.

The degradation of MMT started at 142 °C (T_{onset}). From this point to around 531 °C happened the release and decomposition of the MMT organic modifier, methyl dihydroxyethyl hydrogenated tallow ammonium.¹⁸¹ The thermogram shows two peaks of weight loss (295 °C and 392 °C), which can be explained by the different sites where the functionalization of the nanoclay may occur: in the interlayer space, at the external surface, and at the edges.¹⁸⁰ It is believed that the first peak is related to the decomposition of the molecules bonded to the edges and external surfaces of the clay, since they can be released easier, and the second peak represents the molecules that are less accessible in the interlayers. Moreover, the TGA data indicates a 28 wt% content of organic modifier (weight lost from T_{onset} until 531 °C), which is in agreement with what was indicated by the supplier i.e., between 25 and 30 wt% (**Section 3.1**). Above 531 °C, the MMT nanoclay kept losing weight due to dehydroxylation of the aluminosilicate structure.¹⁸⁰⁻¹⁸² The T_{dec} was not detected in the temperature range studied, which means that it is superior to 600 °C. According to the literature, the T_{dec} for the used nanoclay is above 900 °C.¹⁸¹

From these results, it can be concluded that the thermal stability of nanoclays is greatly dependent on the amount of organic modifier present in the structure.¹⁸¹ The results also indicate that MMT is appropriate to be incorporated into membranes for the separation of CO₂ from post-combustion streams since its weight remains nearly constant up to 120 °C.

The prepared iongel membranes, as well as their starting materials, were submitted to TGA to study their thermal stability and check if they can also withstand temperatures up to 120 °C. The thermograms acquired for [C₂mim][Tf₂N] IL, PEGDA before polymerization and the neat iongel are represented in **Figure 4.6** and **Figure C.1** from **Appendix C**, as weight loss and weight loss velocity, respectively, both as a function of temperature. The thermograms of the prepared iongel MMMs are illustrated in **Figure 4.7** and **Figure C.2** from **Appendix C** also as weight loss and weight loss velocity, respectively, both as a function of temperature. The black lines named "Neat iongel" are the same for all these figures. **Table 4.1** provides the T_{onset} , T_{dec} , total weight losses, and the temperature ranges of the iongel membranes.

Looking at **Figure 4.6**, it can be seen that the decomposition of the IL occurred in one stage, from 334 °C (T_{onset}) to 478 °C with the maximum peak of weight loss at 455 °C. At 446 °C (T_{dec}), the sample had lost 50% of its weight and after the heating ended the residue was 4%. These results are similar to those found in the literature.^{134,183,184}

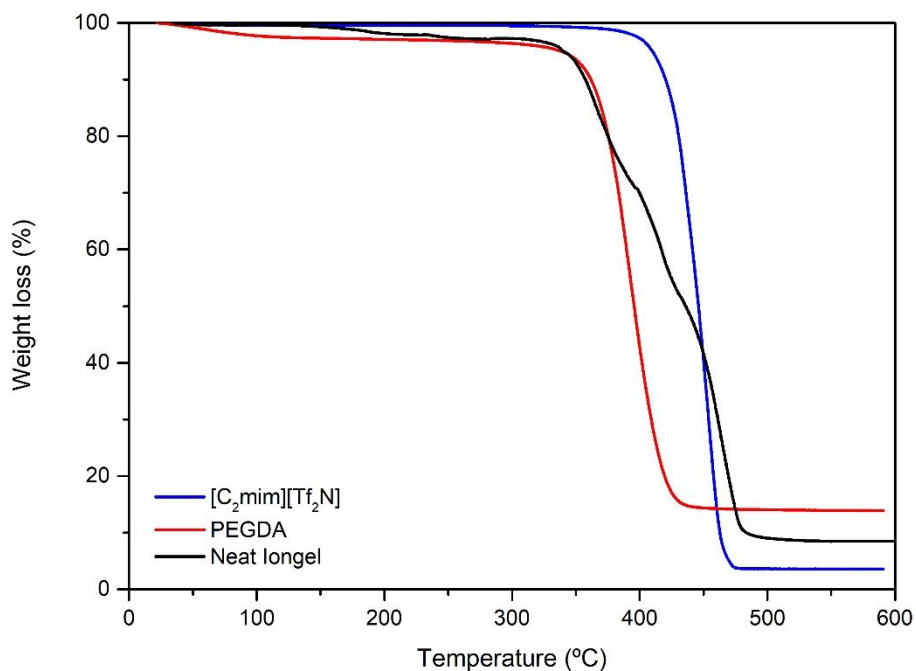


Figure 4.6 - TGA profiles of [C₂mim][Tf₂N], PEGDA and the neat iongel.

The thermogram obtained for PEGDA before polymerization is also in agreement with the literature.^{134,185,186} PEGDA presented a two-stage decomposition process that started with a small weight loss of 3%. This first loss happened mainly from room temperature to around 100 °C and corresponds to the humidity that was present in the sample. The second and most significant stage occurred between the T_{onset} of 194 °C and 519 °C, with a peak at the T_{dec} of 397 °C and was due to the decomposition of the polymer backbone chain with 83% weight loss.¹⁸⁵ At 600 °C there was 14% of weight remaining, which agrees with the temperature for the total decomposition of PEGDA (800 °C) reported in the literature.¹⁸⁶

For the iongel membranes, it was anticipated an intermediate behavior to those observed for their two major components, which was confirmed by the obtained results (**Table 4.1**). For instance, the values obtained for T_{onset} and T_{dec} are between those for PEGDA and [C₂mim][Tf₂N] IL, bearing in mind that the IL has higher thermal stability and is present into the iongel membranes in a higher amount. This expected tendency was also reported for an iongel membrane prepared by Martins *et al.* with the same composition as the one mentioned here as neat iongel (without MMT).¹³⁴

This characterization also demonstrated that the incorporation of MMT seems to have produced iongels with slightly better thermal stability since the T_{onset} increased. For instance, the T_{onset} increased 12 °C from adding 0.2 wt% of nanoclay in comparison with the neat iongel. However, this trend is not linear since increasing the MMT loading five times (from 0.2 wt% to 1 wt%), resulted only in a 3 °C variation of T_{onset} . The enhancement in the thermal stability slows down as the concentration of MMT reaches 1 wt%. A likely explanation is that by incorporating more MMT into the membranes, the quantity of MMT's organic modifier, which starts

to degrade at 142 °C, increases as well, limiting the enhancement of thermal stability provided by the aluminosilicate structure of the nanoclay. On the other hand, Noskov *et al.* reported that the interaction of [C₂mim][Tf₂N] IL with non-modified MMT reduced the thermal stability of this clay/IL composite, explaining that the bonds between the IL's cation and anion become weaker due to the formation of intermolecular bonds between IL and clay.⁶³ To better understand the results obtained, in future work it would be interesting to do a thermal analysis on iongels with concentrations of MMT above 1 wt%.

Table 4.1 – Onset and decomposition temperatures, total weight loss, and respective temperature range of the iongel membranes with 0.0, 0.2, 0.5, and 1.0 wt% MMT loading.

MMT loading (wt%)	T_{onset} (°C)	T_{dec} (°C)	Total weight loss (%)	Temperature range (°C)
0.0	284	436	3	38 – 284
			26	282 – 396
			19	397 – 432
			43	432 – 519
0.2	296	433	3	83 – 297
			25	296 – 389
			22	388 – 431
0.5	298	440	44	431 – 505
			31	129 – 406
			14	405 – 430
1.0	299	434	46	430 – 510
			4	80 – 299
			27	299 – 396
			62	396 – 502

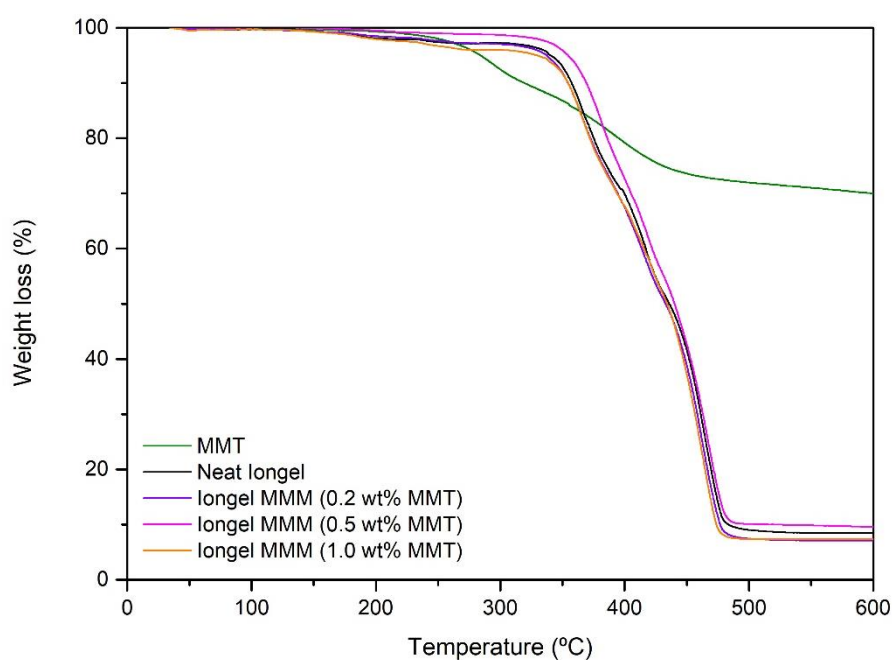


Figure 4.7 – TGA profiles of MMT, the neat iongel and the iongel MMMs with 0.2, 0.5 and 1.0 wt% MMT loading.

Considering the thermograms from **Figure 4.7**, it was observed a similar thermal behavior for all the membranes prepared, since their compositions do not differ much from each other. Their major decomposition occurred in three stages, mainly between 300 °C and 500 °C. Additionally, the iongels' thermograms allowed to check if the membranes could withstand temperatures up to 120 °C. Considering that at this temperature the membrane's weight loss was not meaningful (less than 0.5%) and corresponded to water removal, it can be concluded that the iongels are thermally stable as much as necessary to withstand the conditions of CO₂ separation from post-combustion streams.

4.3. CO₂ Solubility Measurements

A gas absorption experiment with pure CO₂ was done to access if there is any affinity/solubility of this gas towards the MMT nanoclay. The results are shown in **Figure 4.8**, where the CO₂ pressure is represented as a function of time.

As it can be seen from **Figure 4.8**, and despite the MMT nanoclay being in contact with CO₂ for almost two days, the pressure remained approximately constant at around 0.56 bar, which means that the nanoclay did not absorb any moles of CO₂. On the other hand, it was not found in the literature any report suggesting that the selected MMT has an affinity for CO₂. Therefore, it is expected that the incorporation of MMT into the iongel membranes will not influence the solubility of CO₂ and it may only affect the diffusion of this gas into the iongel matrix.

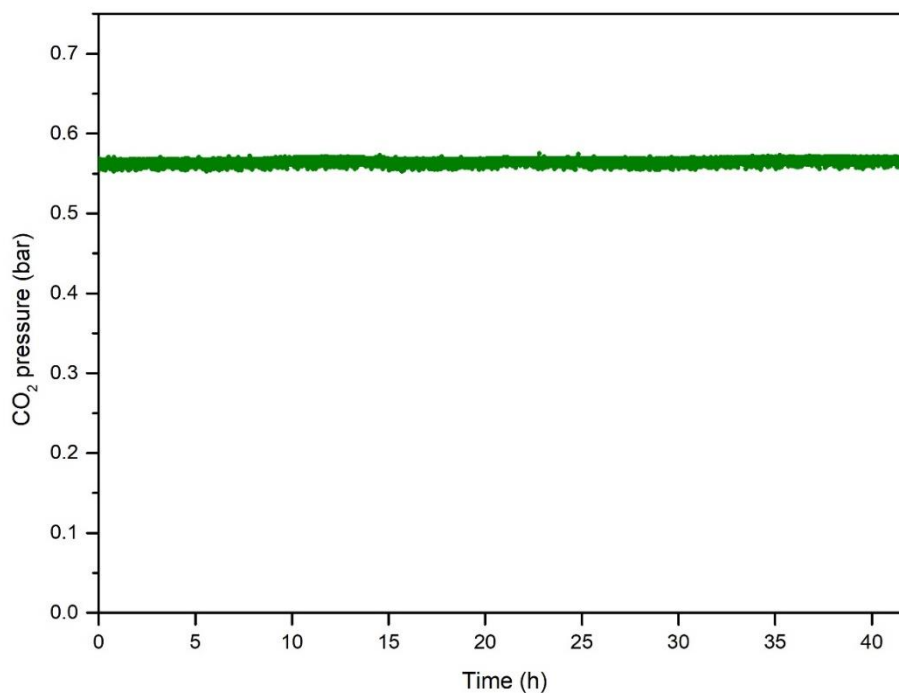


Figure 4.8 - Pressure decay method applied to determine the CO₂ solubility in MMT.

4.4. Scanning Electron Microscopy

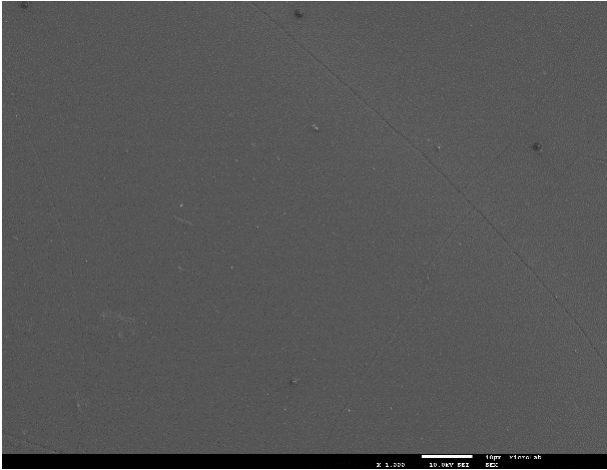
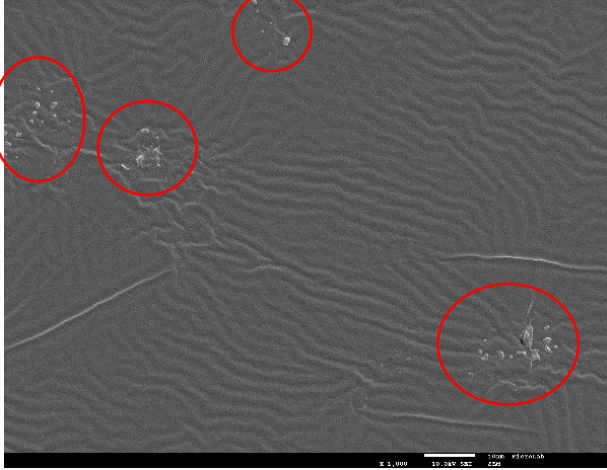
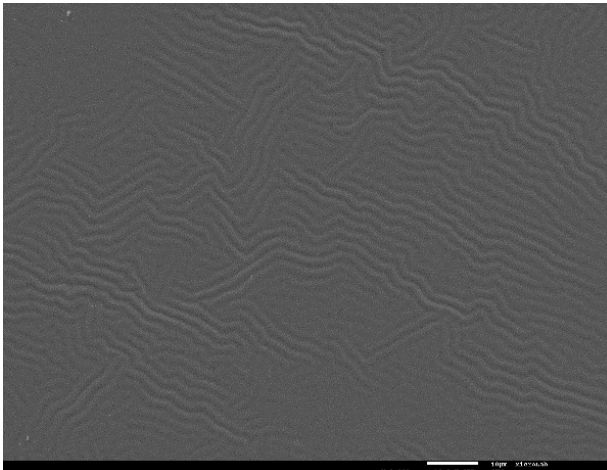
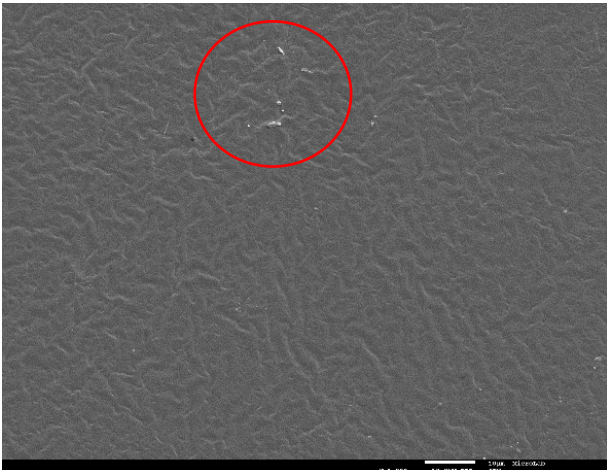
The morphology of the prepared iongel membranes and the compatibility between their components were studied using SEM images of the membranes' surfaces at different magnifications. In order to accomplish good gas separation performances, the iongel membranes should have a homogeneous and dense morphology. **Table 4.2** shows the images of the iongel membranes' surfaces with a magnification of 1000x as it allows for the best observation of details. The images of the iongel membranes' cross-sections are available in **Table D.1** from **Appendix D**. These images show many deformations originated by the fracture of the samples by hand, which do not allow conclusions to be taken from them. In the future, the samples should be fractured under liquid nitrogen, which makes a cleaner cut and minimizes deformations.

Looking at **Table 4.2**, a smooth surface without defects or pores can be seen for the neat iongel, which suggests a dense structure and good miscibility between $[C_2mim][Tf_2N]$ and PEGDA. Despite the deformations presented, due to the preparation of the sample, the respective cross-section image in **Table D.1** agrees with this conclusion, since it does not reveal the formation of agglomerations or phase separation throughout the membrane's thickness. A dense, defect-free neat iongel with the same composition was also reported by Martins *et al.*¹³⁴

Regarding the iongel MMMs, in particular the one with 0.2 wt% MMT, the surface image showed a dense morphology. Nevertheless, when the concentration of MMT increased to 0.5 wt%, the formation of agglomerations started to appear (identified in the figure of **Table 4.2** by red circles), and a heterogeneous surface was obtained. However, it should be mentioned that the preparation of perfectly exfoliated polymer-clay nanocomposites is challenging to accomplish, as it has been reported in the literature.^{67,187} Therefore, the iongel MMMs probably had a morphology that combined intercalated and exfoliated areas. The iongel MMMs with 0.2 wt% and 0.5 wt% MMT loading also had a more wrinkled texture in comparison to the neat iongel, which is accentuated when the nanofiller content is higher (0.5 wt% MMT) and accompanied by the appearance of creases. The agglomerations within the polymeric network might have reduced the cross-linking density, which enhanced the fragility of the iongel MMM with 0.5 wt% MMT and originated some fractures that appear in the surface image as creases (see **Table 4.2**).

When the MMT loading was increased to 1.0 wt%, the iongel MMM also had a wrinkled surface with agglomerations. Moreover, when the iongel MMM surface image is zoomed in, it is possible to see small holes at the surface, as can be observed in **Figure 4.9**. Hence, the iongel MMM containing 1.0 wt% MMT was not tested in terms of pure gas permeation experiments (discussed in **Section 4.8**) since its morphology is not suitable for the solution-diffusion mechanism, and it would behave as an unselective barrier for gas permeation.

Table 4.2 - SEM images of the surface of the iongels with 0.0, 0.2, 0.5, and 1.0 wt% loading of MMT with an ampliation of 1000x. The red circles identify agglomerations.

MMT loading (wt%)	Surface (1000x)	MMT loading (wt%)	Surface (1000x)
0.0		0.5	
0.2		1.0	

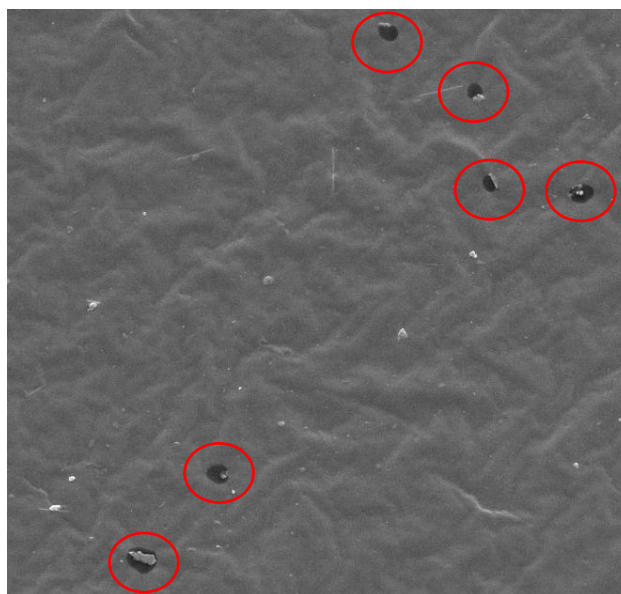


Figure 4.9 - SEM image of the iongel MMM with 1.0 wt% loading of MMT with an ampliation of 1000x. The red circles identify holes on the surface.

4.5. Differential Scanning Calorimetry

In order to investigate the properties and phase transitions of the iongel membranes, DSC experiments were performed. The glass transition temperature (T_g) results are provided in **Table 4.3**. The T_g is defined as the temperature at which the structure of an amorphous polymer becomes rubbery upon heating or glass-like upon cooling, becoming brittle and stiff.^{188,189}

Table 4.3 - Glass transition temperatures (T_g) of the iongel membranes with 0.0, 0.2, 0.5, and 1.0 wt% of MMT loading.

MMT loading (wt%)	T_g (°C)
0.0	-57.1
0.2	-59.7
0.5	-56.6
1.0	-61.7

Looking at **Table 4.3**, it can be seen that all the obtained T_g are far below room temperature, indicating that all the prepared iongel membranes are amorphous. On the other hand, a single T_g for the neat iongel confirmed that its components were well combined. For the iongel MMMs, a good combination of the starting materials could not be proven, since the low quantities of MMT used (≤ 1 wt%) do not originate relevant variations in terms of T_g results.

Regarding the neat iongel, a T_g of -57.1 °C was obtained. Martins *et al.* reported neat PEGDA, with the same M_w as the one used, as a rubbery amorphous polymer with

a single T_g of $-20\text{ }^\circ\text{C}$.¹³⁴ The supplier of $[\text{C}_2\text{mim}][\text{Tf}_2\text{N}]$ IL indicated a T_g of $-98\text{ }^\circ\text{C}$ for this material.¹⁶¹ As expected, the result obtained for the neat iongel is between the values of its neat components. This makes sense because the incorporation of an elevated amount of IL (60 wt%) into a polymeric network increases the mobility of the chains, making the polymer more flexible, which may translate into a decrease of PEGDA's T_g .

In the same study mentioned above, Martins *et al.* also reported a neat iongel with the same composition as the one that was prepared, indicating the respective T_g as $-47\text{ }^\circ\text{C}$.¹³⁴ A possible explanation for the difference between the result obtained ($-57.1\text{ }^\circ\text{C}$) and the value reported in the literature ($-47\text{ }^\circ\text{C}$) could be related with the different amounts of photoinitiator that were used in the preparation of the neat iongels. The neat iongel prepared in the scope of this thesis was produced with 3 wt% to PEGDA of photoinitiator, while in the one reported was used 5 wt% to PEGDA. A higher concentration of radical photoinitiator in the prepared solutions might have increased the cross-linking density, which decreased the polymer chains' mobility and free volume, leading to a higher T_g result.¹⁸⁹

Considering the iongel MMMs, the T_g results vary from $-62\text{ }^\circ\text{C}$ to $-56\text{ }^\circ\text{C}$ without an obvious trend, possibly due to the low loadings of MMT incorporated, as already mentioned. As a conclusion it can be stated that the iongel MMMs maintained the same amorphous nature as the neat iongel after incorporating MMT.

4.6. Contact Angle

The contact angles formed between the iongel membranes' surface, and a drop of liquid, water or glycerol, were measured to evaluate their hydrophilicity. The smaller the angle, the more hydrophilic is the surface. However, it was not possible to measure the contact angles using water due to the spreading of the water drops onto the surface of the iongel membranes, a sign of great hydrophilicity to this solvent. Therefore, the results were obtained using an organic solvent, glycerol, and are depicted in **Figure 4.10**.

The results for the iongel membranes according to MMT concentration were: $60.6^\circ \pm 0.2^\circ$ for 0.0 wt%, $59.1^\circ \pm 0.4^\circ$ for 0.2 wt%, $59.7^\circ \pm 0.4^\circ$ for 0.5 wt%, and $60.5^\circ \pm 0.3^\circ$ for 1.0 wt%.

PEGDA monomer is described in the literature as being composed of hydrophilic ethylene oxide units and hydrophobic acrylate units. Longer PEGDA chain networks, like the one used in this work, have higher contents in ethylene oxide units making the material more hydrophilic. Ju *et al.* studied the contact angle between a drop of n-decane and the surface of a cross-linked PEGDA identical to the one used and reported a contact angle of 52° .¹⁹⁰ Zhang *et al.* reported PEGDA hydrogels, made with PEGDA with a similar

molecular weight as the one used in this work, with contact angles to water around 47°, which characterizes them as hydrophilic materials as well.¹⁹¹

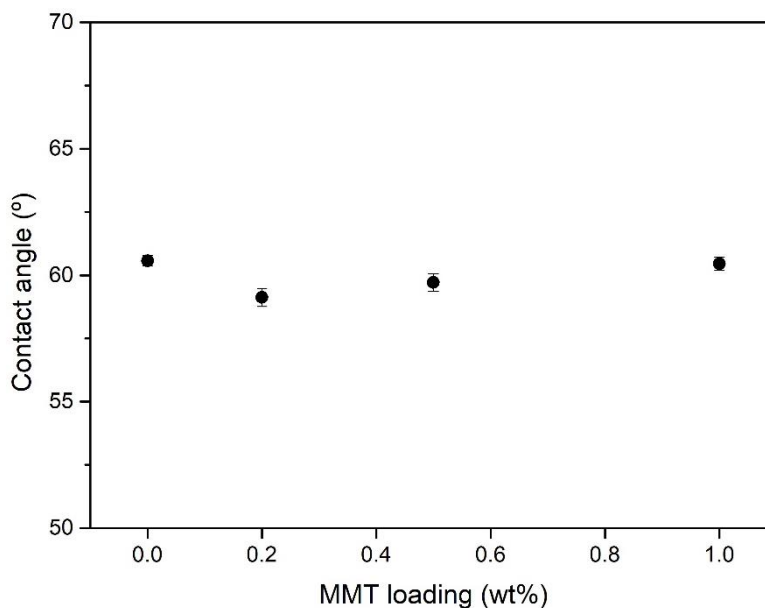


Figure 4.10 - Contact angles obtained for the iongels with 0.0, 0.2, 0.5 and 1.0 wt% MMT loading.

The incorporation of a hydrophobic IL, such as $[C_2mim][Tf_2N]$,^{192,193} into a cross-linked PEGDA reduced the hydrophilic character of the polymeric network, which resulted in a contact angle for the neat iongel above the values previously mentioned for PEGDA. On the other hand, **Figure 4.10** shows that the iongel MMMs have slightly lower contact angles than the neat iongel. However, the variation between these results is very small (in the range of 1.5°). In other words, this could represent a tendency for MMT to increase the hydrophobicity of the iongel membranes but the reduced concentrations of nanoclay in the iongel MMMs (≤ 1 wt%) did not cause a variation that was significant enough to prove this speculation. Regarding the iongel MMM with 1.0 wt% MMT loading, it is important that the holes on its surface detected by SEM (**Figure 4.9**) are taken into consideration and the contact angle obtained for this iongel membrane to be interpreted with caution.¹⁶⁹ The holes observed might have originated a smaller contact angle than expected, due to the penetration of the solvent into them.

The hydrophilic character of all the prepared iongel membranes comes as an advantage for CO₂ transport. The permeability of CO₂ is affected by diffusivity and solubility and, generally, the solubility of CO₂ in hydrophilic polymers is reported as being higher than in more hydrophobic ones.³⁴

4.7. Mechanical Properties

The mechanical properties of the prepared iongel membranes were evaluated by puncture tests. The puncture stress, the normalized puncture stress, and the elongation upon puncture were determined according to **Section 3.3**. These results are displayed in **Table 4.4** to show the effect of the incorporation of MMT in the mechanical properties of the iongel membranes. As an example, **Figure E.1** from **Appendix E** shows the graphic representation of a puncture test with force as a function of distance.

Table 4.4 - Puncture test results (thickness, puncture stress, normalized puncture stress, and elongation upon puncture) of the iongels with 0.0, 0.2, 0.5, and 1.0 wt% MMT loading.

MMT loading (wt%)	Thickness (μm)	Puncture stress (MPa)	Normalized puncture stress (MPa/mm)	Elongation upon puncture (%)
0.0	111 \pm 2	0.45 \pm 0.01	4.1 \pm 0.1	8.3 \pm 0.6
0.2	106 \pm 4	0.56 \pm 0.02	5.3 \pm 0.3	8.0 \pm 0.7
0.5	114 \pm 1	0.48 \pm 0.05	4.2 \pm 0.4	6.9 \pm 1.5
1.0	109 \pm 3	0.57 \pm 0.07	5.3 \pm 0.5	12.2 \pm 0.8

Considering the results obtained for the iongel MMMs of normalized puncture stress, it can be seen that when a dense membrane with evenly dispersed nanoclay was produced, like the one with 0.2 wt%, their mechanical resistance is improved. In particular, an increase of 30% of normalized puncture stress was obtained for the iongel MMM with 0.2 wt% MMT comparatively to the neat iongel. The nanoclay particles distributed within the iongel MMM's matrix probably caused its rigidification by reducing the mobility of the polymer chains and decreasing the free volume. Conversely, when the MMT loading was increased to 0.5 wt%, the respective SEM image (**Table 4.2**) suggested that the dispersion of the clay was not as good as for 0.2 wt%, which could have restricted the mechanical resistance of the iongel MMM. Moreover, the formation of agglomerations detected in the SEM images (**Table 4.2**) could have decreased the cross-linking density and added points of concentrated stress, making the iongel MMM more fragile and with the lowest normalized puncture stress of the iongel MMMs, with a result similar to the neat iongel.

Regarding the results obtained for the elongation upon puncture, it can be stated that the iongel membranes become slightly less stretchable when 0.2 wt% and 0.5 wt% of MMT are incorporated. This effect is less accentuated in the iongel MMM with 0.2 wt% MMT probably due to the homogeneity of its matrix. This may be justified by the additional rigidity verified for the iongel MMM with 0.2 wt% and by the additional fragility of the iongel MMM with 0.5 wt% MMT loading.

Regarding the iongel MMM with 1.0 wt% MMT, despite the nanoclay concentration being 5 times higher than in the iongel MMM with 0.2 wt% MMT, their variation in

normalized puncture stress was the same (30% higher than the neat iongel). This means that even with the holes and the likely agglomerations that this iongel MMM had, the presence of 1.0 wt% of nanoclay particles was enough to provide an improvement in its mechanical properties. Additionally, it was also verified a considerable improvement in flexibility with an elongation upon puncture 48% higher than the neat iongel, due to a structure that had a lower cross-linking density caused by the presence of holes (**Figure 4.9**).

To conclude, the results discussed above indicate that the incorporation of nanoclay particles into an iongel membrane can be beneficial to its mechanical properties as expected, but only if an effective dispersion of the filler is accomplished. This may allow the production of PEGDA-based iongel membranes containing higher IL loadings (> 60 wt%) that provide superior affinity towards CO₂ and better gas separations while maintaining mechanical stability.

4.8. Pure Gas Permeation Experiments

The pure gas permeation experiments provide some of the most important results of this thesis. They determine the iongel membranes' potential to be used for CO₂ separation from N₂ in post-combustion streams, and CH₄ for biogas upgrading. The iongel membranes' performance is characterized by their permeability to CO₂ and ideal selectivity of the gas pairs CO₂/N₂ and CO₂/CH₄.

As an example, the pressure variation obtained during an experiment and the linear fitting to determine the permeability of N₂ are shown in **Figure F.1** and **Figure F.2** from **Appendix F**, respectively. The iongel membranes' permeability for the tested gases as a function of MMT loading is illustrated in **Figure 4.11**. The results of the iongel membranes' performance are presented in **Table 4.5**, as well as their thicknesses. As already mentioned in **Section 4.4**, the iongel MMM with 1.0 wt% MMT loading was not considered for these experiments due to its inappropriate morphology demonstrated by SEM images.

Looking at **Table 4.5** is possible to see that the incorporation of 0.2 wt% MMT did not have a significant impact on the CO₂ permeability, which was maintained around 40 Barrer. Conversely, that same concentration of MMT was able to cause a small decrease in the N₂ and CH₄ permeabilities. These results can be explained by the morphology obtained for this iongel MMM. As already discussed, a good dispersion of nanoclay particles within the iongel matrix must have caused a rigidification of the membrane by filling the spaces in the cross-linked network. This reduced the free volume available for the diffusion of the gas molecules, an effect that is more noticeable in bigger molecules like N₂ (0.36 nm)²⁶ and CH₄ (0.38 nm)²⁶ while the smaller CO₂ molecules (0.33 nm)²⁶ were not

significantly affected. This means that by adding 0.2 wt% MMT to the iongel MMM, it was possible to produce a membrane that was more selective and mechanically resistant, without compromising the CO₂ permeation.

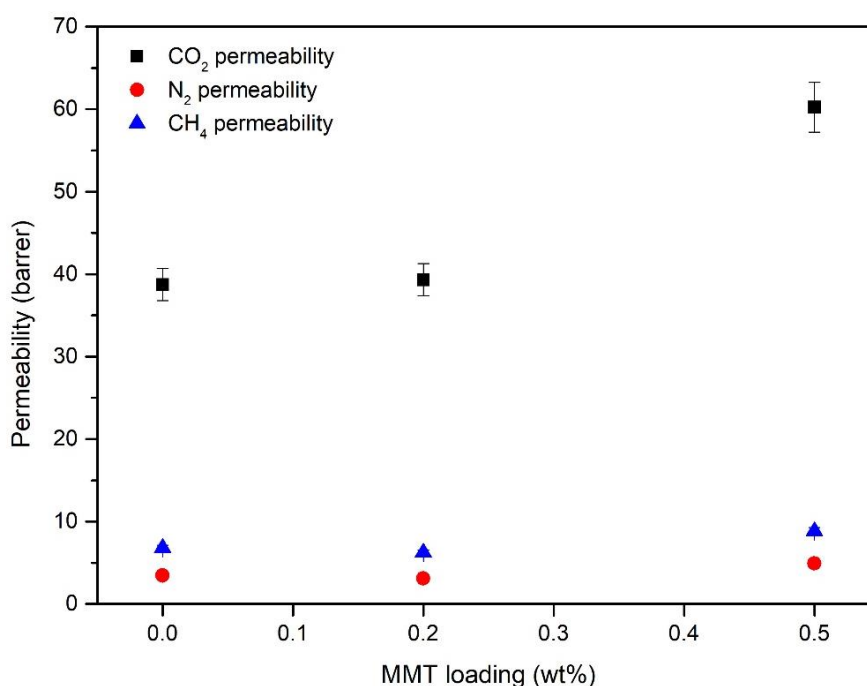


Figure 4.11 - CO₂, N₂ and CH₄ permeabilities of the iongels with 0.0, 0.2 and 0.5 wt% MMT loading.

Table 4.5 - Membrane thicknesses, CO₂, N₂, and CH₄ permeabilities, and ideal selectivities of the iongels with 0.0, 0.2, and 0.5 wt% MMT loading.

MMT loading (wt%)	Membrane thickness (μm)	Permeability (Barrer)			Ideal selectivity	
		CO ₂	N ₂	CH ₄	α (CO ₂ /N ₂)	α (CO ₂ /CH ₄)
0.0	123.8 ± 0.7	38.7 ± 1.9	3.5 ± 0.2	6.8 ± 0.3	11.2 ± 0.6	5.7 ± 0.3
0.2	124.6 ± 0.9	39.3 ± 2.0	3.1 ± 0.2	6.2 ± 0.3	12.6 ± 0.6	6.3 ± 0.3
0.5	120.8 ± 0.4	60.3 ± 3.0	4.9 ± 0.2	8.8 ± 0.4	12.2 ± 0.6	6.8 ± 0.3

Regarding the iongel MMM with 0.5 wt%, it was verified a significant increase in the permeability of all gases. The heterogeneous structure obtained for this membrane, included agglomerations of MMT particles, which probably reduced the cross-linking density of PEGDA and increased the distance between polymer chains, providing more free volume and facilitating gas diffusion. As previously mentioned, the other factor that affects gas diffusion is the size of gas molecules. Consequently, the permeability of the gases increased according to the reduction of their diameter, that is 29%, 40%, and 56% for CH₄ (0.38 nm) > N₂ (0.36 nm) > CO₂ (0.33 nm)²⁶, respectively, compared to the neat iongel. Despite this result, it was still possible to achieve an increase in selectivity for both gas pairs relative to the neat iongel. However, when comparing the iongel MMMs with

0.2 wt% and 0.5 wt%, the results demonstrate that the addition of a superior quantity of MMT did not have an impact on the selectivity of the membrane, probably due to its unsuccessful filler dispersion. Although, it is believed that by optimizing the preparation of the membranes it may be possible to produce iongel MMMs with improved CO₂ separation performance.

Regarding the abovementioned results about the effect of MMT on the iongel membranes' CO₂ separation performance, it is important to take into consideration the CO₂ solubility measurements performed on MMT (**Section 4.3**). These results demonstrated no affinity between CO₂ and the nanoclay particles, establishing that the increased CO₂ permeability was only a consequence of higher diffusivity, not being affected by solubility.

In general, the CO₂ permeability of all the iongel membranes is significantly superior to those of N₂ and CH₄, as expected. The reason may be related to diffusivity, but also with solubility (**Equation 9**). As previously mentioned, CO₂ is a highly condensable gas and has a high affinity for the iongel due to the interactions established between the quadrupole of the molecule and the electrical charges of the IL, which is the major component of the iongel membranes (60 wt%). Therefore, it can be assumed that the superior CO₂ permeation through the iongel membranes relative to the other light gases is explained by a combination of enhanced diffusivity and solubility, while the permeation of N₂ and CH₄ is mainly controlled by diffusivity.

Comparing the selectivity results of the considered gas pairs, CO₂/N₂ and CO₂/CH₄, the results demonstrated that the prepared iongel membranes have more potential to separate the first pair, aiming for their application on the separation of CO₂ from post-combustion streams.

Lastly, in order to compare the obtained results with those already published in the literature, the values were represented in typical Robeson plots⁴¹ of CO₂ permeability as a function of ideal selectivity, illustrated in **Figure 4.12** for the gas pair CO₂/N₂ and in **Figure 4.13** for the pair CO₂/CH₄.

Examining these figures is possible to compare the performance between the typical MMMs (without IL) and the prepared iongel MMMs, both with nanoclay fillers incorporated into them. The figures show that the iongel MMMs have significantly improved CO₂ permeability and overall have better CO₂ separation results against the majority of typical MMMs, especially considering the gas pair CO₂/N₂ (**Figure 4.12**).

Regarding the PIL/IL membranes, the figures show that the prepared iongel membranes have CO₂ permeabilities similar to or higher than most PIL/IL membranes. However, when the IL loading added to PIL membranes is increased (mostly up to 60 wt%), the respective CO₂ permeabilities become one order of magnitude higher than the

prepared iongel membranes. Bearing this in mind, it is expected that concentrations of $[C_2mim][Tf_2N]$ IL higher than 60 wt% incorporated into the iongel membranes could significantly improve their separation performance. For that composition to be accomplished, it seems reasonable to rely on the incorporation of nanoclay particles for extra mechanical resistance, considering the results presented in **Section 4.7**.

Regardless of not surpassing the 2008 Robeson upper bound, these iongel membranes represent a step forward on the way to improving the design of high-performance self-standing membranes with a novel study focused on material science about the combination of nanoclays with a UV cross-linked PEGDA iongel using a simple and promising strategy.

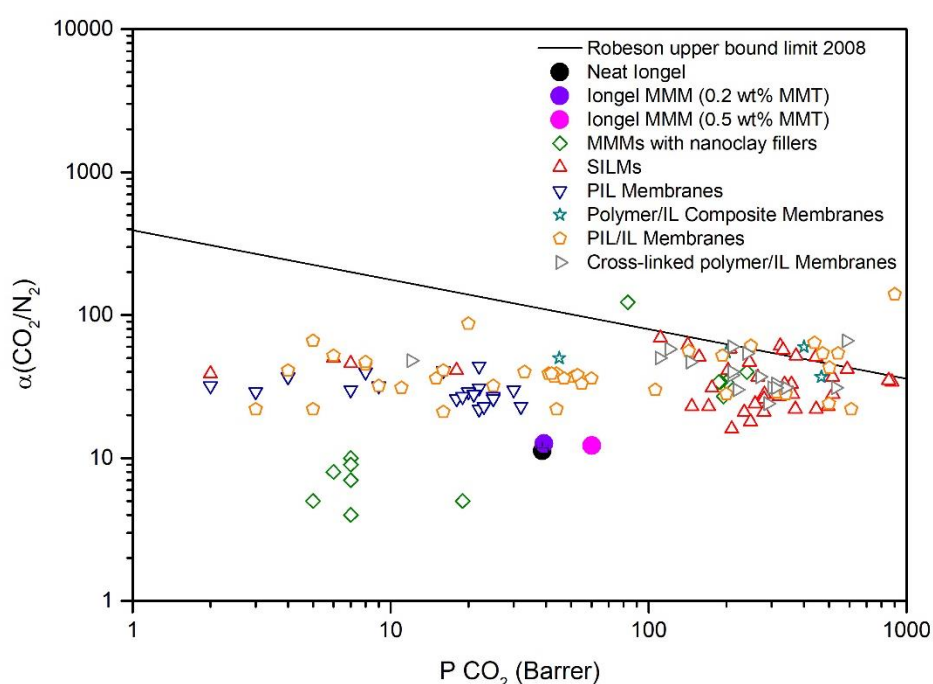


Figure 4.12 – CO_2 separation performance of the prepared iongel membranes and of other membranes reported in the literature^{65,69–71,90,92,93,96,97,100–102,104–106,116,121,124,126–131,134,136,140,144,147–152,156–158,202} (see **Appendix A**) plotted on a CO_2/N_2 Robeson plot. Data are plotted on a log-log scale and the upper bound is adapted from Robeson.⁴¹

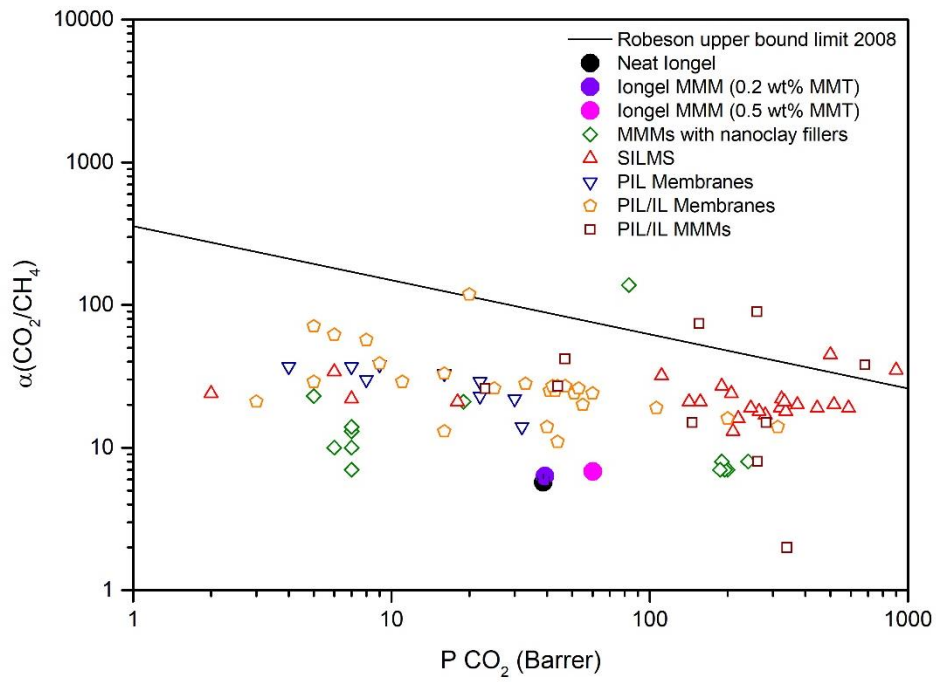


Figure 4.13 – CO₂ separation performance of the prepared iongel membranes and of other membranes reported in the literature^{29,48,65,69–72,92,93,97,99,104,105,116,121,124,126,128,134,147–149,154,156–158,201} (see **Appendix A**) plotted on a CO₂/CH₄ Robeson plot. Data are plotted on a log-log scale and the upper bound is adapted from Robeson.⁴¹

CONCLUSION

The purpose of this thesis was to improve the mechanical properties of iongel membranes developed for CO₂ separation from post-combustion streams and biogas upgrading by incorporating MMT nanoclay particles. In this line, UV cross-linked PEGDA iongel membranes containing 60 wt% of [C₂mim][Tf₂N] IL were prepared with different MMT loadings, and their properties were studied using several techniques, as well as their CO₂/N₂ and CO₂/CH₄ separation performances.

After the preparation, solid and malleable free-standing iongel membranes were obtained for all the compositions. They looked homogeneous and defect-free by visual inspection. The lack of transparency presented by the iongel MMMs compared to the neat iongel suggested that the incorporation of MMT was successful. However, it was not possible to confirm this by ATR-FTIR, since the MMT concentrations used were very low (≤ 1 wt%). On the other hand, this technique showed that the [C₂mim][Tf₂N] IL was successfully incorporated into the PEGDA iongel membranes and also confirmed the proper photopolymerization of the acrylate groups.

The TGA indicated that with the addition of MMT, the iongel MMMs start to degrade at slightly higher temperatures than the neat iongel. On the other hand, their thermal stability depends on the type and quantity of nanoclay organic modifier used. All the prepared iongel membranes can withstand temperatures up to 120 °C, that is typical of post-combustion streams. The SEM images revealed a dense, defect-free and homogeneous surface for the neat iongel and the iongel MMM with 0.2 wt% MMT loading. However, this technique suggested that increasing the nanoclay concentration up to 1.0 wt% resulted in the formation of agglomerations, turning the membranes into heterogeneous materials, which are inappropriate for gas permeation experiments. DSC revealed that the iongel membranes are amorphous materials and that the addition of MMT did not affect the iongel MMMs' crystallinity in a meaningful way. All the iongel membranes proved to be hydrophilic, an advantage when considering their application for CO₂

separation. The study of the mechanical properties showed that the addition of MMT can be beneficial, but only if a membrane with a homogeneous structure is accomplished, focusing on an effective dispersion of the nanoclay particles.

Regarding the results of the gas permeation experiments, the iongel membranes showed more affinity towards CO₂ relative to the N₂ and CH₄, having more potential for the separation of the CO₂/N₂ gas pair. The MMT particles were homogeneously incorporated into the iongel MMMs, probably filling some of the free space of the cross-linked PEGDA network within the IL phase, making the diffusion of molecules with kinetic diameters superior to CO₂ (0.33 nm)²⁶ slightly more difficult. The CO₂ solubility measurements demonstrated that the incorporation of MMT did not affect the solubility of CO₂ in the iongel MMMs, which was mainly a consequence of the interactions established with the IL.

Overall, this study allowed the development of a new simple approach with potential to improve the mechanical resistance of PEGDA-based iongel membranes, which should be further researched in order to incorporate higher contents of IL (< 60 wt%) and produce self-standing high-performance iongel membranes for CO₂ separation from light gases, that may lead to an improvement over some of the membranes already studied.

FUTURE WORK

Considering the aimed application, the targeted membranes could either be completely dense or asymmetric (with a dense layer and a porous layer for support). A dense and homogeneous layer is the key to good gas separation performance. Therefore, despite the neat iongel being appropriate, the iongel MMMs need their preparation to be optimized in future studies in order to allow the incorporation of higher IL loadings (> 60 wt%).

This optimization could be approached considering two characteristics of nanoclays: their ability to be dispersed into individual layers when incorporated into a polymeric matrix and the ability to manipulate their surface chemistry by ion-exchange reactions using different organic or inorganic cations.⁶⁴ The characteristics are related to each other since the degree of dispersion of the clay depends on the compatibility between the interlayer exchangeable cations and the polymer.

Bearing in mind that the iongel membranes are prepared with a hydrophilic polymer, due to the PEG units, it would be interesting trying to use MMT in its pristine state i.e., without modification, since it contains hydrated Na^+ or K^+ ions in the interlayers, probably making the clays miscible with hydrophilic polymers.⁶⁴ With this approach, the preparation method would differ from the one presented here, because the nanoclay particles should be added to PEGDA in the first place.

Considering that the iongel membranes are mainly composed of a hydrophobic IL, another potential approach would be the use of MMT functionalized with a different organic modifier from the one used (methyl dihydroxyethyl hydrogenated tallow ammonium) that has higher compatibility with the matrix.¹⁸⁷ To produce a more compatible clay, organic modifiers like primary, secondary, tertiary, and quaternary alkyl ammonium, or alkyl phosphonium cations can be used in ion-exchange reactions with pristine MMT (**Table 1.2**) or different commercially available organically modified clays can be considered, like those listed in **Table 6.1**, which are recommended to incorporate into polyethylene-based polymeric matrices.⁶⁴

Additionally, in further studies, different lengths or types of alkyl chains can be used, the number of polar groups can be altered and the modifier concentration can be varied.⁶⁴

Table 6.1 - Commercially available surface modified MMT nanoclays suggested as fillers.

Commercial name	Organic modifier	Ref.
Nanomer I.31PS	15-35 wt% octadecylamine; 0.5-5 wt% aminopropyltriethoxysilane	194
Nanomer I.44P	35-45 wt% dimethyl dialkyl (C ₁₄ -C ₁₈) amine	195

To further improve the iongel membranes' performance, MOFs can also be considered as additional fillers since they have been reported to enhance CO₂ permeability with concentrations up to 30 wt%, producing PIL/IL-based MMMs that exceeded the 2008 Robeson upper bound.^{29,133} Nevertheless, the preparation of homogeneous iongel MMMs would become more challenging. Moreover, MOF selection must be done carefully so that the respective pores may have an appropriate size to preferably allow the permeation of CO₂ as opposed to other light gases. The results reported in the literature regarding the performance of polymeric membranes filled with MOFs indicate Cu-BTC and MIL-53 as potential filler options for CO₂/N₂ and CO₂/CH₄ separation, respectively.^{52,53,196-200}

Later on, permeation experiments with mixed gases and operational conditions similar to those verified in industrial applications must be done, to evaluate the iongel MMMs' potential considering CO₂ separation from post-combustion streams and biogas upgrading. The effect of higher temperatures (up to 120 °C) and pressure differentials (up to 1.5 bar) on the CO₂ separation performance of iongel MMMs should also be investigated.

REFERENCES

- (1) bp Statistical Review of World Energy 2021|70th edition <https://www.bp.com/content/dam/bp/business-sites/en/global/corporate/pdfs/energy-economics/statistical-review/bp-stats-review-2021-full-report.pdf> (accessed Sep 8, 2021).
- (2) Fossil Fuels & Health <https://www.hsph.harvard.edu/c-change/subtopics/fossil-fuels-health/> (accessed Dec 22, 2020).
- (3) Environment at a Glance Indicators: Climate Change <https://www.oecd.org/environment/environment-at-a-glance/Climate-Change-Archive-March-2020.pdf> (accessed Dec 22, 2020).
- (4) Lindsey, R. Climate Change: Atmospheric Carbon Dioxide <https://www.climate.gov/news-features/understanding-climate/climate-change-atmospheric-carbon-dioxide> (accessed Dec 22, 2020).
- (5) Energy and the environment explained: Greenhouse gases and the climate <https://www.eia.gov/energyexplained/energy-and-the-environment/greenhouse-gases-and-the-climate.php> (accessed Dec 22, 2020).
- (6) United in Science 2020 https://public.wmo.int/en/resources/united_in_science (accessed Dec 22, 2020).
- (7) Gurría, A. *The Paris Agreement 5 Years on: Taking Stock and Looking Forward*; 2020.
- (8) Key Findings: 1.5°C is possible but requires unprecedented and urgent action <https://www.un.org/en/climatechange/science/key-findings> (accessed Dec 22, 2020).
- (9) Vitillo, J. G.; Smit, B.; Gagliardi, L. Introduction: Carbon Capture and Separation. *Am. Chem. Soc.* **2017**, *117*, 9521–9523. <https://doi.org/10.1021/acs.chemrev.7b00403>.
- (10) CCS Image Library - Carbon capture and storage images: Global CCS Institute <https://www.globalccsinstitute.com/resources/ccs-image-library/> (accessed Sep 16, 2021).
- (11) Olajire, A. A. CO₂ Capture and Separation Technologies for End-of-Pipe Applications - A Review. *Energy* **2010**, *35* (6), 2610–2628. <https://doi.org/10.1016/j.energy.2010.02.030>.
- (12) Patel, H. A.; Byun, J.; Yavuz, C. T. Carbon Dioxide Capture Adsorbents: Chemistry and Methods. *ChemSusChem* **2017**, *10* (7), 1303–1317.

- <https://doi.org/10.1002/cssc.201601545>.
- (13) Wilberforce, T.; Baroutaji, A.; Soudan, B.; Al-Alami, A. H.; Olabi, A. G. Outlook of Carbon Capture Technology and Challenges. *Sci. Total Environ.* **2019**, *657*, 56–72. <https://doi.org/10.1016/j.scitotenv.2018.11.424>.
 - (14) Mertz, B.; Davidson, O.; Coninck, H. de; Loos, M.; Meyer, L. *IPCC Special Report on Carbon Dioxide Capture and Storage*, Cambridge, 2005.
 - (15) Mumford, K. A.; Wu, Y.; Smith, K. H.; Stevens, G. W. Review of Solvent Based Carbon-Dioxide Capture Technologies. *Front. Chem. Sci. Eng.* **2015**, *9* (2), 125–141. <https://doi.org/10.1007/s11705-015-1514-6>.
 - (16) Pires, J. C. M.; Martins, F. G.; Alvim-Ferraz, M. C. M.; Simões, M. Recent Developments on Carbon Capture and Storage: An Overview. *Chem. Eng. Res. Des.* **2011**, *89* (9), 1446–1460. <https://doi.org/10.1016/j.cherd.2011.01.028>.
 - (17) Burdyny, T.; Struchtrup, H. Hybrid Membrane/Cryogenic Separation of Oxygen from Air for Use in the Oxy-Fuel Process. *Energy* **2010**, *35* (5), 1884–1897. <https://doi.org/10.1016/j.energy.2009.12.033>.
 - (18) *Three Basic Methods to Separate Gases*, 2008.
 - (19) Images - CO2CRC: Cooperative Research Centre for Greenhouse Gas Technologies <https://co2crc.com.au/resources/images/> (accessed Sep 16, 2021).
 - (20) Wang, S.; Li, X.; Wu, H.; Tian, Z.; Xin, Q.; He, G.; Peng, D.; Chen, S.; Yin, Y.; Jiang, Z.; Guiver, M. D. Advances in High Permeability Polymer-Based Membrane Materials for CO₂ Separations. *Energy Environ. Sci.* **2016**, *9* (6), 1863–1890. <https://doi.org/10.1039/c6ee00811a>.
 - (21) Sabouni, R.; Kazemian, H.; Rohani, S. Carbon Dioxide Capturing Technologies: A Review Focusing on Metal Organic Framework Materials (MOFs). *Environ. Sci. Pollut. Res.* **2014**, *21* (8), 5427–5449. <https://doi.org/10.1007/s11356-013-2406-2>.
 - (22) Maqsood, K.; Ali, A.; Shariff, A. B. M.; Ganguly, S. Process Intensification Using Mixed Sequential and Integrated Hybrid Cryogenic Distillation Network for Purification of High CO₂ Natural Gas. *Chem. Eng. Res. Des.* **2017**, *117*, 414–438. <https://doi.org/10.1016/j.cherd.2016.10.011>.
 - (23) Yousef, A. M.; El-Maghlany, W. M.; Eldrainy, Y. A.; Attia, A. New Approach for Biogas Purification Using Cryogenic Separation and Distillation Process for CO₂ Capture. *Energy* **2018**, *156*, 328–351. <https://doi.org/10.1016/j.energy.2018.05.106>.
 - (24) Bernardo, P.; Drioli, E.; Golemme, G. Membrane Gas Separation: A Review/State of the Art. *Ind. Eng. Chem. Res.* **2009**, *48* (10), 4638–4663. <https://doi.org/10.1021/ie8019032>.
 - (25) Norahim, N.; Yaisanga, P.; Faungnawakij, K.; Charinpanitkul, T.; Klaysom, C. Recent Membrane Developments for CO₂ Separation and Capture. *Chem. Eng. Technol.* **2018**, *41* (2), 211–223. <https://doi.org/10.1002/ceat.201700406>.
 - (26) Tomé, L. C.; Marrucho, I. M. Ionic Liquid-Based Materials: A Platform to Design Engineered CO₂ Separation Membranes. *R. Soc. Chem.* **2016**, *45* (10), 2785–2824. <https://doi.org/10.1039/c5cs00510h>.

- (27) Xu, J.; Wu, H.; Wang, Z.; Qiao, Z.; Zhao, S.; Wang, J. Recent Advances on the Membrane Processes for CO₂ Separation. *Chinese J. Chem. Eng.* **2018**, *26* (11), 2280–2291. <https://doi.org/10.1016/j.cjche.2018.08.020>.
- (28) Baena-Moreno, F. M.; le Saché, E.; Pastor-Pérez, L.; Reina, T. R. Membrane-Based Technologies for Biogas Upgrading: A Review. *Environ. Chem. Lett.* **2020**, *18* (5), 1649–1658. <https://doi.org/10.1007/s10311-020-01036-3>.
- (29) Sampaio, A. M.; Nabais, A. R.; Tomé, L. C.; Neves, L. A. Impact of MOF-5 on Pyrrolidinium-Based Poly(Ionic Liquid)/Ionic Liquid Membranes for Biogas Upgrading. *Ind. Eng. Chem. Res.* **2020**, *59* (1), 308–317. <https://doi.org/10.1021/acs.iecr.9b04206>.
- (30) García-Gutiérrez, P.; Jacquemin, J.; McCrellis, C.; Dimitriou, I.; Taylor, S. F. R.; Hardacre, C.; Allen, R. W. K. Techno-Economic Feasibility of Selective CO₂ Capture Processes from Biogas Streams Using Ionic Liquids as Physical Absorbents. *Energy and Fuels* **2016**, *30* (6), 5052–5064. <https://doi.org/10.1021/acs.energyfuels.6b00364>.
- (31) He, X. A Review of Material Development in the Field of Carbon Capture and the Application of Membrane-Based Processes in Power Plants and Energy-Intensive Industries. *Energy. Sustain. Soc.* **2018**, *8*(34), 1–14. <https://doi.org/10.1186/s13705-018-0177-9>.
- (32) Valappil, R. S. K.; Ghasem, N.; Al-Marzouqi, M. Current and Future Trends in Polymer Membrane-Based Gas Separation Technology: A Comprehensive Review. *J. Ind. Eng. Chem.* **2021**, *98*, 103–129. <https://doi.org/10.1016/j.jiec.2021.03.030>.
- (33) Nabais, A. R. *Preparação e Caracterização de Membranas de Matriz Mista Para Separação de CO₂*, Universidade Nova de Lisboa, 2016.
- (34) Mulder, M. *Basic Principles of Membrane Technology*, 2nd ed.; Kluwer Academic Publishers: The Netherlands, 1996.
- (35) Neves, L. A.; Crespo, J. G.; Coelho, I. M. Gas Permeation Studies in Supported Ionic Liquid Membranes. *J. Memb. Sci.* **2010**, *357*, 160–170. <https://doi.org/10.1016/j.memsci.2010.04.016>.
- (36) Gu, Y.; Lodge, T. P. Synthesis and Gas Separation Performance of Triblock Copolymer Ion Gels with a Polymerized Ionic Liquid Mid-Block. *Macromolecules* **2011**, *44* (7), 1732–1736. <https://doi.org/10.1021/ma2001838>.
- (37) Farnam, M.; bin Mukhtar, H.; bin Mohd Shariff, A. A Review on Glassy and Rubbery Polymeric Membranes for Natural Gas Purification. *ChemBioEng Rev.* **2021**, *8* (2), 90–109. <https://doi.org/10.1002/cben.202100002>.
- (38) Deng, L.; Xue, Y.; Yan, J.; Lau, C. H.; Cao, B.; Li, P. Oxidative Crosslinking of Copolyimides at Sub-T_g Temperatures to Enhance Resistance against CO₂-Induced Plasticization. *J. Memb. Sci.* **2019**, *583*, 40–48. <https://doi.org/10.1016/j.memsci.2019.04.002>.
- (39) Dong, G.; Li, H.; Chen, V. Plasticization Mechanisms and Effects of Thermal Annealing of Matrimid Hollow Fiber Membranes for CO₂ Removal. *J. Memb. Sci.* **2011**, *369*, 206–220. <https://doi.org/10.1016/j.memsci.2010.11.064>.
- (40) Mazinani, S.; Ramezani, R.; Molelekwa, G. F.; Darvishmanesh, S.; Di Felice, R.; Van der Bruggen, B. Plasticization Suppression and CO₂ Separation Enhancement of Matrimid

- through Homogeneous Blending with a New High Performance Polymer. *J. Memb. Sci.* **2019**, *574*, 318–324. <https://doi.org/10.1016/j.memsci.2018.12.060>.
- (41) Robeson, L. M. The Upper Bound Revisited. *J. Memb. Sci.* **2008**, *320* (1–2), 390–400. <https://doi.org/10.1016/j.memsci.2008.04.030>.
- (42) Comesaña-Gándara, B.; Chen, J.; Bezzu, C. G.; Carta, M.; Rose, I.; Ferrari, M. C.; Esposito, E.; Fuoco, A.; Jansen, J. C.; McKeown, N. B. Redefining the Robeson Upper Bounds for CO₂/CH₄ and CO₂/N₂ Separations Using a Series of Ultraporous Benzotriptycene-Based Polymers of Intrinsic Microporosity. *Energy Environ. Sci.* **2019**, *12* (9), 2733–2740. <https://doi.org/10.1039/c9ee01384a>.
- (43) Lai, T.; Yin, H.; Lind, M. L. The Hydrogen Permeability of Cu-Zr Binary Amorphous Metallic Membranes and the Importance of Thermal Stability. *J. Memb. Sci.* **2015**, *489*, 264–269. <https://doi.org/10.1016/j.memsci.2015.03.098>.
- (44) Chuah, C. Y.; Lee, J.; Song, J.; Bae, T. H. Carbon Molecular Sieve Membranes Comprising Graphene Oxides and Porous Carbon for CO₂/N₂ Separation. *Membranes (Basel)*. **2021**, *11*, 1–13. <https://doi.org/10.3390/membranes11040284>.
- (45) Ping, E. W.; Zhou, R.; Funke, H. H.; Falconer, J. L.; Noble, R. D. Seeded-Gel Synthesis of SAPO-34 Single Channel and Monolith Membranes, for CO₂/CH₄ Separations. *J. Memb. Sci.* **2012**, *415–416*, 770–775. <https://doi.org/10.1016/j.memsci.2012.05.068>.
- (46) Lara-Medina, J. J.; Torres-Rodríguez, M.; Gutiérrez-Arzaluz, M.; Mugica-Alvarez, V. Separation of CO₂ and N₂ with a Lithium-Modified Silicalite-1 Zeolite Membrane. *Int. J. Greenh. Gas Control* **2012**, *10*, 494–500. <https://doi.org/10.1016/j.ijggc.2012.07.014>.
- (47) Muntha, S. T.; Kausar, A.; Siddiq, M. Progress in Applications of Polymer-Based Membranes in Gas Separation Technology. *Polym. - Plast. Technol. Eng.* **2016**, *55* (12), 1282–1298. <https://doi.org/10.1080/03602559.2016.1163592>.
- (48) Singh, Z. V.; Cowan, M. G.; McDanel, W. M.; Luo, Y.; Zhou, R.; Gin, D. L.; Noble, R. D. Determination and Optimization of Factors Affecting CO₂/CH₄ Separation Performance in Poly(Ionic Liquid)-Ionic Liquid-Zeolite Mixed-Matrix Membranes. *J. Memb. Sci.* **2016**, *509*, 149–155. <https://doi.org/10.1016/j.memsci.2016.02.034>.
- (49) Ahmad, M. Z.; Martin-Gil, V.; Supinkova, T.; Lambert, P.; Castro-Muñoz, R.; Hrabanek, P.; Kocirik, M.; Fila, V. Novel MMM Using CO₂ Selective SSZ-16 and High-Performance 6FDA-Polyimide for CO₂/CH₄ Separation. *Sep. Purif. Technol.* **2021**, *254*, 117582. <https://doi.org/10.1016/j.seppur.2020.117582>.
- (50) Nasir, R.; Mukhtar, H.; Man, Z.; Shaharun, M. S.; Bakar, M. Z. A. Development and Performance Prediction of Polyethersulfone-Carbon Molecular Sieve Mixed Matrix Membrane for CO₂/CH₄ Separation. *Chem. Eng. Trans.* **2015**, *45*, 1417–1422. <https://doi.org/10.3303/CET1545237>.
- (51) Zhao, D.; Ren, J.; Wang, Y.; Qiu, Y.; Li, H.; Hua, K.; Li, X.; Ji, J.; Deng, M. High CO₂ Separation Performance of Pebax®/CNTs/GTA Mixed Matrix Membranes. *J. Memb. Sci.* **2017**, *521*, 104–113. <https://doi.org/10.1016/j.memsci.2016.08.061>.
- (52) Nabais, A. R.; Ribeiro, R. P. P. L.; Mota, J. P. B.; Alves, V. D.; Esteves, I. A. A. C.; Neves, L. A. CO₂/N₂ Gas Separation Using Fe(BTC)-Based Mixed Matrix Membranes: A View on the Adsorptive and Filler Properties of Metal-Organic Frameworks. *Sep. Purif. Technol.* **2018**,

- 202 (March), 174–184. <https://doi.org/10.1016/j.seppur.2018.03.028>.
- (53) Monteiro, B.; Nabais, A. R.; Casimiro, M. H.; Martins, A. P. S.; Francisco, R. O.; Neves, L. A.; Pereira, C. C. L. Impact on CO₂/N₂ and CO₂/CH₄ Separation Performance Using Cu-BTC with Supported Ionic Liquids-Based Mixed Matrix Membranes. *Membranes (Basel)*. **2018**, *8* (93), 1–11. <https://doi.org/10.3390/membranes8040093>.
- (54) van Essen, M.; van den Akker, L.; Thür, R.; Houben, M.; Vankelecom, I. F. J.; Borneman, Z.; Nijmeijer, K. The Influence of Pore Aperture, Volume and Functionality of Isoreticular Gmelinite Zeolitic Imidazolate Frameworks on the Mixed Gas CO₂/N₂ and CO₂/CH₄ Separation Performance in Mixed Matrix Membranes. *Sep. Purif. Technol.* **2021**, *260*, 118103. <https://doi.org/10.1016/j.seppur.2020.118103>.
- (55) Amini, Z.; Asghari, M. Preparation and Characterization of Ultra-Thin Poly Ether Block Amide/Nanoclay Nanocomposite Membrane for Gas Separation. *Appl. Clay Sci.* **2018**, *166*, 230–241. <https://doi.org/10.1016/j.clay.2018.09.025>.
- (56) Shen, J.; Zhang, M.; Liu, G.; Guan, K.; Jin, W. Size Effects of Graphene Oxide on Mixed Matrix Membranes for CO₂ Separation. *AIChE J.* **2016**, *62* (8), 2843–2852. <https://doi.org/10.1002/aic.15260>.
- (57) Azizi, S.; Azizi, N.; Homayoon, R. Experimental Study of CO₂ and CH₄ Permeability Values Through Pebax®-1074/Silica Mixed Matrix Membranes. *Silicon* **2019**, *11* (4), 2045–2057. <https://doi.org/10.1007/s12633-018-0021-z>.
- (58) Azizi, N.; Isanejad, M.; Mohammadi, T.; Behbahani, R. M. Effect of TiO₂ Loading on the Morphology and CO₂/CH₄ Separation Performance of PEBA-X-Based Membranes. *Front. Chem. Sci. Eng.* **2019**, *13* (3), 517–530. <https://doi.org/10.1007/s11705-018-1781-0>.
- (59) Nor, F. M.; Karim, N. H. A.; Abdullah, I.; Othaman, R. Permeability of Carbon Dioxide and Nitrogen Gases through SiO₂ and MgO Incorporated ENR/PVC Membranes. *J. Elastomers Plast.* **2016**, *48* (6), 483–498. <https://doi.org/10.1177/0095244315580459>.
- (60) Shindo, R.; Kishida, M.; Sawa, H.; Kidesaki, T.; Sato, S.; Kanehashi, S.; Nagai, K. Characterization and Gas Permeation Properties of Polyimide/ZSM-5 Zeolite Composite Membranes Containing Ionic Liquid. *J. Memb. Sci.* **2014**, *454*, 330–338. <https://doi.org/10.1016/j.memsci.2013.12.031>.
- (61) Mohshim, D. F.; Mukhtar, H.; Man, Z. The Effect of Incorporating Ionic Liquid into Polyethersulfone-SAPO34 Based Mixed Matrix Membrane on CO₂ Gas Separation Performance. *Sep. Purif. Technol.* **2014**, *135*, 252–258. <https://doi.org/10.1016/j.seppur.2014.08.019>.
- (62) Jamil, A.; Ching, O. P.; Shariff, A. B. M. Current Status and Future Prospect of Polymer-Layered Silicate Mixed-Matrix Membranes for CO₂/CH₄ Separation. *Chem. Eng. Technol.* **2016**, *39* (8), 1393–1405. <https://doi.org/10.1002/ceat.201500395>.
- (63) Noskov, A. V.; Alekseeva, O. V.; Shibaeva, V. D.; Agafonov, A. V. Synthesis, Structure and Thermal Properties of Montmorillonite/Ionic Liquid Ionogels. *RSC Adv.* **2020**, *10* (57), 34885–34894. <https://doi.org/10.1039/d0ra06443b>.
- (64) Sinha Ray, S. Chapter 1: An Overview of Pure and Organically Modified Clays. In *Clay-containing Polymer Nanocomposites: From Fundamentals to Real Applications*, Elsevier, 2013; pp 1–24. <https://doi.org/10.1016/C2011-0-07134-X>.

- (65) Behroozi, M.; Pakizeh, M. Study the Effects of Cloisite15A Nanoclay Incorporation on the Morphology and Gas Permeation Properties of Pebax2533 Polymer. *J. Appl. Polym. Sci.* **2017**, *134* (37), 1–11. <https://doi.org/10.1002/app.45302>.
- (66) Jamil, A.; Ching, O. P.; Shariff, A. B. M. Polymer-Nanoclay Mixed Matrix Membranes for CO₂/CH₄ Separation: A Review. *Appl. Mech. Mater.* **2014**, *625*, 690–695. <https://doi.org/10.4028/www.scientific.net/AMM.625.690>.
- (67) Coelho, I.; Ferreira, A. R.; Alves, V. Biodegradable Barrier Membranes Based on Nanoclays and Carrageenan/Pectin Blends. *Int. J. Membr. Sci. Technol.* **2014**, *1* (2), 23–30. <https://doi.org/10.15379/2410-1869.2014.01.01.3>.
- (68) Pavlidou, S.; Paspaspyrides, C. D. A Review on Polymer-Layered Silicate Nanocomposites. *Prog. Polym. Sci.* **2008**, *33* (12), 1119–1198. <https://doi.org/10.1016/j.progpolymsci.2008.07.008>.
- (69) Zulhairun, A. K.; Ismail, A. F.; Matsuura, T.; Abdullah, M. S.; Mustafa, A. Asymmetric Mixed Matrix Membrane Incorporating Organically Modified Clay Particle for Gas Separation. *Chem. Eng. J.* **2014**, *241*, 495–503. <https://doi.org/10.1016/j.cej.2013.10.042>.
- (70) Qiao, Z.; Zhao, S.; Wang, J.; Wang, S.; Wang, Z.; Guiver, M. D. A Highly Permeable Aligned Montmorillonite Mixed-Matrix Membrane for CO₂ Separation. *Angew. Chemie - Int. Ed.* **2016**, *55* (32), 9321–9325. <https://doi.org/10.1002/anie.201603211>.
- (71) Jamil, A.; Zulfiqar, M.; Arshad, U.; Mahmood, S.; Iqbal, T.; Rafiq, S.; Iqbal, M. Z. Development and Performance Evaluation of Cellulose Acetate-Bentonite Mixed Matrix Membranes for CO₂ Separation. *Adv. Polym. Technol.* **2020**, *2020*, 1–12. <https://doi.org/10.1155/2020/8855577>.
- (72) Kalantari, K.; Moradihamedani, P.; Ibrahim, N. A.; Abdullah, A. H. Bin; Afifi, A. B. M. Polysulfone Mixed-Matrix Membrane Incorporating Talc Clay Particles for Gas Separation. *Polym. Bull.* **2018**, *75* (8), 3723–3738. <https://doi.org/10.1007/s00289-017-2234-5>.
- (73) Fan, P.; Liu, H.; Marosz, V.; Samuels, N. T.; Suib, S. L.; Sun, L.; Liao, L. High Performance Composite Polymer Electrolytes for Lithium-Ion Batteries. *Adv. Funct. Mater.* **2021**, *2101380*, 1–29. <https://doi.org/10.1002/adfm.202101380>.
- (74) Bordes, P.; Pollet, E.; Avérous, L. Nano-Biocomposites: Biodegradable Polyester/Nanoclay Systems. *Prog. Polym. Sci.* **2009**, *34* (2), 125–155. <https://doi.org/10.1016/j.progpolymsci.2008.10.002>.
- (75) Yan, X.; Anguille, S.; Bendahan, M.; Moulin, P. Ionic Liquids Combined with Membrane Separation Processes: A Review. *Sep. Purif. Technol.* **2019**, *222*, 230–253. <https://doi.org/10.1016/j.seppur.2019.03.103>.
- (76) Porcarelli, L.; Shaplov, A. S.; Salsamendi, M.; Nair, J. R.; Vygodskii, Y. S.; Mecerreyes, D.; Gerbaldi, C. Single-Ion Block Copoly(Ionic Liquid)s as Electrolytes for All-Solid State Lithium Batteries. *ACS Appl. Mater. Interfaces* **2016**, *8* (16), 10350–10359. <https://doi.org/10.1021/acsami.6b01973>.
- (77) Karimi-Maleh, H.; Fakude, C. T.; Mabuba, N.; Peleyeju, G. M.; Arotiba, O. A. The Determination of 2-Phenylphenol in the Presence of 4-Chlorophenol Using Nano-Fe₃O₄/Ionic Liquid Paste Electrode as an Electrochemical Sensor. *J. Colloid Interface Sci.*

- 2019, 554, 603–610. <https://doi.org/10.1016/j.jcis.2019.07.047>.
- (78) Mohammed, H.; Al-Othman, A.; Nancarrow, P.; Elsayed, Y.; Tawalbeh, M. Enhanced Proton Conduction in Zirconium Phosphate/Ionic Liquids Materials for High-Temperature Fuel Cells. *Int. J. Hydrogen Energy* **2021**, *46* (6), 4857–4869. <https://doi.org/10.1016/j.ijhydene.2019.09.118>.
- (79) Chen, S. T.; Renny, M. N.; C. Tomé, L.; Olmedo-Martínez, J. L.; Udabe, E.; Jenkins, E. P. W.; Mecerreyes, D.; Malliaras, G. G.; McLeod, R. R.; Proctor, C. M. Reducing Passive Drug Diffusion from Electrophoretic Drug Delivery Devices through Co-Ion Engineering. *Adv. Sci.* **2021**, *8* (2003995), 1–9. <https://doi.org/10.1002/advs.202003995>.
- (80) Velasco-Bosom, S.; Karam, N.; Carnicer-Lombarte, A.; Gurke, J.; Casado, N.; Tomé, L. C.; Mecerreyes, D.; Malliaras, G. G. Conducting Polymer-Ionic Liquid Electrode Arrays for High-Density Surface Electromyography. *Adv. Healthc. Mater.* **2021**, No. 2100374, 1–6. <https://doi.org/10.1002/adhm.202100374>.
- (81) Li, Q.; Zhang, S.; Wang, Y.; Xiang, J.; Hu, S.; Yuan, X.; Gholizadeh, M.; Hu, X. Ionic Liquid Coupled with Nickel Salt for Enhancing the Hydro-Liquefaction Efficiency of the Major Biomass Components. *Renew. Energy* **2021**, *175*, 296–306. <https://doi.org/10.1016/j.renene.2021.04.143>.
- (82) De Oliveira, H. F. N.; Farès, C.; Rinaldi, R. Beyond a Solvent: The Roles of 1-Butyl-3-Methylimidazolium Chloride in the Acid-Catalysis for Cellulose Depolymerisation. *Chem. Sci.* **2015**, *6* (9), 5215–5224. <https://doi.org/10.1039/c5sc00393h>.
- (83) Zhou, Y.; Boudesocque, S.; Mohamadou, A.; Dupont, L. Extraction of Metal Ions with Task Specific Ionic Liquids: Influence of a Coordinating Anion. *Sep. Sci. Technol.* **2015**, *50*(1), 38–44. <https://doi.org/10.1080/01496395.2014.952747>.
- (84) Lopez, A. M.; Hestekin, J. A. Improved Organic Acid Purification through Wafer Enhanced Electrodeionization Utilizing Ionic Liquids. *J. Memb. Sci.* **2015**, *493*, 200–205. <https://doi.org/10.1016/j.memsci.2015.06.008>.
- (85) Andrzejewska, E.; Marcinkowska, A.; Zgrzeba, A. Ionogels - Materials Containing Immobilized Ionic Liquids. *Polimery* **2017**, *62* (5), 344–352. <https://doi.org/10.14314/polimery.2017.344>.
- (86) Dai, Z.; Noble, R. D.; Gin, D. L.; Zhang, X.; Deng, L. Combination of Ionic Liquids with Membrane Technology: A New Approach for CO₂ Separation. *J. Memb. Sci.* **2016**, *497*, 1–20. <https://doi.org/10.1016/j.memsci.2015.08.060>.
- (87) Akhmetshina, A. A.; Davletbaeva, I. M.; Grebenschikova, E. S.; Sazanova, T. S.; Petukhov, A. N.; Atlaskin, A. A.; Razov, E. N.; Zaripov, I. I.; Martins, C. F.; Neves, L. A.; Vorotyntsev, I. V. The Effect of Microporous Polymeric Support Modification on Surface and Gas Transport Properties of Supported Ionic Liquid Membranes. *Membranes (Basel)*. **2015**, *6*(1). <https://doi.org/10.3390/membranes6010004>.
- (88) Myers, C.; Pennline, H.; Luebke, D.; Ilconich, J.; Dixon, J. N. K.; Maginn, E. J.; Brennecke, J. F. High Temperature Separation of Carbon Dioxide/Hydrogen Mixtures Using Facilitated Supported Ionic Liquid Membranes. *J. Memb. Sci.* **2008**, *322*, 28–31. <https://doi.org/10.1016/j.memsci.2008.04.062>.
- (89) Cichowska-Kopczyńska, I.; Joskowska, M.; Debski, B.; Aranowski, R.; Hupka, J. Separation

- of Toluene from Gas Phase Using Supported Imidazolium Ionic Liquid Membrane. *J. Memb. Sci.* **2018**, *566*, 367–373. <https://doi.org/10.1016/j.memsci.2018.08.058>.
- (90) Albo, J.; Santos, E.; Neves, L. A.; Simeonov, S. P.; Afonso, C. A. M.; Crespo, J. G.; Irabien, A. Separation Performance of CO₂ through Supported Magnetic Ionic Liquid Membranes (SMILMs). *Sep. Purif. Technol.* **2012**, *97*, 26–33. <https://doi.org/10.1016/j.seppur.2012.01.034>.
- (91) Gouveia, A. S. L.; Tomé, L. C.; Lozinskaya, E. I.; Shaplov, A. S.; Vygodskii, Y. S.; Marrucho, I. M. Exploring the Effect of Fluorinated Anions on the CO₂/N₂ Separation of Supported Ionic Liquid Membranes. *Phys. Chem. Chem. Phys.* **2017**, *19* (42), 28876–28884. <https://doi.org/10.1039/c7cp06297d>.
- (92) Tomé, L. C.; Patinha, D. J. S.; Ferreira, R.; Garcia, H.; Pereira, C. S.; Freire, C. S. R.; Rebelo, L. P. N.; Marrucho, I. M. Cholinium-Based Supported Ionic Liquid Membranes: A Sustainable Route for Carbon Dioxide Separation. *ChemSusChem* **2014**, *7*(1), 110–113. <https://doi.org/10.1002/cssc.201300613>.
- (93) Tomé, L. C.; Patinha, D. J. S.; Freire, C. S. R.; Rebelo, L. P. N.; Marrucho, I. M. CO₂ Separation Applying Ionic Liquid Mixtures: The Effect of Mixing Different Anions on Gas Permeation through Supported Ionic Liquid Membranes. *RSC Adv.* **2013**, *3*(30), 12220–12229. <https://doi.org/10.1039/c3ra41269e>.
- (94) Alkhouzaam, A.; Khraisheh, M.; Atilhan, M.; Al-Muhtaseb, S. A.; Qi, L.; Rooney, D. High-Pressure CO₂/N₂ and CO₂/CH₄ Separation Using Dense Polysulfone-Supported Ionic Liquid Membranes. *J. Nat. Gas Sci. Eng.* **2016**, *36*, 472–485. <https://doi.org/10.1016/j.jngse.2016.10.061>.
- (95) Kulkarni, P. S.; Neves, L. A.; Coelho, I. M.; Afonso, C. A. M. M.; Crespo, G. J.; Crespo, J. G. Supported Ionic Liquid Membranes for Removal of Dioxins from High-Temperature Vapor Streams. *Environ. Sci. Technol.* **2012**, *46* (1), 462–468. <https://doi.org/10.1021/es2024302>.
- (96) Neves, L. A.; Nemestóthy, N.; Alves, V. D.; Cserjési, P.; Bélafi-Bakó, K.; Coelho, I. M. Separation of Biohydrogen by Supported Ionic Liquid Membranes. *Desalination* **2009**, *240*(1–3), 311–315. <https://doi.org/10.1016/j.desal.2007.10.095>.
- (97) Bara, J. E.; Gabriel, C. J.; Carlisle, T. K.; Camper, D. E.; Finotello, A.; Gin, D. L.; Noble, R. D. Gas Separations in Fluoroalkyl-Functionalized Room-Temperature Ionic Liquids Using Supported Liquid Membranes. *Chem. Eng. J.* **2009**, *147* (1), 43–50. <https://doi.org/10.1016/j.cej.2008.11.021>.
- (98) Hojniak, S. D.; Silverwood, I. P.; Khan, A. L.; Vankelecom, I. F. J.; Dehaen, W.; Kazarian, S. G.; Binnemans, K. Highly Selective Separation of Carbon Dioxide from Nitrogen and Methane by Nitrile/Glycol-Difunctionalized Ionic Liquids in Supported Ionic Liquid Membranes (SILMs). *J. Phys. Chem. B* **2014**, *118* (26), 7440–7449. <https://doi.org/10.1021/jp503259b>.
- (99) Shahkaramipour, N.; Adibi, M.; Seifkordi, A. A.; Fazli, Y. Separation of CO₂/CH₄ through Alumina-Supported Geminal Ionic Liquid Membranes. *J. Memb. Sci.* **2014**, *455*, 229–235. <https://doi.org/10.1016/j.memsci.2013.12.039>.
- (100) Mahurin, S. M.; Dai, T.; Yeary, J. S.; Luo, H.; Dai, S. Benzyl-Functionalized Room

- Temperature Ionic Liquids for CO₂/N₂ Separation. *Ind. Eng. Chem. Res.* **2011**, *50* (24), 14061–14069. <https://doi.org/10.1021/ie201428k>.
- (101) Hillesheim, P. C.; Mahurin, S. M.; Fulvio, P. F.; Yeary, J. S.; Oyola, Y.; Jiang, D. E.; Dai, S. Synthesis and Characterization of Thiazolium-Based Room Temperature Ionic Liquids for Gas Separations. *Ind. Eng. Chem. Res.* **2012**, *51* (35), 11530–11537. <https://doi.org/10.1021/ie3015632>.
- (102) Mahurin, S. M.; Yeary, J. S.; Baker, S. N.; Jiang, D. en; Dai, S.; Baker, G. A. Ring-Opened Heterocycles: Promising Ionic Liquids for Gas Separation and Capture. *J. Memb. Sci.* **2012**, *401–402*, 61–67. <https://doi.org/10.1016/j.memsci.2012.01.042>.
- (103) Mahurin, S. M.; Lee, J. S.; Baker, G. A.; Luo, H.; Dai, S. Performance of Nitrile-Containing Anions in Task-Specific Ionic Liquids for Improved CO₂/N₂ Separation. *J. Memb. Sci.* **2010**, *353* (1–2), 177–183. <https://doi.org/10.1016/j.memsci.2010.02.045>.
- (104) Tomé, L. C.; Florindo, C.; Freire, C. S. R.; Rebelo, L. P. N.; Marrucho, I. M. Playing with Ionic Liquid Mixtures to Design Engineered CO₂ Separation Membranes. *Phys. Chem. Chem. Phys.* **2014**, *16* (32), 17172–17182. <https://doi.org/10.1039/c4cp01434k>.
- (105) Santos, E.; Albo, J.; Irabien, A. Acetate Based Supported Ionic Liquid Membranes (SILMs) for CO₂ Separation: Influence of the Temperature. *J. Memb. Sci.* **2014**, *452*, 277–283. <https://doi.org/10.1016/j.memsci.2013.10.024>.
- (106) Kasahara, S.; Kamio, E.; Ishigami, T.; Matsuyama, H. Effect of Water in Ionic Liquids on CO₂ Permeability in Amino Acid Ionic Liquid-Based Facilitated Transport Membranes. *J. Memb. Sci.* **2012**, *415–416*, 168–175. <https://doi.org/10.1016/j.memsci.2012.04.049>.
- (107) Kasahara, S.; Kamio, E.; Matsuyama, H. Improvements in the CO₂ Permeation Selectivities of Amino Acid Ionic Liquid-Based Facilitated Transport Membranes by Controlling Their Gas Absorption Properties. *J. Memb. Sci.* **2014**, *454*, 155–162. <https://doi.org/10.1016/j.memsci.2013.12.009>.
- (108) Yuan, J.; Mecerreyes, D.; Antonietti, M. Poly(Ionic Liquid)s: An Update. *Prog. Polym. Sci.* **2013**, *38* (7), 1009–1036. <https://doi.org/10.1016/j.progpolymsci.2013.04.002>.
- (109) Mecerreyes, D. Polymeric Ionic Liquids: Broadening the Properties and Applications of Polyelectrolytes. *Prog. Polym. Sci.* **2011**, *36* (12), 1629–1648. <https://doi.org/10.1016/j.progpolymsci.2011.05.007>.
- (110) Tomé, L. C.; Gouveia, A. S. L.; Freire, C. S. R.; Mecerreyes, D.; Marrucho, I. M. Polymeric Ionic Liquid-Based Membranes: Influence of Polycation Variation on Gas Transport and CO₂ Selectivity Properties. *J. Memb. Sci.* **2015**, *486*, 40–48. <https://doi.org/10.1016/j.memsci.2015.03.026>.
- (111) Suckow, M.; Roy, M.; Sahre, K.; Häußler, L.; Singha, N.; Voit, B.; Böhme, F. Synthesis of Polymeric Ionic Liquids with Unidirectional Chain Topology by AB Step Growth Polymerization. *Polymer (Guildf.)* **2017**, *111*, 123–129. <https://doi.org/10.1016/j.polymer.2017.01.063>.
- (112) Vygodskii, Y. S.; Shaplov, A. S.; Lozinskaya, E. I.; Lyssenko, K. A.; Golovanov, D. G.; Malyshkina, I. A.; Gavrilova, N. D.; Buchmeiser, M. R. Conductive Polymer Electrolytes Derived from Poly(Norbornene)s with Pendant Ionic Imidazolium Moieties. *Macromol. Chem. Phys.* **2008**, *209* (1), 40–51. <https://doi.org/10.1002/macp.200700378>.

- (113) Xiong, Y. B.; Wang, H.; Wang, Y. J.; Wang, R. M. Novel Imidazolium-Based Poly(Ionic Liquid)s: Preparation, Characterization, and Absorption of CO₂. *Polym. Adv. Technol.* **2012**, *23* (5), 835–840. <https://doi.org/10.1002/pat.1973>.
- (114) Carlisle, T. K.; Nicodemus, G. D.; Gin, D. L.; Noble, R. D. CO₂/Light Gas Separation Performance of Cross-Linked Poly(Vinylimidazolium) Gel Membranes as a Function of Ionic Liquid Loading and Cross-Linker Content. *J. Memb. Sci.* **2012**, *397–398*, 24–37. <https://doi.org/10.1016/j.memsci.2012.01.006>.
- (115) Zhang, G.; Liu, X.; Li, B.; Bai, Y. Free-Radical Solution Copolymerization of the Ionic Liquid Monomer 1-Vinyl-3-Ethylimidazolium Bromide with Acrylonitrile. *J. Appl. Polym. Sci.* **2009**, *112* (6), 3337–3340. <https://doi.org/10.1002/app.29598>.
- (116) Bara, J. E.; Lessmann, S.; Gabriel, C. J.; Hatakeyama, E. S.; Noble, R. D.; Gin, D. L. Synthesis and Performance of Polymerizable Room-Temperature Ionic Liquids as Gas Separation Membranes. *Ind. Eng. Chem. Res.* **2007**, *46* (16), 5397–5404. <https://doi.org/10.1021/ie0704492>.
- (117) Ding, S.; Tang, H.; Radosz, M.; Shen, Y. Atom Transfer Radical Polymerization of Ionic Liquid 2-(1-Butylimidazolium-3-yl)ethyl Methacrylate Tetrafluoroborate. *J. Polym. Sci. Part A Polym. Chem.* **2004**, *42* (22), 5794–5801. <https://doi.org/10.1002/pola.20423>.
- (118) Obadia, M. M.; Jourdain, A.; Serghei, A.; Ikeda, T.; Drockenmuller, E. Cationic and Dicationic 1,2,3-Triazolium-Based Poly(Ethylene Glycol Ionic Liquid)s. *Polym. Chem.* **2017**, *8* (5), 910–917. <https://doi.org/10.1039/C6PY02030E>.
- (119) Seno, K.-I.; Kanaoka, S.; Aoshima, S. Synthesis and LCST-Type Phase Separation Behavior in Organic Solvents of Poly(Vinyl Ethers) with Pendant Imidazolium or Pyridinium Salts. *J. Polym. Sci. Part A Polym. Chem.* **2008**, *46* (17), 5724–5733. <https://doi.org/10.1002/pola.22881>.
- (120) Marcilla, R.; Blazquez, J. A.; Fernandez, R.; Grande, H.; Pomposo, J. A.; Mecerreyes, D. Synthesis of Novel Polycations Using the Chemistry of Ionic Liquids. *Macromol. Chem. Phys.* **2005**, *206* (2), 299–304. <https://doi.org/10.1002/macp.200400411>.
- (121) Tomé, L. C.; Mecerreyes, D.; Freire, C. S. R.; Rebelo, L. P. N.; Marrucho, I. M. Pyrrolidinium-Based Polymeric Ionic Liquid Materials: New Perspectives for CO₂ Separation Membranes. *J. Memb. Sci.* **2013**, *428*, 260–266. <https://doi.org/10.1016/j.memsci.2012.10.044>.
- (122) Li, M.; Yang, L.; Fang, S.; Dong, S. Novel Polymeric Ionic Liquid Membranes as Solid Polymer Electrolytes with High Ionic Conductivity at Moderate Temperature. *J. Memb. Sci.* **2011**, *366* (1–2), 245–250. <https://doi.org/10.1016/j.memsci.2010.10.004>.
- (123) Vijayakumar, V.; Kim, J. H.; Nam, S. Y. Piperidinium Functionalized Poly(2,6 Dimethyl 1,4 Phenylene Oxide) Based Polyionic Liquid/Ionic Liquid (PIL/IL) Composites for CO₂ Separation. *J. Ind. Eng. Chem.* **2021**, *99*, 81–89. <https://doi.org/10.1016/j.jiec.2021.04.013>.
- (124) Kammakakam, I.; Bara, J. E.; Jackson, E. M.; Lertxundi, J.; Mecerreyes, D.; Tomé, L. C. Tailored CO₂-Philic Anionic Poly(Ionic Liquid) Composite Membranes: Synthesis, Characterization, and Gas Transport Properties. *ACS Sustain. Chem. Eng.* **2020**, *8* (15), 5954–5965. <https://doi.org/10.1021/acssuschemeng.0c00327>.

- (125) Camper, D.; Bara, J.; Koval, C.; Noble, R. D. Bulk-Fluid Solubility and Membrane Feasibility of Rmim-Based Room-Temperature Ionic Liquids. *Ind. Eng. Chem. Res.* **2006**, *45* (18), 6279–6283. <https://doi.org/10.1021/ie060177n>.
- (126) Bara, J. E.; Gabriel, C. J.; Hatakeyama, E. S.; Carlisle, T. K.; Lessmann, S.; Noble, R. D.; Gin, D. L. Improving CO₂ Selectivity in Polymerized Room-Temperature Ionic Liquid Gas Separation Membranes through Incorporation of Polar Substituents. *J. Memb. Sci.* **2008**, *321* (1), 3–7. <https://doi.org/10.1016/j.memsci.2007.12.033>.
- (127) Shaligram, S. V.; Wadgaonkar, P. P.; Kharul, U. K. Polybenzimidazole-Based Polymeric Ionic Liquids (PILs): Effects of “substitution Asymmetry” on CO₂ Permeation Properties. *J. Memb. Sci.* **2015**, *493*, 403–413. <https://doi.org/10.1016/j.memsci.2015.07.020>.
- (128) Tomé, L. C.; Aboudzadeh, M. A.; Rebelo, L. P. N.; Freire, C. S. R.; Mecerreyes, D.; Marrucho, I. M. Polymeric Ionic Liquids with Mixtures of Counter-Anions: A New Straightforward Strategy for Designing Pyrrolidinium-Based CO₂ Separation Membranes. *J. Mater. Chem. A* **2013**, *1* (35), 10403–10411. <https://doi.org/10.1039/c3ta12174g>.
- (129) Tomé, L. C.; Isik, M.; Freire, C. S. R.; Mecerreyes, D.; Marrucho, I. M. Novel Pyrrolidinium-Based Polymeric Ionic Liquids with Cyano Counter-Anions: High Performance Membrane Materials for Post-Combustion CO₂ Separation. *J. Memb. Sci.* **2015**, *483*, 155–165. <https://doi.org/10.1016/j.memsci.2015.02.020>.
- (130) Tomé, L. C.; Guerreiro, D. C.; Teodoro, R. M.; Alves, V. D.; Marrucho, I. M. Effect of Polymer Molecular Weight on the Physical Properties and CO₂/N₂ Separation of Pyrrolidinium-Based Poly(Ionic Liquid) Membranes. *J. Memb. Sci.* **2018**, *549* (December 2017), 267–274. <https://doi.org/10.1016/j.memsci.2017.12.019>.
- (131) Teodoro, R. M.; Tomé, L. C.; Mantione, D.; Mecerreyes, D.; Marrucho, I. M. Mixing Poly(Ionic Liquid)s and Ionic Liquids with Different Cyano Anions: Membrane Forming Ability and CO₂/N₂ Separation Properties. *J. Memb. Sci.* **2018**, *552* (December 2017), 341–348. <https://doi.org/10.1016/j.memsci.2018.02.019>.
- (132) Gouveia, A. S. L.; Malcaitè, E.; Lozinskaya, E. I.; Shaplov, A. S.; Tomé, L. C.; Marrucho, I. M. Poly(Ionic Liquid)-Ionic Liquid Membranes with Fluorosulfonyl-Derived Anions: Characterization and Biohydrogen Separation. *ACS Sustain. Chem. Eng.* **2020**, *8* (18), 7087–7096. <https://doi.org/10.1021/acssuschemeng.0c00960>.
- (133) Nabais, A. R.; Martins, A. P. S. S.; Alves, V. D.; Crespo, J. G.; Marrucho, I. M.; Tomé, L. C.; Neves, L. A. Poly(Ionic Liquid)-Based Engineered Mixed Matrix Membranes for CO₂/H₂ Separation. *Sep. Purif. Technol.* **2019**, *222* (November 2018), 168–176. <https://doi.org/https://doi.org/10.1016/j.seppur.2019.04.018>.
- (134) Martins, A. P. S.; De Añastro, A. F.; Olmedo-Martínez, J. L.; Nabais, A. R.; Neves, L. A.; Mecerreyes, D.; Tomé, L. C. Influence of Anion Structure on Thermal, Mechanical and CO₂ Solubility Properties of Uv-Cross-Linked Poly(Ethylene Glycol) Diacrylate Ionogels. *Membranes (Basel)*. **2020**, *10* (46), 1–18. <https://doi.org/10.3390/membranes10030046>.
- (135) Bernardo, P.; Jansen, J. C.; Bazzarelli, F.; Tasselli, F.; Fuoco, A.; Friess, K.; Izák, P.; Jarmarová, V.; Kačírková, M.; Clarizia, G. Gas Transport Properties of Pebax®/Room Temperature Ionic Liquid Gel Membranes. *Sep. Purif. Technol.* **2012**, *97*, 73–82. <https://doi.org/10.1016/j.seppur.2012.02.041>.

- (136) Chen, H. Z.; Li, P.; Chung, T. S. PVDF/Ionic Liquid Polymer Blends with Superior Separation Performance for Removing CO₂ from Hydrogen and Flue Gas. *Int. J. Hydrogen Energy* **2012**, *37* (16), 11796–11804. <https://doi.org/10.1016/j.ijhydene.2012.05.111>.
- (137) Kanehashi, S.; Kishida, M.; Kidesaki, T.; Shindo, R.; Sato, S.; Miyakoshi, T.; Nagai, K. CO₂ Separation Properties of a Glassy Aromatic Polyimide Composite Membranes Containing High-Content 1-Butyl-3-Methylimidazolium Bis(Trifluoromethylsulfonyl)Imide Ionic Liquid. *J. Memb. Sci.* **2013**, *430*, 211–222. <https://doi.org/10.1016/j.memsci.2012.12.003>.
- (138) Friess, K.; Jansen, J. C.; Bazzarelli, F.; Izák, P.; Jarmarová, V.; Kačírková, M.; Schauer, J.; Clarizia, G.; Bernardo, P. High Ionic Liquid Content Polymeric Gel Membranes: Correlation of Membrane Structure with Gas and Vapour Transport Properties. *J. Memb. Sci.* **2012**, *415–416*, 801–809. <https://doi.org/10.1016/j.memsci.2012.05.072>.
- (139) Uchytíl, P.; Schauer, J.; Petrychkovych, R.; Setnickova, K.; Suen, S. Y. Ionic Liquid Membranes for Carbon Dioxide-Methane Separation. *J. Memb. Sci.* **2011**, *383* (1–2), 262–271. <https://doi.org/10.1016/j.memsci.2011.08.061>.
- (140) Uk Hong, S.; Park, D.; Ko, Y.; Baek, I.; Hong, S. U.; Park, D.; Ko, Y.; Baek, I. Polymer-Ionic Liquid Gels for Enhanced Gas Transport. *Chem. Commun.* **2009**, *1* (46), 7227–7229. <https://doi.org/10.1039/b913746g>.
- (141) Erdni-Goryaev, E. M.; Alent'Ev, A. Y.; Belov, N. A.; Ponkratov, D. O.; Shaplov, A. S.; Lozinskaya, E. I.; Vygodskii, Y. S. Gas Separation Characteristics of New Membrane Materials Based on Poly(Ethylene Glycol)-Crosslinked Polymers and Ionic Liquids. *Pet. Chem.* **2012**, *52* (7), 494–498. <https://doi.org/10.1134/S0965544112070031>.
- (142) Yang, Q.; Zhang, Z.; Sun, X. G.; Hu, Y. S.; Xing, H.; Dai, S. Ionic Liquids and Derived Materials for Lithium and Sodium Batteries. *Chem. Soc. Rev.* **2018**, *47* (6), 2020–2064. <https://doi.org/10.1039/c7cs00464h>.
- (143) Cowan, M. G.; Gin, D. L.; Noble, R. D. Poly(Ionic Liquid)/Ionic Liquid Ion-Gels with High “Free” Ionic Liquid Content: Platform Membrane Materials for CO₂/Light Gas Separations. *Acc. Chem. Res.* **2016**, *49* (4), 724–732. <https://doi.org/10.1021/acs.accounts.5b00547>.
- (144) Kasahara, S.; Kamio, E.; Yoshizumi, A.; Matsuyama, H. Polymeric Ion-Gels Containing an Amino Acid Ionic Liquid for Facilitated CO₂ Transport Media. *Chem. Commun.* **2014**, *50* (23), 2996–2999. <https://doi.org/10.1039/c3cc48231f>.
- (145) Deng, J.; Yu, J.; Dai, Z.; Deng, L. Cross-Linked PEG Membranes of Interpenetrating Networks with Ionic Liquids as Additives for Enhanced CO₂ Separation. *Ind. Eng. Chem. Res.* **2019**, *58* (13), 5261–5268. <https://doi.org/10.1021/acs.iecr.9b00241>.
- (146) Tomé, L. C. Development of New Membranes Based on Ionic Liquid Materials for Gas Separation, Universidade Nova de Lisboa, 2014.
- (147) Bara, J. E.; Hatakeyama, E. S.; Gin, D. L.; Noble, R. D. Improving CO₂ Permeability in Polymerized Room-Temperature Ionic Liquid Gas Separation Membranes through the Formation of a Solid Composite with a Room-Temperature Ionic Liquid. *Polym. Adv. Technol.* **2008**, *19* (10), 1415–1420. <https://doi.org/10.1002/pat.1209>.

- (148) Bara, J. E.; Gin, D. L.; Noble, R. D. Effect of Anion on Gas Separation Performance of Polymer-Room-Temperature Ionic Liquid Composite Membranes. *Ind. Eng. Chem. Res.* **2008**, *47* (24), 9919–9924. <https://doi.org/10.1021/ie801019x>.
- (149) Bara, J. E.; Noble, R. D.; Gin, D. L. Effect of “Free” Cation Substituent on Gas Separation Performance of Polymer-Room-Temperature Ionic Liquid Composite Membranes. *Ind. Eng. Chem. Res.* **2009**, *48* (9), 4607–4610. <https://doi.org/10.1021/ie801897r>.
- (150) Zhou, J.; Mok, M. M.; Cowan, M. G.; McDanel, W. M.; Carlisle, T. K.; Gin, D. L.; Noble, R. D. High-Permeance Room-Temperature Ionic-Liquid-Based Membranes for CO₂/N₂ Separation. *Ind. Eng. Chem. Res.* **2014**, *53* (51), 20064–20067. <https://doi.org/10.1021/ie5040682>.
- (151) Carlisle, T. K.; McDanel, W. M.; Cowan, M. G.; Noble, R. D.; Gin, D. L. Vinyl-Functionalized Poly(Imidazolium)s: A Curable Polymer Platform for Cross-Linked Ionic Liquid Gel Synthesis. *Chem. Mater.* **2014**, *26* (3), 1294–1296. <https://doi.org/10.1021/cm403885r>.
- (152) McDanel, W. M.; Cowan, M. G.; Chisholm, N. O.; Gin, D. L.; Noble, R. D. Fixed-Site-Carrier Facilitated Transport of Carbon Dioxide through Ionic-Liquid-Based Epoxy-Amine Ion Gel Membranes. *J. Memb. Sci.* **2015**, *492*, 303–311. <https://doi.org/10.1016/j.memsci.2015.05.034>.
- (153) Gouveia, A. S. L.; Ventaja, L.; Tomé, L. C.; Marrucho, I. M. Towards Biohydrogen Separation Using Poly(Ionic Liquid)/Ionic Liquid Composite Membranes. *Membranes (Basel)*. **2018**, *8* (4). <https://doi.org/10.3390/membranes8040124>.
- (154) Dunn, C. A.; Shi, Z.; Zhou, R.; Gin, D. L.; Noble, R. D. (Cross-Linked Poly(Ionic Liquid)-Ionic Liquid-Zeolite) Mixed-Matrix Membranes for CO₂/CH₄ Gas Separations Based on Curable Ionic Liquid Prepolymers. *Ind. Eng. Chem. Res.* **2019**, *58* (11), 4704–4708. <https://doi.org/10.1021/acs.iecr.8b06464>.
- (155) Ahmadi, M.; Janakiram, S.; Dai, Z.; Ansaloni, L.; Deng, L. Performance of Mixed Matrix Membranes Containing Porous Two-Dimensional (2D) and Three-Dimensional (3D) Fillers for CO₂ Separation: A Review. *Membranes (Basel)*. **2018**, *8* (3). <https://doi.org/10.3390/membranes8030050>.
- (156) Lin, H.; Kai, T.; Freeman, B. D.; Kalakkunnath, S.; Kalika, D. S. The Effect of Cross-Linking on Gas Permeability in Cross-Linked Poly(Ethylene Glycol Diacrylate). *Macromolecules* **2005**, *38* (20), 8381–8393. <https://doi.org/10.1021/ma0510136>.
- (157) Kusuma, V. A.; Macala, M. K.; Liu, J.; Marti, A. M.; Hirsch, R. J.; Hill, L. J.; Hopkinson, D. Ionic Liquid Compatibility in Polyethylene Oxide/Siloxane Ion Gel Membranes. *J. Memb. Sci.* **2018**, *545*, 292–300. <https://doi.org/10.1016/j.memsci.2017.09.086>.
- (158) Kusuma, V. A.; Macala, M. K.; Baker, J. S.; Hopkinson, D. Cross-Linked Poly(Ethylene Oxide) Ion Gels Containing Functionalized Imidazolium Ionic Liquids as Carbon Dioxide Separation Membranes. *Ind. Eng. Chem. Res.* **2018**, *57*, 11658–11667. <https://doi.org/10.1021/acs.iecr.8b02739>.
- (159) Scovazzo, P.; Kieft, J.; Finan, D. A.; Koval, C.; DuBois, D.; Noble, R. D. Gas Separations Using Non-Hexafluorophosphate [PF₆]⁻ Anion Supported Ionic Liquid Membranes. *J. Memb. Sci.* **2004**, *238* (1–2), 57–63. <https://doi.org/10.1016/j.memsci.2004.02.033>.
- (160) Gouveia, A. S. L.; Bumenn, E.; Rohtlaid, K.; Michaud, A.; Vieira, T. M.; Alves, V. D.; Tomé,

- L. C.; Plesse, C.; Marrucho, I. M. Ionic Liquid-Based Semi-Interpenetrating Polymer Network (SIPN) Membranes for CO₂ Separation. *Sep. Purif. Technol.* **2021**, *274* (December 2020). <https://doi.org/10.1016/j.seppur.2021.118437>.
- (161) 1-Ethyl-3-methylimidazolium bis(trifluoromethylsulfonyl)imide, 99% <https://iolitec.de/en/node/89> (accessed May 13, 2021).
- (162) File:End group example.png https://commons.wikimedia.org/wiki/File:End_group_example.png (accessed May 16, 2021).
- (163) Nanoclay, surface modified <https://www.sigmaaldrich.com/catalog/product/aldrich/682640?lang=pt®ion=PT> (accessed May 13, 2021).
- (164) Kekevi, B.; Mert, E. H. Synthesis of β -Myrcene-Based Macroporous Nanocomposite Foams: Altering the Morphological and Mechanical Properties by Using Organo-Modified Nanoclay. *J. Appl. Polym. Sci.* **2021**, *138* (e50074), 1–13. <https://doi.org/10.1002/app.50074>.
- (165) Thermogravimetric Analysis (TGA) - A Beginner's Guide https://www.perkinelmer.com/lab-solutions/resources/docs/GDE_TGABeginnersGuide.pdf (accessed May 7, 2021).
- (166) Neves, L. A.; Afonso, C.; Coelho, I. M.; Crespo, J. G. Integrated CO₂ Capture and Enzymatic Bioconversion in Supported Ionic Liquid Membranes. *Sep. Purif. Technol.* **2012**, *97*, 34–41. <https://doi.org/10.1016/j.seppur.2012.01.049>.
- (167) Swapp, S. Scanning Electron Microscopy (SEM) https://serc.carleton.edu/research_education/geochemsheets/techniques/SEM.html (accessed May 7, 2021).
- (168) Differential Scanning Calorimetry (DSC) - A Beginner's Guide https://www.perkinelmer.com/CMSResources/Images/46-74542GDE_DSCBeginnersGuide.pdf (accessed May 9, 2021).
- (169) Drelich, J. W. Contact Angles: From Past Mistakes to New Developments through Liquid-Solid Adhesion Measurements. *Adv. Colloid Interface Sci.* **2019**, *267*, 1–14. <https://doi.org/10.1016/j.cis.2019.02.002>.
- (170) Drelich, J. W.; Boinovich, L.; Chibowski, E.; Della Volpe, C.; Hołysz, L.; Marmur, A.; Siboni, S. Contact Angles: History of over 200 Years of Open Questions. *Surf. Innov.* **2020**, *8*(1–2), 3–27. <https://doi.org/10.1680/jsuin.19.00007>.
- (171) Cussler, E. L. *Diffusion - Mass Transfer in Fluid Systems*, Third Edit.; Cambridge University Press: New York, 2009.
- (172) Merkel, T. C.; Bondar, V. I.; Nagai, K.; Freeman, B. D.; Pinnau, I. Gas Sorption, Diffusion, and Permeation in Poly(Dimethylsiloxane). *J. Polym. Sci.* **2000**, *38*, 415–434.
- (173) Jarrar, R.; Mohsin, M. A.; Haik, Y. Alteration of the Mechanical and Thermal Properties of Nylon 6/Nylon 6,6 Blends by Nanoclay. *J. Appl. Polym. Sci.* **2012**, *124*, 1880–1890. <https://doi.org/10.1002/app.35215>.
- (174) Patel, H. A.; Somani, R. S.; Bajaj, H. C.; Jasra, R. V. Nanoclays for Polymer

- Nanocomposites, Paints, Inks, Greases and Cosmetics Formulations, Drug Delivery Vehicle and Waste Water Treatment. *Bull. Mater. Sci.* **2006**, *29* (2), 133–145. <https://doi.org/10.1007/BF02704606>.
- (175) Yourdkhani, M.; Mousavand, T.; Chapleau, N.; Hubert, P. Thermal, Oxygen Barrier and Mechanical Properties of Polylactide-Organoclay Nanocomposites. *Compos. Sci. Technol.* **2013**, *82*, 47–53. <https://doi.org/10.1016/j.compscitech.2013.03.015>.
- (176) Madejová, J. FTIR Techniques in Clay Mineral Studies. *Vib. Spectrosc.* **2003**, *31* (1), 1–10. [https://doi.org/10.1016/S0924-2031\(02\)00065-6](https://doi.org/10.1016/S0924-2031(02)00065-6).
- (177) Sownthari, K.; Suthanthiraraj, S. A. Structural , Thermal , and Electrical Studies on Gel Polymer Electrolytes Containing 1-Ethyl-3-Methylimidazolium Bis (Trifluoromethylsulfonyl) Imide. *Ionics (Kiel)*. **2015**, *21*, 1649–1654. <https://doi.org/10.1007/s11581-014-1324-8>.
- (178) Kiefer, J.; Fries, J.; Leipertz, A. Experimental Vibrational Study of Imidazolium-Based Ionic Liquids: Raman and Infrared Spectra of 1-Ethyl-3- Methylimidazolium Bis (Trifluoromethylsulfonyl) Imide and 1-Ethyl-3-Methylimidazolium Ethylsulfate. *Appl. Spectrosc.* **2007**, *61* (12), 1306–1311.
- (179) Peter, M.; Tayalia, P. An Alternative Technique for Patterning Cells on Poly(Ethylene Glycol) Diacrylate Hydrogels. *RSC Adv.* **2016**, *6* (47), 40878–40885. <https://doi.org/10.1039/c6ra08852j>.
- (180) Hashemifard, S. A.; Ismail, A. F.; Matsuura, T. Effects of Montmorillonite Nano-Clay Fillers on PEI Mixed Matrix Membrane for CO₂ Removal. *Chem. Eng. J.* **2011**, *170* (1), 316–325. <https://doi.org/10.1016/j.cej.2011.03.063>.
- (181) Pugazhenthí, G.; Suresh, K.; Vinoth Kumar, R.; Kumar, M.; Rajkumar Surin, R. A Simple Sonication Assisted Solvent Blending Route for Fabrication of Exfoliated Polystyrene (PS)/Clay Nanocomposites: Role of Various Clay Modifiers. *Mater. Today Proc.* **2018**, *5* (5), 13191–13210. <https://doi.org/10.1016/j.matpr.2018.02.310>.
- (182) Defontaine, G.; Barichard, A.; Letaief, S.; Feng, C.; Matsuura, T.; Detellier, C. Nanoporous Polymer - Clay Hybrid Membranes for Gas Separation. *J. Colloid Interface Sci.* **2010**, *343* (2), 622–627. <https://doi.org/10.1016/j.jcis.2009.11.048>.
- (183) Verma, Y. L.; Singh, R. K. Conformational States of Ionic Liquid 1-Ethyl-3-Methylimidazolium Bis(Trifluoromethylsulfonyl)Imide in Bulk and Confined Silica Nanopores Probed by Crystallization Kinetics Study. *J. Phys. Chem. C* **2015**, *119* (43), 24381–24392. <https://doi.org/10.1021/acs.jpcc.5b06672>.
- (184) Liu, S. H.; Chen, C. C.; Zhang, B.; Wu, J. H. Fire and Explosion Hazards of 1-Ethyl-3-Methylimidazolium Bis(Trifluoromethylsulfonyl)Imide. *RSC Adv.* **2020**, *10* (38), 22468–22479. <https://doi.org/10.1039/d0ra01821j>.
- (185) Genier, F. S.; Burdin, C. V.; Biriá, S.; Hosein, I. D. A Novel Calcium-Ion Solid Polymer Electrolyte Based on Crosslinked Poly(Ethylene Glycol) Diacrylate. *J. Power Sources* **2019**, *414*, 302–307. <https://doi.org/10.1016/j.jpowsour.2019.01.017>.
- (186) Rattanawongwiboon, T.; Hemvichian, K.; Lertsarawut, P.; Suwanmala, P. Chitosan-Poly(Ethylene Glycol) Diacrylate Beads Prepared by Radiation-Induced Crosslinking and Their Promising Applications Derived from Encapsulation of Essential Oils. *Radiat. Phys.*

- Chem.* **2020**, *170* (September 2019), 108656.
<https://doi.org/10.1016/j.radphyschem.2019.108656>.
- (187) Alexandre, B.; Langevin, D.; Médéric, P.; Aubry, T.; Couderc, H.; Nguyen, Q. T.; Saiter, A.; Marais, S. Water Barrier Properties of Polyamide 12/Montmorillonite Nanocomposite Membranes: Structure and Volume Fraction Effects. *J. Memb. Sci.* **2009**, *328*, 186–204. <https://doi.org/10.1016/j.memsci.2008.12.004>.
- (188) Schaller, C. 4.4: Glass Transition <https://chem.libretexts.org/@go/page/190669> (accessed May 28, 2021).
- (189) Glass Transition Temperature (T_g) of Plastics - Definition & Values <https://omnexus.specialchem.com/polymer-properties/properties/glass-transition-temperature> (accessed Aug 20, 2021).
- (190) Ju, H.; McCloskey, B. D.; Sagle, A. C.; Kusuma, V. A.; Freeman, B. D. Preparation and Characterization of Crosslinked Poly(Ethylene Glycol) Diacrylate Hydrogels as Fouling-Resistant Membrane Coating Materials. *J. Memb. Sci.* **2009**, *330* (1–2), 180–188. <https://doi.org/10.1016/j.memsci.2008.12.054>.
- (191) Zhang, H.; Wang, L.; Song, L.; Niu, G.; Cao, H.; Wang, G.; Yang, H.; Zhu, S. Controllable Properties and Microstructure of Hydrogels Based on Crosslinked Poly(Ethylene Glycol) Diacrylates with Different Molecular Weights. *J. Appl. Polym. Sci.* **2011**, *121*, 531–540. <https://doi.org/10.1002/app.33653>.
- (192) Mahmoud, M. E. Surface Loaded 1-Methyl-3-Ethylimidazolium Bis(Trifluoromethylsulfonyl)Imide [EMIM⁺Tf₂N⁻] Hydrophobic Ionic Liquid on Nano-Silica Sorbents for Removal of Lead from Water Samples. *Desalination* **2011**, *266*, 119–127. <https://doi.org/10.1016/j.desal.2010.08.011>.
- (193) Khalifa, Y.; Broderick, A.; Newberg, J. T. Water Vapor Electron Scattering Cross-Section Measurements Using a Hydrophobic Ionic Liquid. *J. Electron Spectros. Relat. Phenomena* **2018**, *222*, 162–166. <https://doi.org/10.1016/j.elspec.2017.06.002>.
- (194) Nanoclay, surface modified contains 15-35 wt. % octadecylamine, 0.5-5 wt. % aminopropyltriethoxysilane: Sigma-Aldrich <https://www.sigmaaldrich.com/PT/en/product/aldrich/682632?context=product> (accessed Sep 16, 2021).
- (195) Nanoclay, surface modified contains 35-45 wt. % dimethyl dialkyl (C₁₄-C₁₈) amine: Sigma-Aldrich <https://www.sigmaaldrich.com/PT/en/product/aldrich/682624?context=product> (accessed Sep 16, 2021).
- (196) Chang, Y. W.; Chang, B. K. Influence of Casting Solvents on Sedimentation and Performance in Metal–Organic Framework Mixed–Matrix Membranes. *J. Taiwan Inst. Chem. Eng.* **2018**, *89*, 224–233. <https://doi.org/10.1016/j.jtice.2018.05.006>.
- (197) Dorosti, F.; Omidkhan, M.; Abedini, R. Fabrication and Characterization of Matrimid/MIL-53 Mixed Matrix Membrane for CO₂/CH₄ Separation. *Chem. Eng. Res. Des.* **2014**, *92*, 2439–2448. <https://doi.org/10.1016/j.cherd.2014.02.018>.
- (198) Duan, C.; Jie, X.; Liu, D.; Cao, Y.; Yuan, Q. Post-Treatment Effect on Gas Separation Property of Mixed Matrix Membranes Containing Metal Organic Frameworks. *J. Memb.*

- Sci.* **2014**, *466*, 92–102. <https://doi.org/10.1016/j.memsci.2014.04.024>.
- (199) Feijani, E. A.; Mahdavi, H.; Tavasoli, A. Poly(Vinylidene Fluoride) Based Mixed Matrix Membranes Comprising Metal Organic Frameworks for Gas Separation Applications. *Chem. Eng. Res. Des.* **2015**, *96*, 87–102. <https://doi.org/10.1016/j.cherd.2015.02.009>.
- (200) Dorosti, F.; Alizadehdakhel, A. Fabrication and Investigation of PEBAX/Fe-BTC, a High Permeable and CO₂ Selective Mixed Matrix Membrane. *Chem. Eng. Res. Des.* **2018**, *136*, 119–128. <https://doi.org/10.1016/j.cherd.2018.01.029>.
- (201) Hanioka, S.; Maruyama, T.; Sotani, T.; Teramoto, M.; Matsuyama, H.; Nakashima, K.; Hanaki, M.; Kubota, F.; Goto, M. CO₂ Separation Facilitated by Task-Specific Ionic Liquids Using a Supported Liquid Membrane. *J. Memb. Sci.* **2008**, *314* (1–2), 1–4. <https://doi.org/10.1016/j.memsci.2008.01.029>.
- (202) Moghadam, F.; Kamio, E.; Yoshizumi, A.; Matsuyama, H. An Amino Acid Ionic Liquid-Based Tough Ion Gel Membrane for CO₂ Capture. *Chem. Commun.* **2015**, *51*(71), 13658–13661. <https://doi.org/10.1039/c5cc04841a>.
- (203) Attribution-ShareAlike 2.5 <https://creativecommons.org/licenses/by-sa/2.5/legalcode> (accessed May 16, 2021).
- (204) Attribution-ShareAlike 3.0 Unported <https://creativecommons.org/licenses/by-sa/3.0/legalcode> (accessed May 16, 2021).
- (205) Trepte, A. File:Montmorillonite-en.svg <https://commons.wikimedia.org/wiki/File:Montmorillonite-en.svg> (accessed May 13, 2021).
- (206) Patel, N. P.; Miller, A. C.; Spontak, R. J. Highly CO₂-Permeable and -Selective Membranes Derived from Crosslinked Poly(Ethylene Glycol) and Its Nanocomposites. *Adv. Funct. Mater.* **2004**, *14* (7), 699–707. <https://doi.org/10.1002/adfm.200305136>.
- (207) Poly(ethylene glycol) diacrylate <https://www.sigmaaldrich.com/catalog/product/aldrich/437441?lang=pt®ion=PT#productDetailSafetyRelatedDocs> (accessed May 13, 2021).

APPENDIX: RESULTS REPORTED IN THE LITERATURE

Table A.1 - CO₂/N₂ and CO₂/CH₄ separation performance of MMMs with nanoclay fillers reported in the literature.

MMM	Experimental conditions	P _{CO₂} (Barrer)	Selectivity		Ref.
			α (CO ₂ /N ₂)	α (CO ₂ /CH ₄)	
PSf	25 °C, 5 bar Single gas	5	5	23	69
PSf/0.5 wt% Cloisite15A		-	5	20	
PSf/1.0 wt% Cloisite15A		19	5	21	
PSf/2.0 wt% Cloisite15A		-	1	4	
PSf/MMT	50 °C, 30 bar, Mixed gas	82-85	123	138	70
Pebax2533	25 °C, 2 bar Single gas	240	40	8	65
Pebax2533/2 wt% Cloisite15A		200	34	7	
Pebax2533/4 wt% Cloisite15A		195	27	7	
Pebax2533/6 wt% Cloisite15A		190	34	8	
Pebax2533/10 wt% Cloisite15A		187	34	7	
CA	25 °C, 2 bar Single gas	7	4	7	71
CA/0.5 wt% Bentonite		7	7	10	
CA/1.0 wt% Bentonite		7	10	13	
CA/1.5 wt% Bentonite		7	9	14	
CA/2.0 wt% Bentonite		6	8	10	
PSf	3 bar Single gas	-	-	0	72
PSf/0.1 wt% talc		-	-	0	
PSf/0.3 wt% talc		-	-	∞	
PSf/0.5 wt% talc		-	-	7	

Table A.2 - CO₂/N₂, CO₂/CH₄, and CO₂/H₂ separation performance of SILMs with different cations reported in the literature.

Ionic Liquid	Support	Experimental conditions	P _{CO₂} (Barrer)	Selectivity			Ref.
				α (CO ₂ /N ₂)	α (CO ₂ /CH ₄)	α (CO ₂ /H ₂)	
[C ₄ mim][PF ₆] [C ₆ mim][PF ₆] [C ₈ mim][PF ₆]	Hydrophobic PVDF	30 °C, 0.5 bar Single gas	171 281 370	23 28 22	- - -	6 8 5	96
[C ₄ F ₅ mim][Tf ₂ N] [C ₆ F ₉ mim][Tf ₂ N] [C ₈ F ₁₃ mim][Tf ₂ N]	PES	23 °C, 1 bar Single gas	320 280 210	27 21 16	19 17 13	- - -	97
C ₃ [mim] ₂ [Tf ₂ N] ₂ C ₆ [mim] ₂ [Tf ₂ N] ₂	Alumina	27 °C, 0.3 bar Single gas	190 220	- -	27 16	- -	99
[H ₂ NC ₃ mim][Tf ₂ N]	Cross-linked Nylon 66	37-95 °C, 1 bar Mixed gas	100 - 1000	-	-	0.4 - 1.4	88
[H ₂ NC ₃ mim][Tf ₂ N] [H ₂ NC ₃ mim][CF ₃ SO ₃]	Hydrophilic PTFE	25 °C, 0.1 bar Mixed gas	≈ 500 ≈ 900	- -	≈ 45 ≈ 35	- -	201
[B ₂ py][Tf ₂ N] [B ₂ mpy][Tf ₂ N] [B ₂ 3mpy][Tf ₂ N] [B ₂ 4mpy][Tf ₂ N]	Hydrophobic PTFE	25 °C, 0.35 bar Single gas	518 358 446 496	28 33 22 23	- - - -	- - - -	100
[B ₂ mpyr][Tf ₂ N]	Hydrophobic PTFE	25 °C, 0.35 bar Single gas	280	26	-	-	100
[C ₄ mthiaz][Tf ₂ N] [B ₂ mthiaz][Tf ₂ N] [C ₃ H ₇ O ₂ mthiaz][Tf ₂ N]	PES	25 °C, 0.35 bar Single gas	362 235 248	28 21 18	- - -	- - -	101
[(N ₁₁) ₂ CH][Tf ₂ N] [(N ₁₁) ₂ N][Tf ₂ N]	Alumina	25 °C, 0.35 bar Single gas	1882 1777	28 29	- -	- -	102

Table A.3 – CO₂/N₂ and CO₂/CH₄ separation performance of SILMs with different anions reported in the literature.

Ionic Liquid	Support	Experimental conditions	P _{CO₂} (Barrer)	Selectivity		Ref.
				α (CO ₂ /N ₂)	α (CO ₂ /CH ₄)	
[C ₂ mim][Tf ₂ N]	PES	25 °C Single gas	-	29	-	103
[C ₄ mim][N(CN) ₂]			-	51	-	
[C ₄ mim][C(CN) ₃]			-	45	-	
[C ₂ mim][B(CN) ₄]			-	53	-	
[C ₂ mim][C ₁ SO ₄]	Hydrophilic	20 °C, 1 bar	111	69	32	104
[C ₂ mim][C ₂ SO ₄]	PTFE	Single gas	157	51	21	
[C ₂ mim][Ac]	Hydrophobic	25 °C, 0.45 bar	879	34	-	105
[C ₄ mim][Ac]	PVDF	Single gas	852	35	-	
[Ch][Mal]	Hydrophilic PTFE	20 °C, 1 bar Single gas	2	39	24	92
[Ch][Lev]			18	41	21	
[Ch][Gly]			6	50	34	
[Ch][Lac]			7	46	22	
[P ₄₄₄₄][Gly]	Hydrophilic PTFE	100 °C, 0.1 bar Mixed gas	≈ 5000	≈ 50	-	106
[P ₄₄₄₄][Ala]			≈ 7000	≈ 60	-	
[P ₄₄₄₄][Ser]			≈ 2000	≈ 35	-	
[P ₄₄₄₄][Pro]			≈ 10500	≈ 70	-	
[P _{6,6,6,14}] ₂ [CoCl ₄]	Hydrophobic PVDF	25 °C, 0.45 bar Single gas	147	23	-	90
[P _{6,6,6,14}] ₂ [FeCl ₄]			259	24	-	
[P _{6,6,6,14}] ₂ [MnCl ₄]			203	41	-	
[P _{6,6,6,14}] ₃ [GdCl ₆]			176	31	-	
[C ₂ mim][Tf ₂ N] _{0.5} [Ac] _{0.5}	Hydrophilic PTFE	20 °C, 1 bar Single gas	336	33	18	93
[C ₂ mim][Tf ₂ N] _{0.5} [Lac] _{0.5}			265	37	18	
[C ₂ mim][Tf ₂ N] _{0.5} [N(CN) ₂] _{0.5}			589	42	19	
[C ₂ mim][Tf ₂ N] _{0.5} [SCN] _{0.5}			516	37	20	
[C ₂ mim][C ₁ SO ₄] _{0.5} [SCN] _{0.5}			142	62	21	
[C ₂ mim][C ₁ SO ₄] _{0.5} [N(CN) ₂] _{0.5}			207	58	24	
[C ₂ mim][C ₁ SO ₄] _{0.5} [C(CN) ₃] _{0.5}			246	47	19	
[C ₂ mim][C ₁ SO ₄] _{0.5} [B(CN) ₄] _{0.5}			373	52	20	
[C ₂ mim][SCN] _{0.5} [N(CN) ₂] _{0.5}			324	61	22	
[C ₂ mim][SCN] _{0.5} [C(CN) ₃] _{0.5}			332	57	21	
[C ₂ mim][SCN] _{0.5} [B(CN) ₄] _{0.5}			445	51	19	

Table A.4 - CO₂/N₂ and CO₂/CH₄ separation performance of PIL membranes reported in the literature.

PIL Membrane	Experimental conditions	P _{CO₂} (Barrer)	Selectivity		Ref.
			α (CO ₂ /N ₂)	α (CO ₂ /CH ₄)	
Styrene-based: Methyl substituent	20 °C Single gas	9	32	38	116
Styrene-based: Butyl substituent		30	30	22	
Styrene-based: Hexyl substituent		32	23	14	
Acrylate-based: Methyl substituent		7	30	37	
Acrylate-based: Butyl substituent		22	31	23	
Oligo(ethylene glycol) ₁ -type	22 °C, 2 bar Single gas	16	41	33	126
Oligo(ethylene glycol) ₂ -type		22	44	29	
C ₃ CN-type		4	37	37	
C ₅ CN-type		8	40	30	
[DBDMPBI-BuI][Tf ₂ N]	35 °C, 19 bar Single gas	20	29	-	127
[DBDMPBI-BuI][HFB]		21	28	-	
[DBzDMPBI-BuI][Tf ₂ N]		25	27	-	
[DBzDMPBI-BuI][HFB]		25	26	-	
PBI-BuI		2	32	-	
[DBDMPBI-HFA][Tf ₂ N]		18	26	-	
[DBDMPBI-HFA][HFB]		19	27	-	
[DBzDMPBI-HFA][Tf ₂ N]		22	22	-	
[DBzDMPBI-HFA][HFB]		23	23	-	
PBI-HFA		3	29	-	

Table A.5 - CO₂/N₂ and CO₂/H₂ separation performance of polymer/IL composite membranes reported in the literature.

Polymer/IL Composite Membrane	Experimental conditions	P _{CO₂} (Barrer)	Selectivity		Ref.
			α (CO ₂ /N ₂)	α (CO ₂ /H ₂)	
PVDF-HFP/33 wt% [C ₆ mim][BF ₄]	35-45 °C, 2 bar Mixed gas	45	50	-	140
PVDF-HFP/50 wt% [C ₆ mim][BF ₄]		200	55	-	
PVDF-HFP/66 wt% [C ₆ mim][BF ₄]		400	60	-	
PVDF/33 wt%[C ₄ mim][B(CN) ₄]	35 °C, 2 bar Single gas	467	37	10	136
PVDF/50 wt%[C ₄ mim][B(CN) ₄]		1228	40	12	
PVDF/66 wt%[C ₄ mim][B(CN) ₄]		1778	41	13	
PVP/70 wt% [P ₄₄₄₄][Pro]	100 C, 1 bar Mixed gas	6700	170	-	144

Table A.6 - CO₂/N₂, CO₂/CH₄, and CO₂/H₂ separation performance of PIL/IL membranes reported in the literature.

PIL/IL Composite Membrane	Experi- mental conditions	P _{CO₂} (Barrer)	Selectivity			Ref.
			α (CO ₂ /N ₂)	α (CO ₂ /CH ₄)	α (CO ₂ /H ₂)	
Imidazolium PIL	22 °C, 2 bar	9	32	39	-	147
Imidazolium PIL/20 mol% [C ₂ mim][Tf ₂ N]	Single gas	44	39	27	-	
Imidazolium PIL	22 °C, 2 bar Single gas	16	41	33	-	148
Imidazolium PIL/20 mol% [C ₂ mim][Tf ₂ N]		60	36	24	-	
Imidazolium PIL/20 mol% [C ₂ mim][N(CN) ₂]		41	39	25	-	
Imidazolium PIL/20 mol% [C ₂ mim][OTf]		43	37	25	-	
Imidazolium PIL/20 mol% [C ₂ mim][SbF ₆]		42	39	27	-	
PIL (Imidazolium)	22 °C, 2 bar Single gas	16	41	33	-	149
PIL/20 mol% [Alkyl cation][Tf ₂ N]		51	37	24	-	
PIL/20 mol% [Ether cation][Tf ₂ N]		53	38	26	-	
PIL/20 mol% [Nitrile cation][Tf ₂ N]		33	40	28	-	
PIL/20 mol% [Fluoroalkyl cation][Tf ₂ N]		47	36	27	-	
PIL/20 mol% [Siloxane cation][Tf ₂ N]		55	33	20	-	
Imidazolium PIL/58 wt% [C ₂ mim][Tf ₂ N]	Single gas	610	22	-	-	150
Cross-linked Imidazolium PIL/80 wt% [C ₂ mim][Tf ₂ N]	22 °C Single gas	500	24	-	-	151
Epoxide/amine PIL/75 wt% [C ₂ mim][N(CN) ₂]	Mixed gas	900	140	-	-	152
Double polymer network/80 wt% [P ₄₄₄₄][Pro]	100 °C, 1 bar	4000	100	-	-	202
PIL: Poly([pyr ₁₁][Tf ₂ N]; IL: [pyr ₁₄][Tf ₂ N] PIL	21 °C, 1 bar Single gas	5	22	29	-	121
PIL/20 wt% IL		25	32	26	-	
PIL/40 wt% IL		106	30	19	-	
PIL/60 wt% IL		200	28	16	-	
PIL/80 wt% IL (PVDF supported) IL (PVDF supported)		313 340	29 28	14 14	- -	
PIL: Poly([pyr ₁₁][Tf ₂ N]; IL: [pyr ₁₄][Tf ₂ N] PIL(Tf ₂ N)/20 wt% IL	20 °C, 1 bar Single gas	25	32	26	-	128
PIL(Tf ₂ N/PF ₆)/20 wt% IL		11	31	29	-	
PIL(Tf ₂ N/NSA)/20 wt% IL		3	22	21	-	
PIL(Tf ₂ N/DS)/20 wt% IL		44	22	11	-	
PIL(Tf ₂ N/DBSA)/20 wt% IL		16	21	13	-	
PIL: Poly([pyr ₁₁][N(CN) ₂]; IL: [C ₂ mim][N(CN) ₂] PIL/20 wt% IL	20 °C, 1 bar Single gas	4	41	-	-	129
PIL: Poly([pyr ₁₁][C(CN) ₃]; IL: [C ₂ mim][C(CN) ₃] PIL/20 wt% IL		8	45	-	-	
PIL/40 wt% IL		143	56	-	-	
PIL/60 wt% IL		439	64	-	-	

Table A.6 (continued) - CO₂/N₂, CO₂/CH₄, and CO₂/H₂ separation performance of PIL/IL membranes reported in the literature.

PIL/IL Composite Membrane	Experimental conditions	P _{CO₂} (Barrer)	Selectivity			Ref.
			α (CO ₂ /N ₂)	α (CO ₂ /CH ₄)	α (CO ₂ /H ₂)	
PIL: Poly([pyr ₁₁₁][C(CN) ₃] ₃); IL: [C ₂ mim][C(CN) ₃]	20 °C, 1 bar Single gas	15 193 542 8 143 439	36 52 54 45 56 64	-	-	130
Medium M _w PIL/20 wt% IL						
Medium M _w PIL/40 wt% IL						
Medium M _w PIL/60 wt% IL						
High M _w PIL/20 wt% IL						
High M _w PIL/40 wt% IL						
High M _w PIL/60 wt% IL						
Poly([pyr ₁₁₁][N(CN) ₂] ₂ /60 wt% [C ₂ mim][C(CN) ₃]	20 °C, 1 bar Single gas	249 439 473 502	61 64 54 43	-	-	131
Poly([pyr ₁₁₁][C(CN) ₃] ₃ /60 wt% [C ₂ mim][C(CN) ₃]						
Poly([pyr ₁₁₁][C(CN) ₃] ₃ /60 wt% [C ₂ mim][B(CN) ₄]						
Poly([pyr ₁₁₁][B(CN) ₄] ₄ /60 wt% [C ₂ mim][C(CN) ₃]						
Poly[pyr ₁₁₁][TFSAM]/20 wt% [C ₂ mim][TFSAM]	35 °C, 1 bar Single gas	40 177 38 201 72	-	-	3.2 7.2 3.6 8.9 3.5	132
Poly[pyr ₁₁₁][TFSAM]/40 wt% [C ₂ mim][TFSAM]						
Poly[pyr ₁₁₁][FSI]/20 wt% [C ₂ mim][FSI]						
Poly[pyr ₁₁₁][FSI]/40 wt% [C ₂ mim][FSI]						
Poly[pyr ₁₁₁][TSAC]/20 wt% [C ₂ mim][TSCA]						
Cross-linking monomers: MIL-CF ₃ ; MIL-C ₇ H ₇ (MIL - methacryloxy-based IL) IL: [C ₂ mim][Tf ₂ N]	20 °C, 3 bar Single gas	8 6 5 20	47 52 66 87	57 62 71 119	3 3 3 4	124
MIL-CF ₃ /20 wt% PEGDA/0.5 mol equiv IL						
MIL-CF ₃ /20 wt% PEGDA/1.0 mol equiv IL						
MIL- C ₇ H ₇ /20 wt% PEGDA/0.5 mol equiv IL						
MIL- C ₇ H ₇ /20 wt% PEGDA/1.0 mol equiv IL						

Table A.7 - CO₂/CH₄ and CO₂/H₂ separation performance of PIL/IL-based MMMs reported in the literature.

PIL/IL-based MMM	Experimental conditions	P _{CO₂} (Barrer)	Selectivity		Ref.
			α (CO ₂ /CH ₄)	α (CO ₂ /H ₂)	
PIL: Poly([smim][Tf ₂ N]); IL: [C ₂ mim][Tf ₂ N] PIL/20 wt% IL PIL/16 wt% IL/20 wt% SAPO-34 PIL/20 wt% IL/30 wt% SAPO-34 PIL/30 wt% IL/40 wt% SAPO-34	25 °C, 2 bar Single gas	44 155 260 680	27 74 90 38	- - - -	48
PIL: curable IL prepolymer IL: [C ₂ mim][Tf ₂ N] PIL/20 wt% IL PIL/16 wt% IL/20 wt% SAPO-34	21 °C, 1 bar Single gas	23 47	26 42	- -	154
PIL: Poly[pyr ₁₁][Tf ₂ N]; IL: [C ₄ mpyr][Tf ₂ N] PIL/40 wt% IL PIL/40 wt% IL/10 wt% MIL-53 PIL/40 wt% IL/20 wt% MIL-53 PIL/40 wt% IL/30 wt% MIL-53 PIL/40 wt% IL/10 wt% Cu-BTC PIL/40 wt% IL/20 wt% Cu-BTC PIL/40 wt% IL/30 wt% Cu-BTC PIL/40 wt% IL/10 wt% ZIF-8 PIL/40 wt% IL/20 wt% ZIF-8 PIL/40 wt% IL/30 wt% ZIF-8	30 °C, 0.7 bar Single gas	47 35 50 90 40 75 78 55 84 97	- - - - - - - - - -	2 3 7 13 3 3 7 3 3 4	133
PIL: Poly[pyr ₁₁][Tf ₂ N]; IL: [C ₂ mim][BETI] PIL/40 wt% IL PIL/40 wt% IL/10 wt% MOF-5 PIL/40 wt% IL/20 wt% MOF-5 PIL/40 wt% IL/30 wt% MOF-5	30 °C, 0.7 bar Single gas	146 261 282 340	15 8 15 2	- - - -	29

Table A.8 - CO₂/N₂ separation performance of PEG-based cross-linked iongel membranes reported in the literature.

PIL/IL-based MMM	Experimental conditions	P _{CO₂} (Barrer)	Selectivity α (CO ₂ /N ₂)	Ref.
Semi-crystalline PEG	35 °C,	12	48	156
Cross-linked PEGDA	Single gas	110	50	
PEGDA	40 °C, 1 bar Single gas	120	58	157
PEGDA/40 vol% [C ₂ mim][Tf ₂ N]		270	37	
PEGDA/40 vol% [C ₂ mim][N(CN) ₂]		210	60	
PEGDA/40 vol% [P ₁₄₄₄][Tf ₂ N]		290	24	
PEGDA/40 vol% [N ₄₁₁₁][Tf ₂ N]		220	30	
PEGDA/40 vol% [C ₂ mpy][Tf ₂ N]		210	38	
PEGDA-siloxane		210	40	
PEGDA-siloxane/40 vol% [C ₂ mim][Tf ₂ N]		340	31	
PEGDA-siloxane/40 vol% [C ₂ mim][N(CN) ₂]		240	54	
PEGDA-siloxane/40 vol% [N ₄₁₁₁][Tf ₂ N]		310	33	
PEGDA-siloxane/40 vol% [C ₂ mpy][Tf ₂ N]		300	31	
PEGDA-siloxane/40 vol% [C ₄ mpyrr][Tf ₂ N]		310	31	
PEG	40 °C, 1 bar	145	47	158
PEG/60 vol% [C ₂ mim][Tf ₂ N]	Single gas	530	31	
PEGDA/70 wt% [C ₂ mim][C(CN) ₃] PA supported	30 °C, 0.7 bar Single gas	583	66	134

APPENDIX: FOURIER-TRANSFORM INFRARED (FTIR) SPECTROSCOPY

Table B.1 - Assignments of FTIR peaks of MMT.

Wavenumber (cm ⁻¹)				Vibrational assignment
This study	Ref. ¹⁷³	Ref. ¹⁷⁴	Ref. ¹⁷⁵	
517	500	529	-	Si-O bending.
799	836	836	-	AlMgOH bending.
885	875	875	-	AlFeOH bending.
918	915	915	-	AlAlOH bending.
1012	1000-1125	1035	-	Si-O stretching.
2851	-	-	2846	C-H bending of CH ₂ and CH ₃ groups of the organic modifier.
2924	-	-	2920	C-H bending of CH ₂ and CH ₃ groups of the organic modifier.
3630	3630	3623	3624	OH group stretching for Al-OH, Si-OH and the organic modifier.

Table B.2 - Assignments of FTIR peaks of PEGDA.

Wavenumber (cm ⁻¹)				Vibrational assignment
This study	Ref. ¹⁷⁹	Ref. ¹³⁴	Ref. ¹⁴⁵	
951	954-955	-	-	C-O-C stretching.
1100	1111-1112	-	1100	C-O-C symmetric stretching from ether groups.
1271	1243-1283	-	-	C-O asymmetric bending.
1350	1351-1352	-	-	C-O asymmetric bending.
1408	1411	-	1407	C-H bending.
1619	-	1619	-	C=C asymmetric stretching from terminal acrylate groups.
1636	1636-1647	1635	1635	C=C symmetric stretching from terminal acrylate groups.
1721	1731	1720	-	C=O symmetric stretching.
2869	2885-2887	2866	-	C-H stretching.

Table B.3 - Assignments of FTIR peaks of [C₂mim][Tf₂N].

Wavenumber (cm ⁻¹)				Vibrational assignment
This study	Ref. ¹³⁴	Ref. ¹⁷⁷	Ref. ¹⁷⁸	
569	-	-	569	In plane-symmetric bending of the imidazolium ring (cation), CF ₃ asymmetric bending (anion).
600	-	-	600	SO ₂ asymmetric bending (anion), in plane symmetric bending of the imidazolium ring and CH ₃ (N)CN stretching (cation).
612	-	-	611	SO ₂ asymmetric bending (anion), out of plane asymmetric bending of the imidazolium ring and CH ₃ (N)CN stretching (cation).
650	-	-	650	Out of plane asymmetric bending of the imidazolium ring (cation) and SNS bending (anion).
740	-	743	741	CF ₃ symmetric bending (anion), CH ₃ (N) bending, CH ₂ (N) bending and in-plane bending of the imidazolium ring (cation).
789	-	791	789	C=C asymmetric bending (cation) and CS stretching (anion).
842	-	843	843	C=C bending (cation).
960	-	-	960	C=C bending (cation).
1051	-	1055	1051	SNS asymmetric stretching (anion), in-plane asymmetric stretching of the imidazolium ring and CH ₃ (N) twisting (cation).
1133	1134	1137	1132	S=O symmetric stretching (anion).
1168	1165	-	-	CF ₃ asymmetric stretching (anion).
1330	-	-	1331	S=O asymmetric stretching (anion), in plane symmetric stretching of the imidazolium ring, CH ₂ (N) stretching and CH ₃ (N)CN stretching (cation).
1347	1346	1348	1348	S=O asymmetric stretching (anion).
1574	-	1574	1574	In plane-symmetric/asymmetric stretching of the imidazolium ring, CH ₃ (N)CN stretching and CH ₂ (N) stretching (cation).
2990	-	-	2991	C-H asymmetric stretching (cation).
3160	3162	-	3165	C-H asymmetric stretching and in plane symmetric stretching of the imidazolium ring (cation).

C. |

APPENDIX: THERMOGRAVIMETRIC ANALYSIS

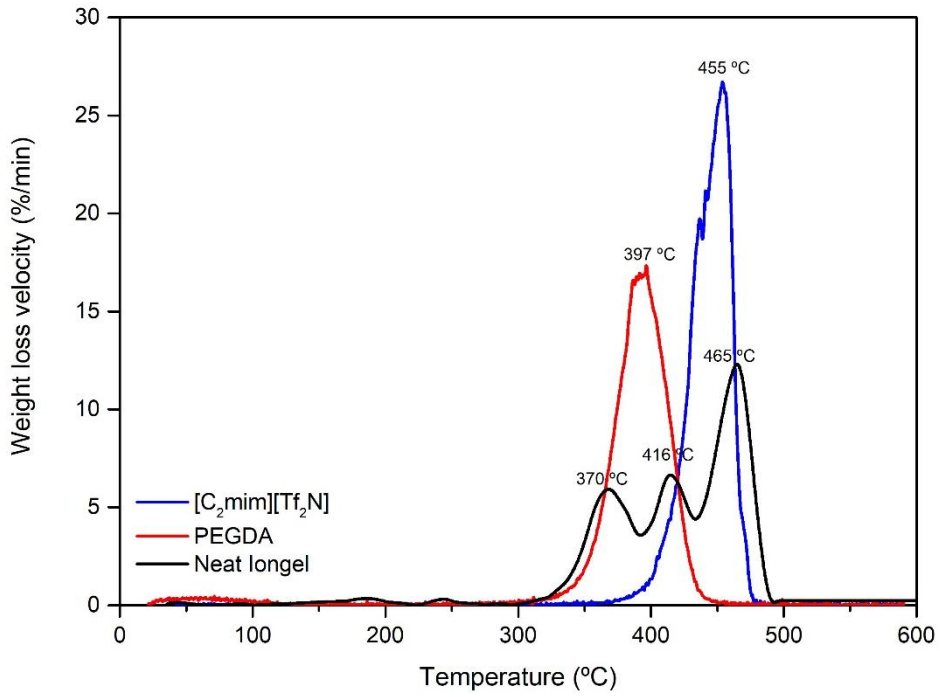


Figure C.1 – dTGA profiles of [C₂mim][Tf₂N], PEGDA and the neat iongel.

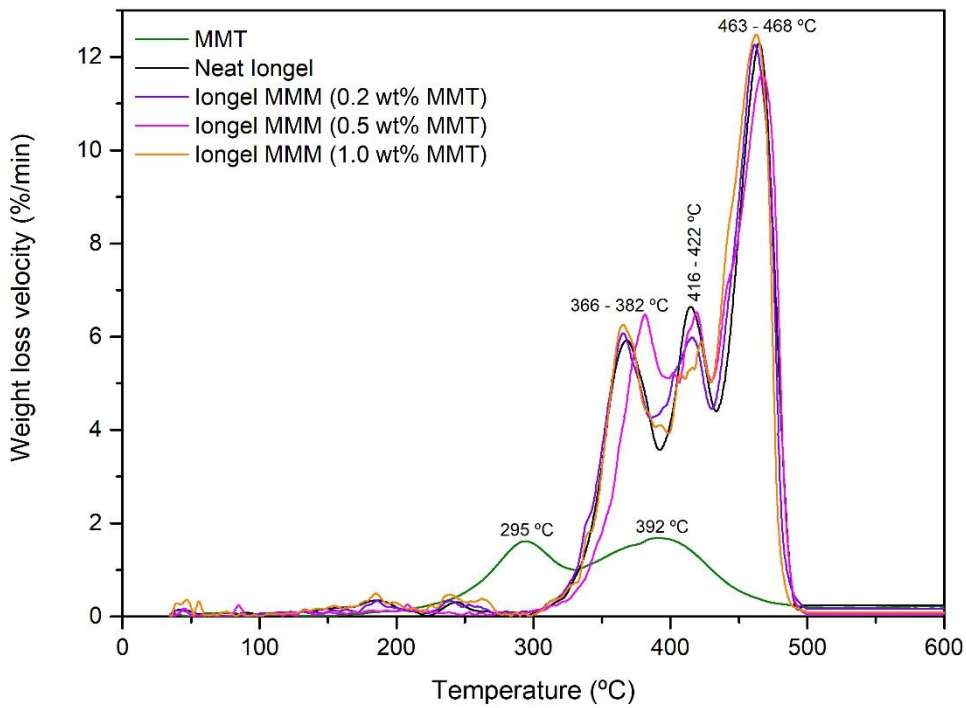
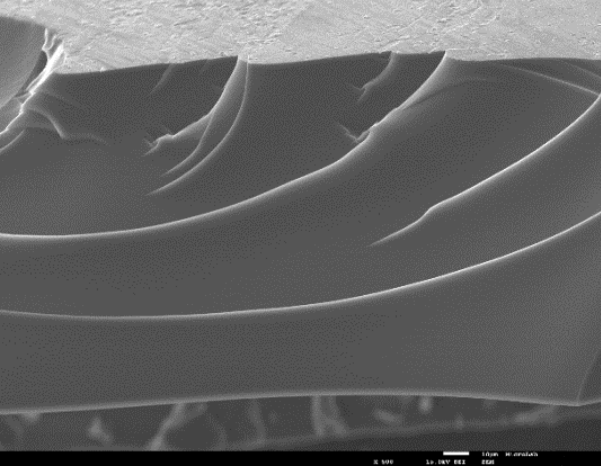
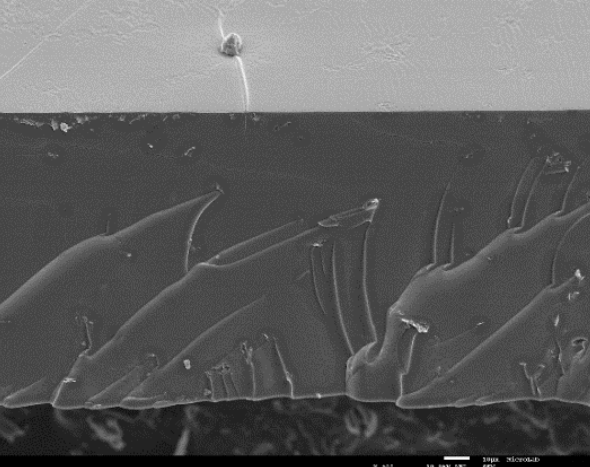
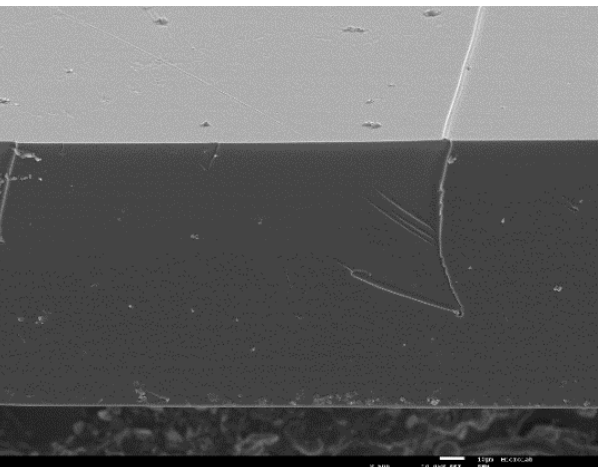
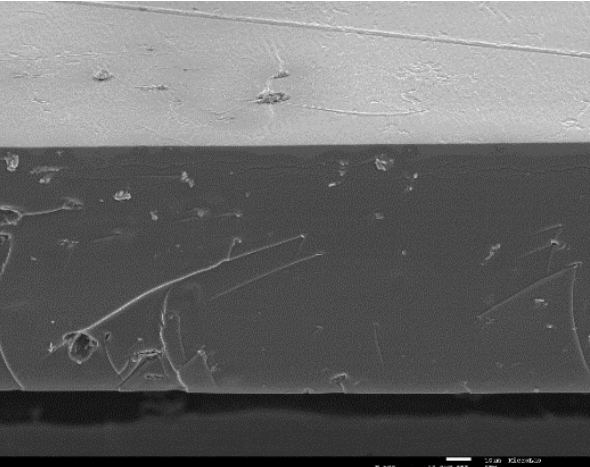


Figure C.2 – dTGA profiles of MMT, the neat iongel and the iongel MMMs with 0.2, 0.5 and 1.0 wt% MMT loading.

D. |

APPENDIX: SCANNING ELECTRON MICROSCOPY

Table D.1 - SEM images of the cross-section of the iongels with 0.0, 0.2, 0.5, and 1.0 wt% loading of MMT with an ampliation of 500x.

MMT loading (wt%)	Cross-section (500x)	MMT loading (wt%)	Cross-section (500x)
0.0		0.5	
0.2		1.0	

APPENDIX: MECHANICAL PROPERTIES

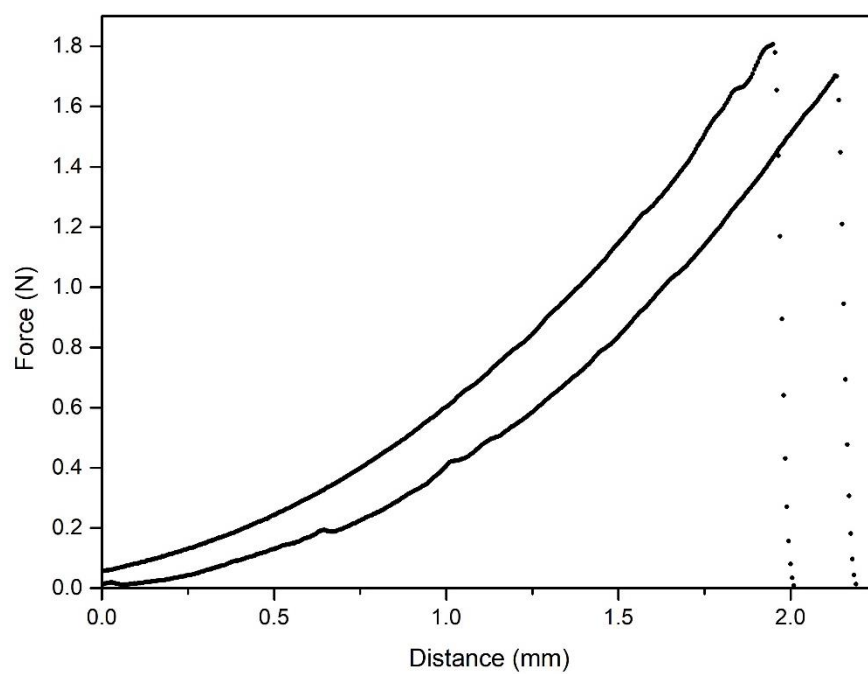


Figure E.1 - Graphic representation of the puncture test for the iongel with 0.2 wt% MMT loading (two replicates).

APPENDIX: PURE GAS PERMEATION EXPERIMENTS

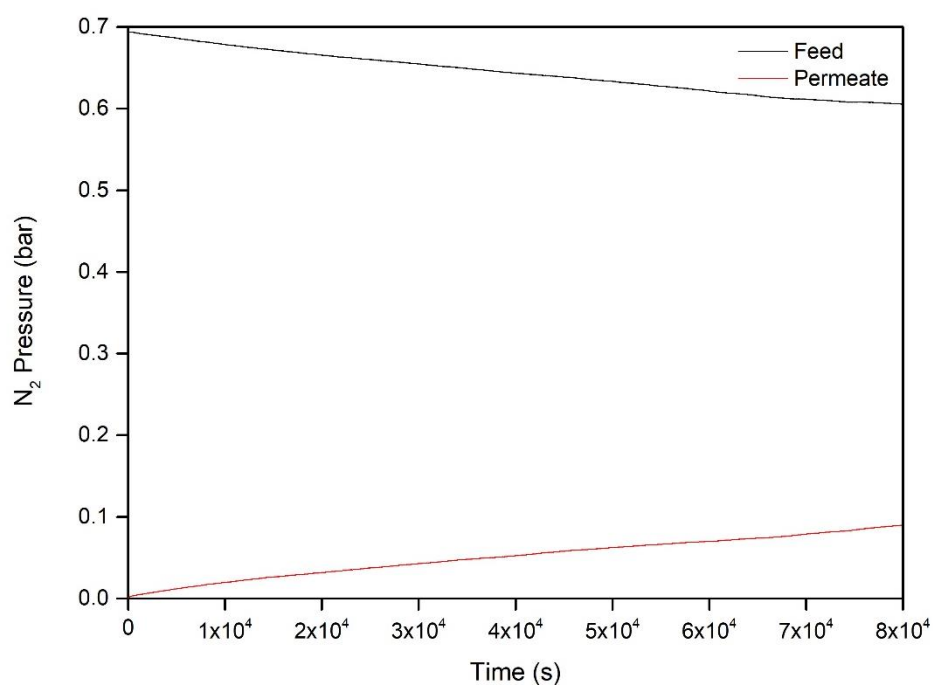


Figure F.1 - N₂ pressure variation in the feed and permeate compartments as a function of time for the iongel with 0.5 wt% MMT loading.

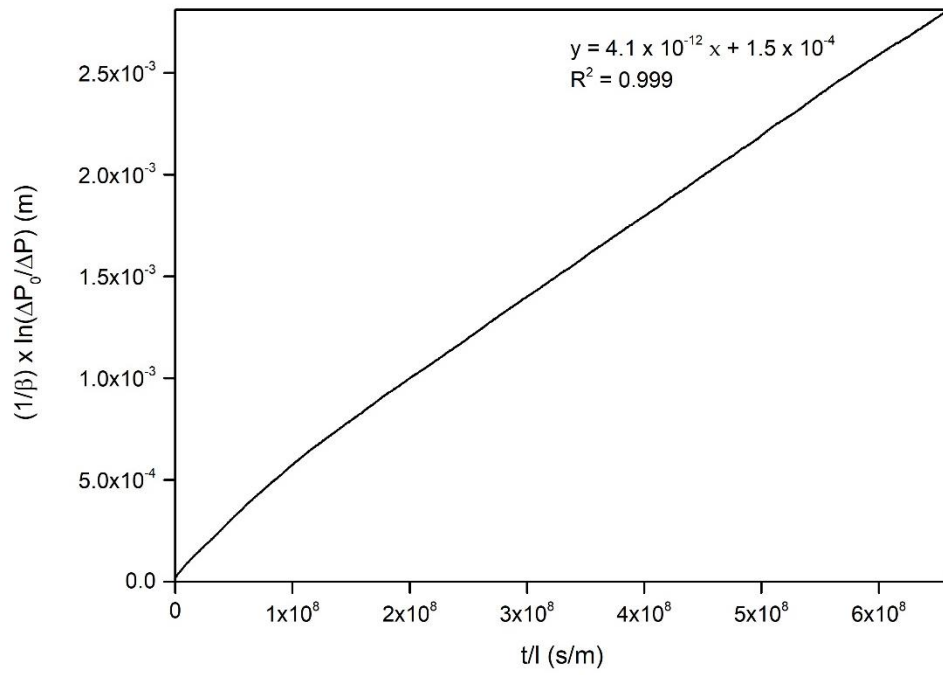


Figure F.2 - Linear fitting of the iongel with 0.5 wt% MMT loading for N₂ permeability calculations.



2021

RUTE RITA MENDES CANCELA
OLIVEIRA FRANCISCO

POLY(ETHYLENE GLYCOL) DIACRYLATE IONGEL
MEMBRANES REINFORCED WITH NANOCCLAYS FOR CO₂
SEPARATION